מכון ויצמן למדע
WEIZMANN INSTITUTE OF SCIENCE

עבודת גמר (תזה) לתואר
דוקטור לפילוסופיה

מוגשת למועצה המדעית של
מכון ויצמן למדע
רחובות, ישראל

Thesis for the degree
Doctor of Philosophy

Submitted to the Scientific Council of the
Weizmann Institute of Science
Rehovot, Israel

מאת
סיון נבון

By
Sivan Navon

פענוח הקוד של הקודונים: סלקציה מעבר לרצף חומצות האמינו.

Deciphering the codons' code: Selection beyond amino acid sequence.

מנחה:
פרופ' יצחק פלפל

Advisor:
Prof. Yitzhak Pilpel

כסלו התשע"ד

November 2013

Table of Contents

1 Abstract

The base of protein production is the translation process in which the codon sequence is decoded into amino acids by tRNAs. The actual codons used for a certain protein can influence different aspects of its gene expression. Codon choices were shown to influence protein levels and folding, mRNA stability and even the host fitness. In my research I focused on how codon usage affects different aspects of gene expression. My research includes a combination of three projects meant to better understand the sequence effects on the gene's translation on one hand, and its mRNA stability on the other.

In my first project I examine how the distribution of codons along the mRNA affects the protein levels. Here I reanalyzed data from two experiments in *Escherichia coli*, examining how regions with "slow codons", i.e. codons which take longer to be translated, influence the translation rate and its efficiency. I found that localizing the slowest codons in the 5'-end results in higher protein levels and the slower this region is the higher the protein levels.

A major parameter which affects the codon's translational speed is the availability of the tRNA which translates it. In my second project we studied the tRNA pool of *S. cerevisiae* through a comprehensive deletion library of tRNAs. We found extensive backup between the tRNA copies and differential contribution to the cell's fitness of identical tRNA copies. In addition, we found up-regulation of RNA Polymerase III genes in some deletion strains all suggesting additional levels of regulation of the tRNA transcription.

In my third project I studied the mRNA degradation in *Escherichia coli* and its coupling to the translation process. By combining mapping of 5' RNA fragments with ribosome profiling data, I studied the relationship between the gene's translation and degradation properties. I suggest that the ribosomes play a dual role in mRNA degradation: on one hand they enhance cleavage of the transcript in its local vicinity, immediately up stream to its attenuation site, yet globally on the transcript they protect it from degradation.

Together my studies shed light on some of the forces behind codon usage. My studies show how codons can attenuate ribosome elongation and reveal that ribosome attenuation is also coupled with the mRNA degradation process.

2 תקציר

הבסיס של ייצור חלבון הוא תהליך התרגום שבו רצף קודונים מפוענח לחומצות אמינו על ידי רנ"א- מוביל (tRNA). הקודונים הספציפיים לקידוד החלבון יכולים להשפיע על היבטים שונים של ביטוי הגן. נמצא כי הקודונים משפיעים על רמות חלבון וקיפולו, יציבות הרנ"א-שליח ואפילו כשירות התא. במחקר שלי התמקדתי בשאלה כיצד הקודונים משפיעים על ההיבטים שונים של ביטוי גנים. המחקר שלי הינו שילוב של שלושה פרויקטים אשר אמורים לשפוך אור על השפעות רצף הקודונים על תרגומו של הגן מצד אחד, ויציבות הרנ"א שלו מצד שני.

בפרויקט הראשון שלי בחנתי כיצד פיזור הקודונים לאורך הרנ"א משפיע על רמות החלבון. בפרוייקט ניתחתי נתונים משני ניסויים באשריכיה קולי ובחנתי כיצד אזורים עם "קודונים איטיים", כלומר קודונים אשר לוקחים זמן רב יותר כדי להיות מתורגמים, משפיעים על קצב התרגום והיעילות שלו. מצאתי כי מיקום של הקודונים האיטיים ביותר בקצה ה5' הינו במתאם עם רמות חלבון גבוהות יותר וככל שהאיזור איטי יותר רמות החלבון גבוהות יותר.

פרמטר מרכזי שמשפיע על מהירות התרגום של קודון הוא זמינות של הtRNA שמתרגם אותו. בפרויקט השני שלי חקרנו את מאגר הtRNAs של בשמר S. cerevisiae דרך ספריית מחיקה של גני ה - tRNAs. מצאנו גיבוי נרחב בין עותקי tRNA השונים וכן השפעה שונה לכשירות התא של מחיקת עותקי tRNA זהים. בנוסף, מצאנו עליה של גנים הקשורים RNA פולימראז III במספר זנים. כל אלה מצביעים כי יתכן וקיימת רגולציה על מאגר הtRNAs ובפרט רגולציה על שעתוק הtRNA.

בפרויקט השלישי שלי חקרתי את תהליך הפירוק של רנ"א-שליח בחיידק אי-קולי והצימוד שלו לתהליך התרגום. על ידי שילוב של מידע על מיקומי חלקי רנ"א בתא עם פרופילי תרגום של ריבוזומים, בחנתי את הקשר בין מאפייני התרגום והפירוק של הגן. מן התוצאות משתמע כי הריבוזומים משחקים תפקיד כפול בפירוק הרנ"א: מחד הם מגבירים את הסיכוי לחיתוך של הרנ"א מידית במעלה הרצף, ומצד שני, באופן גלובלי, הריבוזומים מגנים על הרנ"א מפני פירוק.

יחדיו החלקים השונים של המחקר שלי שופכים אור על גורמים המשפיעים על השימוש בקודונים השונים. המחקרים שלי מראים כי קודונים יכולים להשפיע על תנועת הריבוזום וחושפים קשר בין תהליך התרגום לתהליך פירוק של רנ"א-שליח.

3 Introduction

3.1 Codon Usage and Bias

During the translation process the nucleotide sequence of a gene is translated into the amino acid sequence of a protein. For translation, the nucleotides are grouped into triplets, resulting in 64 codons; these codons are commonly translated to 20 amino acids and stop codons. As a result, 18 out of the 20 amino-acids are translated by two to six different codons, called synonymous codons.

Although translated into the same amino acid, synonymous codons are not perceived the same by the translation system. Commonly across various genomes, there are around 40 different tRNA types per species. Some codons are translated by a fully matching tRNA while others are translated by non-fully matched ones, through the wobble interactions, originally described by Crick (Crick, 1966). According to the wobble hypothesis only the first two positions of a triplet codon need to be precisely paired with the tRNA anti-codon, while the pairing of the third nucleotide position of the codon may be ambiguous, and it varies according to the nucleotide present in this position. Crick's wobble hypothesis was later extended to take into account different covalent modifications that occur on the tRNA molecule (Yarus, 1982, Agris, 1991, Agris, 2004). These modifications which are usually on the 34th nucleotide of the tRNA molecule (the first nucleotide of the anti-codon pair) either disable potential pairing between codon-anticodon pairing of different amino-acids or enable better pairing when the third position does not match (Yarian *et al.*, 2002, reviewed in:Agris, 2004).

Two major observations suggest that there should be significant differences between codons that still code for the same amino acid. The first, the tRNA levels in the cytoplasm can be significantly different between different tRNAs for the same amino acid (Ikemura, 1981, Ikemura, 1982). Although relatively few measurements of such tRNA abundance levels were done (Ikemura, 1981, Ikemura, 1982, Dittmar *et al.*, 2005, Zaborske *et al.*, 2009) a quite reliable proxy for these levels was found in the form of the tRNA gene copy number (tGCN) (Percudani *et al.*, 1997, Kanaya *et al.*, 1999, Tuller *et al.*, 2010a). From this

genome proxy, which can be examined at every fully sequenced genome, it is clear that the various codons are translated by a set of tRNAs which are very different in their relative abundance. The second observation is that there is a codon bias in genes, namely a nonrandom use of synonymous codons found in genomes of both unicellular and multi-cellular organisms (Ikemura, 1985). This bias was found to be particularly pronounced for highly express genes (Sharp & Li, 1986). It was also found that the genome codon bias correlates to the tGCN (Ikemura, 1981, Ikemura, 1982, Duret, 2000), suggesting connection between codon bias and tGCN to translation efficiency. Particularly, highly expressed genes were found to be preferentially encoded by codons that correspond to high abundance tRNAs (Sharp & Li, 1986).

3.2 Translation Efficiency

Based on the fact that highly expressed genes are biased toward "optimal" codons which correspond to the most abundant tRNA genes in the cell (Sharp & Li, 1986), two indices which calculate the adaptation of a sequence to the cellular translation capabilities were developed. The first index is the Codon Adaptation Index (CAI) (Sharp & Li, 1987). For each species a reference set of highly expressed genes is used to assess the relative translation efficiency score of each codon. Then a score for a gene can be calculated by the geometric mean of the translation efficiency values of its codons: $CAI = \left(\prod_{k=1}^{L} w_k \right)^{\frac{1}{L}}$ where L is the number of codons in the gene and w_k is the relative translation efficiency score of the kth codon. This value reflects the usage frequency of the gene's codons in the set of highly expressed genes. The second index is the tRNA Adaptation index (tAI) (dos Reis *et al.*, 2004). This index assumes that the codon efficiency is derived from its tRNA concentration and its tRNA binding affinity. The affinities between each tRNA to each codon were calculated by optimizing the tAI index for highly expressed genes in yeast; these affinities are assumed to be the same for all organisms. As a proxy of the tRNA concentration the tRNA gene copy number (tGCN) of each tRNA type in every species is used. After the initial calculation of affinities which was done in the original paper (dos Reis et al., 2004), the species' codons efficiency (W_i) can easily be

calculated by simply multiplying its tGCN by the previously calculate affinities $(1 - s_{ij})$, $W_i = \sum_{j=1}^{n_i}(1 - s_{ij}) \cdot tGCN_{ij}$. As for the CAI, the tAI score of a gene is calculated as the genomic mean of all its codons: $tAI = \left(\prod_{k=1}^{L} W_k\right)^{\frac{1}{L}}$ where L is the number of codons in the gene and w_k is the normalized codon's efficiency of the kth codon $w_k = W_k / \max(W_i)$.

Although these indices were shown to be good predictors for expression of natural genes (Sharp & Li, 1986, Man & Pilpel, 2007), in recent synthetic libraries experiments they failed to predict the abundance of a protein across different nucleotide sequence variants (Kudla *et al.,* 2009, Welch *et al.,* 2009). This failure suggests other sequence parameters affect the translation efficiency, shedding light on one of the potential limitations of both indices: they are indifferent to the order of the codons along genes, scoring equally alternative genes with same codon composition and yet different order of high and low efficiency codons.

In recent years other sequence parameters were shown to also affect translation efficiency. One of the most significant parameter is the mRNA secondary structure, in particular the folding energy of the ribosome binding site (RBS) region, which is also affected by codons close to the ATG (Lu *et al.*, 2007, Kudla et al., 2009, Gu *et al.,* 2010, Tuller *et al.*, 2010b, Goodman *et al.,* 2013). In addition codons near the ORF start were found to be under selection for low folding energy (Gu et al., 2010) but also for less efficient codons (Tuller et al., 2010a); suggesting that the codons regulate the flow of ribosomes on the transcript (Tuller et al., 2010a). To date it is quite clear that changes to the secondary structure significantly affect translation efficiency (Goodman et al., 2013, Kudla et al., 2009). Yet it is still unclear to what extent changes in each of these sequence parameters away from the ATG affects the translation efficiency of a given transcript and whether we have identified them all. However, it is clear that changes of synonymous codons, while not changing the amino acid sequence, do influence all the above sequence parameters thus changing translation efficiency.

3.3 The tRNA pool

The tRNA (transfer RNA) is one of the fundamental components of the translation machinery. The tRNA pool, numerically represented by the tRNA concentrations in the cell, was shown to play an important role in the dynamics of translation in previous papers (Ikemura, 1981, Ikemura, 1982, Dittmar et al., 2005, Man & Pilpel, 2007, Subramaniam *et al.*, 2013). This is attributed to the fact that the rate limiting step in the elongation cycle of polypeptides is tRNA search and selection, (Varenne *et al.*, 1984)

The tRNAs are transcribed by RNA Polymerase III (Pol III) which, along with RNA Polymerase I, dominates cellular transcription, together reaching more than 80% of total RNA synthesis in growing cells (Paule & White, 2000). The tRNA promoters are composed of two highly conserved sequence elements that reside within the transcribed region called the A-box and the B-box (reviewed in: Paule & White, 2000). For many years these two internal promoter elements along with the Pol III terminator were considered the main elements to regulate tRNA transcription. However, more recent papers have shown that the tRNA transcription levels also depend on upstream regulatory motifs (Giuliodori *et al.*, 2003, Parthasarthy & Gopinathan, 2006).

tRNA genes may be present in multiple copies in a genome, e.g, *S. cerevisiae* has 274 tRNA genes encoding 42 different isoacceptors, human has 506 tRNAs encoding 48 different isoacceptors, and *E. coli* K12 has 86 tRNAs with 39 different isoacceptors (Chan & Lowe, 2009). It is assumed that the requirement for large quantities of tRNAs is met by multiple copies of the tRNA gene in addition to multiple rounds of transcription of each tRNA gene (Duret, 2000, Percudani et al., 1997, Kanaya et al., 1999). Indeed it was shown that the tRNA genome copy number is a reliable proxy for the tRNA levels (Percudani et al., 1997, Kanaya et al., 1999, Tuller et al., 2010a).

The tRNA pool is often assumed to be constant throughout the life of a cell (Tuller et al., 2010a, dos Reis et al., 2004). However recent papers reveal a more complex picture. Absolute tRNA levels were shown to change across growth conditions (Dittmar et al., 2005) and in different tissues (Dittmar *et al.*, 2006). The binding of Pol III to the genome was also shown to vary between the

different tRNAs genes (Canella *et al.*, 2010, Kutter *et al.*, 2011). These new finding suggests the tRNA pool has the potential to be dynamic and to undergo regulated change in different growth conditions. A dynamic tRNA pool could grant the cell the ability to adapt the translation efficiencies to better fit the immediate demand. The questions of how dynamic is the tRNA pool and what are the mechanism that enable it to change still remains to be answered.

3.4 Transcript Degradation

The amount of protein synthesized in the cell is determined by two primary parameters: the mRNA levels of the genes and the rate of translation of this mRNA. mRNA levels in turn, are determined by both the rate of transcription and the rate of degradation. In bacteria the half-life of different transcripts varies significantly, from less than a minute to about an hour (Bernstein *et al.*, 2002), thus allowing the stability of the mRNA to play a key role in regulating the transcriptome.

A mature bacterial transcript initially bears a triphosphate at its 5' and a stem & loop structure at its 3'. In *Escherichia coli*, the degradation of most mRNAs is thought to begin with an internal endonucleolytic cleavage (Deana & Belasco, 2005), resulting in two RNA fragments. The upstream fragment is no longer protected by a 3' stem loop and is thus promptly degraded by 3' exonucleases. The downstream fragment is only monophosphorylated, leading to its rapid degradation by a series of internal cleavages and 3' degradations (Deana & Belasco, 2005).

Since in bacteria the degradation is initiated from an internal cleavage, it is not surprising that translation parameters influence the mRNA degradation. Two ribosome-related mechanisms have a potential to stabilize the mRNA (reviewed in: Deana & Belasco, 2005). The first, closely spaced translating ribosomes can protect potential cleavage sites. The second, ribosome occupying the 5' terminus of the transcript can impede access to cleavage site by disrupting the cleavage mechanism. Indeed it was found that a ribosome binding to the RBS helps to protect mRNAs, and as a consequence a less efficient RBS can give rise to destabilization of the mRNA (reviewed in: Deana & Belasco, 2005). On the other hand, stalled ribosomes could have either a stabilizing effect (Bechhofer &

Zen, 1989) or a destabilizing affect (Hayes & Sauer, 2003, Sunohara *et al.*, 2004). In particularly it was shown that clusters of rare codon have a destabilizing effect (Sunohara et al., 2004). Furthermore stalled ribosomes were found to causes cleavage in variety of location without an identified nucleases, naming them "killer ribosomes" (reviewed in: Dreyfus, 2009).

It thus appears from biochemical analyses that the control of translation and mRNA degradation might be coupled. In particular features that affect translation efficiency may also influence the decay rate of the corresponding mRNAs. As described above, different codons have the potential to change both the secondary structure of the transcript and the ribosomes flow along it. As a result, degradation of mRNA might be sensitive to, and perhaps regulated by codon usage. To date the exact features which determine where and when a transcript will be cleaved are still unknown. Exact cleavages sites were mapped only for a handful of genes over the years (Cormack & Mackie, 1992, McDowall *et al.*, 1994, Braun *et al.*, 1996, Ehretsmann *et al.*, 1992) and the nucleases cleavage preferences were not completely characterize. Thus, any hope to predict mRNA stability requires more work to understand both the cleavage mechanism and its potential coupling with translation.

4 Methods

4.1 The role of codon selection in regulation of translation efficiency deduced from synthetic libraries (Navon *et al.* Genome Biology 2011)

4.1.1 Defining the bottleneck

In this project we analyzed how a region of non-optimal codons can affect translation. We defined this region as the bottleneck, a region on the gene where the harmonic mean of the codons' tAI (dos Reis et al., 2004) values is minimal. The codon tAI values are assumed to be proportional to the speed of its translation (Tuller et al., 2010a); higher tAI value, correspond to high tRNA abundance and affinity, thus faster translation. A harmonic mean of speeds is simply an arithmetic mean of the corresponding times. Hence looking for the region with the minimum harmonic mean of speed is equivalent to looking for the region which takes the longest time to translate. For each region the harmonic mean of speed is: $\frac{n}{\sum_{c \in Region} \frac{1}{tAI_c}}$; where n is the region size, and c is the set of all the codons in the region (n codons). For more details the see the Methods in the paper attached to the results chapter, 5.1

4.1.2 Choosing the bottleneck window size (*n*)

Under a maximal density scenario (fast initiation rate), the distance between two consecutive ribosomes will be minimal. In this case, when two ribosomes are translating the same mRNA simultaneously, the minimum possible distance between the two translated codon (one by each of the ribosome) is one ribosome size (*H* codons). At any given moment during the translation process, two adjacent ribosomes would have translated exactly the same codons apart from the last *H* codons - the first of the two ribosomes has already translated them, and second is just about to start them. If the time it took the first ribosome to finish translating the *n*th codon $T(n,1)$ is larger than the time it takes the second ribosome to translate the *n-H*th codon $T(n-H,2)$ the second ribosome will "bump" into the first one. Therefore the region of *H* codons with maximum translation time determines whether and where a traffic jam will be

created (for detailed calculations see the Methods in the paper attached to the results chapter, 5.1). Consequently the minimal distance between two ribosomes should determine our window size. We adopted the average ribosome-to-ribosome distance measured by Brandt *et al.* (Brandt *et al.*, 2009). They measured the mean distance between the center of mass of two ribosomes on actual bacterial polysomes to be 21.6*nm* which is about 21 codons (0.34*nm* per base). For more details see the Methods in the paper attached to the results chapter, 5.1.

4.1.3 The bottleneck parameters

A bottleneck is characterized by two parameters: its "location" and its "strength":

The "**location**" of the bottleneck is defined as the location in the gene of the bottleneck's first codon (*k* codons from the ATG).

The "**strength**" of the bottleneck is defined as the arithmetic average of 1/tAI values for the codons in the region, e.g. $\frac{1}{n}\sum_{c\in Region}\frac{1}{tAI_c}$ (the inverse of the harmonic mean).

The **relative strength** of the bottleneck is defined as the strength of the bottleneck divided by the average 1/tAI for the entire gene, e.g. $\frac{\frac{1}{n}\sum_{c\in bottleneck}\frac{1}{tAI_c}}{\frac{1}{l}\sum_{c=1}^{l}\frac{1}{tAI_c}}$; where l is the number of codon in the gene (excluding the stop codon).

The **relative location** of the bottleneck is defined as the location of the bottleneck divided by number of possible windows; e.g. $\frac{k}{l-n+1}$; where k is the location of the bottleneck, and l is the length of the gene and n is the window size.

4.1.4 Finding the main anti-correlated codons

We used partial correlation to find the codons which contribute the most to the decrease in the cell's fitness. The highest contributors were filtered according to the following steps:

1. Find codons which have a negative correlation to the OD.
2. For all codons left, we calculated the partial correlation matrix M(*i*,*j*) = partial correlation (codon *i*, OD | codon *j*).
3. Find the minimum absolute value of the partial correlation, for each codon. Rank the codons in a descending order accordingly.

For more details see the Methods in the paper attached to the results chapter, 5.1.

4.1.5 Calculating the codon usage in the genome and transcriptome

To calculate the codon usage in the genome we counted each codon appearance in all the ORFs and normalized by the total number of codons. For this analysis we used the genome of *E. coli* B21 strain (which was used by Kudla *et al.*) was downloaded from NCBI; [Refseq: NC_012947 (Jan 11, 2010)].

To calculate the codon usage of the transcriptome of each gene was calculated by multiplying the mRNA levels measurements for the gene by the codon usage of the same gene. The contributions of all genes were summed for each codon and then divided by the total sum of all codons. mRNA levels were taken from Lu *et al*. (Lu et al., 2007). For details see the Methods in the paper attached to the results chapter, 5.1.

4.2 A Comprehensive tRNA deletion library unravels the genetic architecture of the tRNA pool

4.2.1 Characterizing the growth dynamics and the phenotype of a deletion strain

To assess the contribution of each tRNA gene to cellular growth, we characterized the growth dynamics of each deletion strain. We chose to characterize each deletion strain by two growth parameters: growth rate and the size of the population upon entering the stationary phase, denoted "growth yield". For each strain the relative-growth-rate and relative-growth-yield were calculated by normalizing its parameters to the wild type parameters measured in the same experiment. These parameters are then projected on a distribution of the wild type growth parameters (which was created by measuring the wild type multiple times in multiple days) and the number of standard deviations is calculated (σ), see Figure 1. Any deviations larger than two standard deviations from the mean were considered as "phenotypes" and deviations above three standard deviations were considered a "strong phenotype". A negative deviation denotes impairment (worse than the wild type (WT)) while a positive deviation denotes improvement (better than the WT).

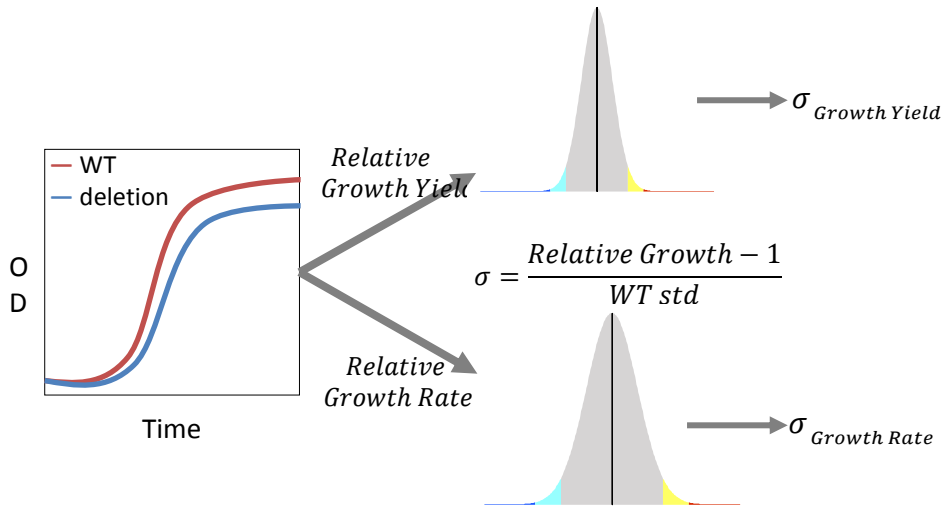

Figure 1. Characterizing a deletion strain. Schematic representation of growth measurements, analysis, and scoring. For each strain relative-growth-rate and relative-growth-yield were calculated in relation to the wild type strain. These parameters are then projected on a distribution of the wild type growth parameters. Sigma (σ) is denotes the number of standard deviations from the mean of the wild type.

4.2.2 Motif Analysis

A sequence motif analysis was performed using the MEME online software (Bailey & Elkan, 1994) to identify motifs which are can explain difference in tRNA deletion strain fitness. The motif search was done on the upstream sequence of tRNA genes which exhibited a yield impairment phenotype in rich medium upon deletion (42 genes) versus the upstream sequence of tRNA genes which exhibited a phenotype in no more than two out of the six measured conditions (99 genes). To apply location constrains on the motifs, the MEME analysis was done in windows of size 9bp, looking for motifs of 4-8bp in length.

4.2.3 Microarray analysis

For five tRNA deletion strains the transcriptome was measured using to Affymetrix yeast 2.0 microarrays. The microarray background adjustment was done using the Robust Multi-array Average (RMA) procedure followed by quintile normalization. For each strain, the fold change in expression for all genes was calculated by comparing the wild-type measurement in the same batch and averaged over two biological repeats.

The five strains were clustered. The cluster tree was based on the correlation between the mRNA fold changes of the different strains. For the clustering we used the top 50% of the sorted genes based by the gene variance across the strains.

4.2.4 Gene Set Enrichment

To expose what are the responses and underling molecular pathways that differentiate these two groups of tRNA deletion strains, we used Gene Set Enrichment Analysis (GSEA) software. GSEA computationally determines whether pre-defined set of genes shows statistically significant difference in representation between two biological groups (Subramanian *et al.*, 2005, Mootha *et al.*, 2003). For the pre-defined set of genes we used *S. cerevisiae* pathways as defined by KEGG (Kanehisa & Goto, 2000, Kanehisa *et al.*, 2012).

4.3 Ribosome density governs patterns of mRNA cleavage in *Escherichia coli*

4.3.1 Identifying cleavage sites

In order to identify cleavages sites for both *E. coli* and *P. aeruginosa* we used data derived from a modified RNA deep sequencing protocol (Wurtzel *et al.*, 2010) to deduce location of endonucleolytic cleavage sites. The Mapping of *E. coli* 5'-end monophosphorylated RNA fragments were taken from the Quax *et al*. paper (Quax *et al.*, 2013), which was downloaded from: http://www.weizmann.ac.il/molgen/Sorek/Navon_data.fasta.gz. and the *P. aeruginosa* mapping were taken from Wurtzel *et al.* paper (Wurtzel *et al.*, 2012).

The 5'-end mapping for both datasets were filtered, keeping only the most reliable cleavage sites thus filtering out potential transcription-start-sites (TSS) and less reliable reads. For details on the filtering see the Material and Methods in the paper attached to the results chapter, 5.3.

4.3.2 mRNA folding energy and unpairing score calculations

To calculate the mRNA secondary structure around the cleavage sites we used Vienna RNAfold package (Lorenz *et al.*, 2011). For more details see the Material and Methods in the paper attached to the results chapter, 5.3.

4.3.3 Calculating the genes' ribosome density

For this paper the ribosome density were constructed from ribosome occupancy data deposited in GSE35641 (Li *et al.*, 2012). The ribosome occupancy for each gene was normalized to the sum of the ribosome occupancy over all the mRNA including its UTRs (50 nucleotides upstream and downstream). For more details see the Material and Methods in the paper attached to the results chapter 5.3.

5 Results

5.1 The role of codon selection in regulation of translation efficiency deduced from synthetic libraries (Navon *et al.* Genome Biology 2011)

Although translated into the same amino acid, synonymous codons are not perceived the same by the translation system. The translation efficiency of a codon is affected by the availability of the tRNAs translating it and their affinity to translate it. Thus, some codons will be perceived as more optimal than others by the translation system. The aim of this project was to study how regions of less than optimal codons affect the gene expression level and the host fitness.

Genome Biology

RESEARCH Open Access

The role of codon selection in regulation of translation efficiency deduced from synthetic libraries

Sivan Navon, Yitzhak Pilpel*

Abstract

Background: Translation efficiency is affected by a diversity of parameters, including secondary structure of the transcript and its codon usage. Here we examine the effects of codon usage on translation efficiency by re-analysis of previously constructed synthetic expression libraries in *Escherichia coli*.

Results: We define the region in a gene that takes the longest time to translate as the bottleneck. We found that localization of the bottleneck at the beginning of a transcript promoted a high level of expression, especially if the computed dwell time of the ribosome within this region was sufficiently long. The location and translation time of the bottleneck were not correlated with the cost of expression, approximated by the fitness of the host cell, yet utilization of specific codons was. Particularly, enhanced usage of the codons UCA and CAU was correlated with increased cost of production, potentially due to sequestration of their corresponding rare tRNAs.

Conclusions: The distribution of codons along the genes appears to affect translation efficiency, consistent with analysis of natural genes. This study demonstrates how synthetic biology complements bioinformatics by providing a set-up for well controlled experiments in biology.

Background

Understanding the mechanisms that control the efficiency of protein translation is a major challenge for proteomics, computational biology and biotechnology. Efficient translation of proteins, either in their natural biological context or in heterologous expression systems, amounts to maximizing production, while minimizing the costs of the process. Abundant genome sequence data now make it possible to decipher sequence design elements that govern the efficiency of translation. The codon adaptation index (CAI) [1] was the first measure to be introduced for gauging translation efficiency directly from nucleotide sequences of genes. This measure quantifies the extent to which the codon bias of a gene resembles that of highly expressed genes. The tRNA adaptation index (tAI) assesses the extent to which the codons of a gene are biased towards the more abundant tRNAs in the organism [2]. Despite several simplifying assumptions, both tAI and CAI are good measurements for predicting protein abundance from sequence [3,4]. Perhaps the most critical simplification of the two models is that they represent the translation efficiency of an entire gene by a single number - the average translation efficiency value over all its codons. As such, both CAI and tAI ignore the order in which codons of high and low translation efficiency appear in the sequence. Thus, two genes may share the same value of CAI or tAI and yet the order of high and low efficiency codons differs between them.

By analyzing dozens of genomes, we have recently shown that the order of high and low efficiency codons in biological sequences is under selection [5,6]. Specifically, examining such genomes revealed a clustering of low efficiency codons at the beginning of ORFs, mainly in the first approximately 50 codons. We termed this design the 'translation ramp', or 'ramp' for short, which might constitute a strategic early bottleneck in the flow of the ribosomes. Our model suggests that such ramps attenuate the ribosomes at the beginning of genes, thus allowing a jam-free flow of ribosomes beyond the ramp. We have shown that this design is predominantly

* Correspondence: pilpel@weizmann.ac.il
Department of Molecular Genetics, Weizmann Institute of Science, PO Box 26, Rehovot, 76100, Israel

obeyed by highly expressed genes [5,7], suggesting that it might support efficient production. Investigating natural genes has two obvious advantages: their availability in very high numbers, and the fact that they have been subject to selection and optimization by evolution. Similarly, using the totally asymmetrical simple exclusion process (TASEP), it was theoretically shown that slow codons can affect ribosome density and production rates depending on initiation rate, termination rate, and the rate of the slow codons and their distribution [8-12].

Yet, analysis of natural sequences also poses limitations. Natural genes represent a wide variety but their variability is uncontrolled and is influenced by confounding factors at many levels. For instance, even if two genes share the same translation efficiency profile, they may differ with respect to the strength of their promoter, the un-translated regions, the secondary structure and the amino acid sequence, all factors that may affect protein levels. Synthetic biology, which now offers the ability to synthesize and express designed genes, may complement the picture obtained from bioinformatics analysis of natural genes. Although the number of genes that can be synthesized is by orders of magnitude lower than the number of natural sequences, synthetic genes enable us to modify one variable at a time while keeping others constant. In several pioneering studies of this type, the nucleotide sequence of a single gene was randomized while amino acid sequence was kept constant. In particular, these studies generated libraries of artificial variants of genes' nucleotide coding sequences, while fixing other features, such as the untranslation regions and promoters. Analysis of one such library led to an important finding - that the stability of the mRNA, especially in the 5' region, is a main determinant of protein abundance [13]. Those authors further found that the CAI of a gene had no effect on protein expression levels but that it was rather correlated with, and perhaps affected, the fitness of the host cell.

Here we set to re-analyze the data from these libraries [13,14]. We were motivated by the realization that, due to their simplifying assumptions, the CAI and tAI do not capture the full capacity of codon selection to affect translation efficiency, particularly since these models ignore codon order that is under tight selection [5,6]. We show that obeying the design we observed in nature, namely localization of the bottleneck at the beginning of the ORF sequence, indeed promotes higher levels of expression. This was especially true if the predicted dwell time of the ribosome at these bottleneck regions was sufficiently long. On the other hand, the bottleneck characteristics did not affect the fitness of the host cell. We did find, however, that the extent of utilization of two particular codons (UCA and CAU) does correlate negatively with a cell's fitness, potentially due to sequestration of the corresponding rare tRNAs. The results further demonstrate how correlative conclusions made from observations of natural gene sequences can be complemented by synthetic genes, allowing decoding of the sequence features that govern the efficiency of translation and its costs.

Results and discussion

Translation efficiency

Looking for the effects of codon usage on translation efficiency and whether the order of the codons is important, we set out to re-analyze data from the three synthetic libraries [13,14]. The original tAI value [2] is defined for an entire gene based on all its codons as:

$$tAI_g = \left(\prod_{k=1}^{\ell_g} w_{i_k} \right)^{1/\ell_g}$$

where l_g is the length of the gene in codons and w_{i_k} is the relative adaptiveness value of the codon defined by the kth triplet in the gene.

Here we refer to the w_i value of a single codon as the codon's tAI. This measure is an approximation of the codon's translation speed, since a codon is assigned with a high tAI if the various tRNAs that translate it are at high abundance and have high affinity towards it. Besides the tAI, there are other alternative approximations for the codon's translation speed [8,15,16] (see discussion in Additional file 1). Note that all current models have approximation as their basis, necessarily introducing inaccuracies in analyses that are based on them.

To investigate the effect of regions with less than optimal codons, for each gene we defined the 'bottleneck' as a region of a fixed number of codons, n, where the (harmonic) mean of the codons' tAI value is minimal (the value of n is related to the distance between two consecutive ribosomes on the mRNA (see Materials and methods). Assuming the codon's tAI value is an approximation for the translation speed, then 1/tAI can be regarded as the codon's translation time and the bottleneck is the region with the longest average translation time.

The bottleneck of each gene is characterized by two parameters: the location of the bottleneck - that is, number of codons from the ATG in which it occurs - and the 'strength' of the bottleneck - the average time to translate all the codons within it. To allow comparisons between the different genes and libraries below, we refer to the relative, rather than absolute, form of these variables - the relative location of the bottleneck is its

location divided by the length of the gene, and the relative strength is the strength divided by the average strength (that is, the time it takes to translate the bottleneck regions divided by the total time of translation of the mRNA, or 1/tAI of the entire gene).

We first analyzed 154 synthetic GFP genes in a library constructed by Kudla *et al.* [13]. All the synthetic GFP variants had the same amino acid sequence but different codon sequences. For these genes we calculated the bottleneck parameters using a window of length $n = 21$ codons. Note that there is uncertainty regarding the exact value of this parameter (see Materials and methods); however, experimentation with other window sizes in the range $14 < n < 30$ did not affect results qualitatively (not shown). Figure 1a shows the relative location of the bottleneck of all GFP genes versus the protein abundance of each translated gene (see Materials and methods). The relative location is anti-correlated to the protein abundance (Pearson correlation -0.43, *P*-value 3.4×10^{-8}; Spearman correlation -0.46, *P*-value 2.8×10^{-9}), indicating that genes that have the bottleneck closer to the ATG (designated here as the 'proximal bottleneck') tend to have higher protein abundance levels compared to genes whose bottleneck are located towards the 3' end of the gene (designated the 'distal bottleneck').

As for the relative strength of the bottleneck, when examining the entire library of 154 genes we found a modest yet significant correlation with the protein abundance (Pearson correlation 0.38, *P*-value 1.9×10^{-6}; Spearman correlation 0.31, *P*-value 1.2×10^{-4}); that is, genes with long dwell times of the ribosome in the bottleneck regions tended to have higher expression levels. However, as seen in Figure 1b, this correlation is mainly contributed by genes that have a proximal bottleneck. Focusing on 86 of the genes with a proximal bottleneck (located between relative positions 0.16 to 0.28) a significant positive correlation emerged between the relative strength and the protein abundance (Pearson correlation 0.47, *P*-value 3.9×10^{-6}; Spearman correlation 0.44, *P*-value 2.1×10^{-5}). From Figure 1a it is seen that there are relatively few genes with a distal bottleneck that also have a similar relative strength; therefore, the influence of the relative strength on distal genes cannot be deduced.

Summarizing the analysis of the GFP library, the distribution of the codons along the transcript appears to affect the final GFP levels in the cell. A region of less efficient codons at the beginning of a transcript - for example, a proximal bottleneck - seems to enable higher protein levels. For genes with a proximal bottleneck it is also beneficial to have a relatively long dwell time of the ribosome, that is, a strong enough bottleneck. From this library we were not able to learn about the significance of the bottleneck strength in the case of genes with distal bottlenecks; however, other libraries with different distributions of bottlenecks can shed light on the question.

In another recent paper, by Welch *et al.* [14], two different proteins were synthesized: the DNA polymerase of Bacillus phage and an antibody fragment (scFv). For each protein there are approximately 40 different

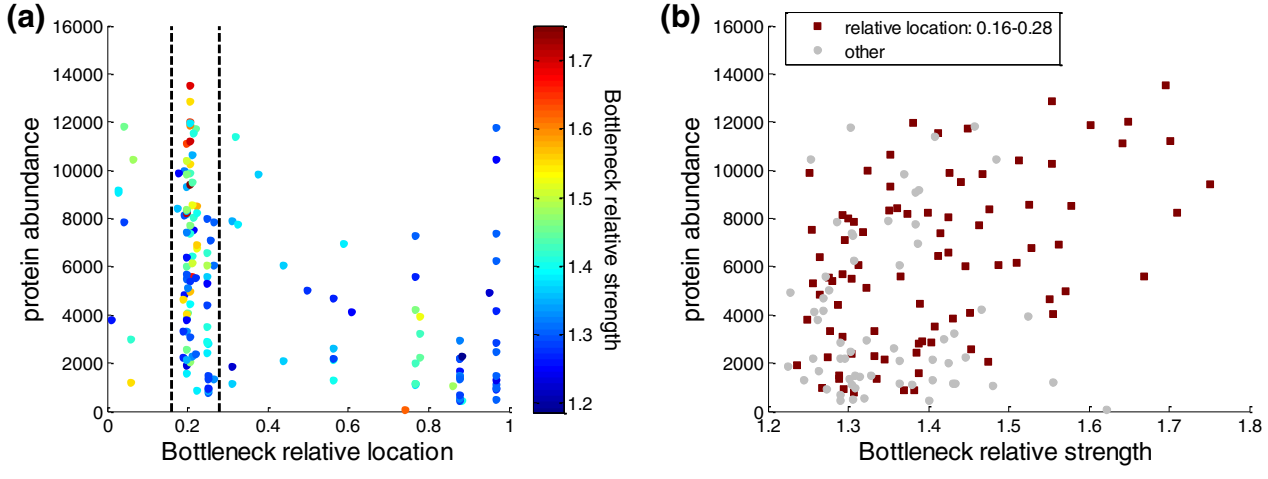

Figure 1 Protein abundance versus relative location and strength of the bottleneck in the GFP library. **(a)** All the genes in the GFP library. The x-axis is the relative location of the bottleneck in every gene; the y-axis is the per-cell protein abundance. The color of each dot is the relative strength of the bottleneck in every gene. Eighty-six of the genes are located between the two black lines that correspond to relatively early bottlenecks - that is, relative location between 0.16 and 0.28. **(b)** The correlation between the bottleneck relative strength and per-cell protein abundance for all the genes in the GFP library. The 86 genes that have a relative location between 0.16 and 0.28 are plotted as red squares, and the rest of the genes are plotted as grey circles.

sequences in which the amino acid was kept the same while changing the codon sequence. For both proteins, the location of the bottleneck is quite far from the ATG in most synthetic variants (relative distance of approximately 0.5 and higher; Figure S1 in Additional file 2), excluding the possibility of examining the effect of the proximal bottleneck on the expression of these two proteins. Nonetheless, we could still compute the correlation between the bottleneck's parameters and protein abundance. Although less significant than in the case of the GFP library, both libraries showed an anti-correlation between protein abundance levels and the relative location of the bottleneck (Spearman correlation -0.34 (*P*-value 0.06) and -0.40 (*P*-value 0.03); Pearson correlation -0.34 (*P*-value 0.06) and -0.16 (*P*-value 0.40) for the scFv and the polymerase, respectively). Similar to the GFP library, such negative correlation indicates that proximal bottlenecks are often associated with higher expression levels. As was done for the GFP library, we looked at the correlation between protein abundance and the bottleneck relative strength (Figure 2) for specific locations, chosen based on Figure S1 in Additional file 2 (for correlations see Table S1 in Additional file 1). Interestingly, while in the case of the GFP library a proximal bottleneck became more effective with increased relative strength, in the cases of scFv and the polymerase, which featured a distal bottleneck, the strength actually showed the opposite correlation; that is, genes with long dwell times in the bottleneck regions showed lower protein abundance (Spearman correlation -0.43 (*P*-value 0.02) and -0.67 (*P*-value 7.1×10^{-5}) for all genes of scFv and the polymerase, respectively). It is our understanding that a proximal bottleneck can have beneficial effects on protein production [5]. The bottleneck can delay the translating ribosome, causing a ribosome backlog (when in polysome), and can also reduce the density of the ribosome downstream. A proximal bottleneck minimizes the number of jammed ribosomes, thus reducing ribosome sequestering and collisions, two potential causes for a decrease in protein production. Assuming the bottleneck reduces the density of ribosomes downstream, a slower bottleneck (that is, a bottleneck with increased relative strength) will reduce even more downstream ribosome collisions, improving protein production, as seen with the GFP library. On the other hand, a distal bottleneck at the end of the ORF causes a long backlog, with no beneficial effects on expression levels. Since a bottleneck at the end of the ORF seems to have mainly negative effects on the protein translation rate, reducing its relative strength is beneficial, as seen in the case of the scFv and the polymerase.

To further verify our assumption that the bottleneck may have beneficial effects on protein abundance when they are located at the beginning of a gene, we looked at the distribution of locations of the bottleneck in natural *Escherichia coli* genes [Refseq: NC_012947] (Figure 3; Figure S2 in Additional file 2). Indeed, for most genes with a bottleneck of high relative strength (higher than 1.3), the bottleneck region is located in the first quadrant of the transcript (relative location smaller than 0.25). For 41% of genes with a bottleneck of high relative strength, the bottleneck is located in the first quadrant (hyper-geometric significant enrichment *P*-value

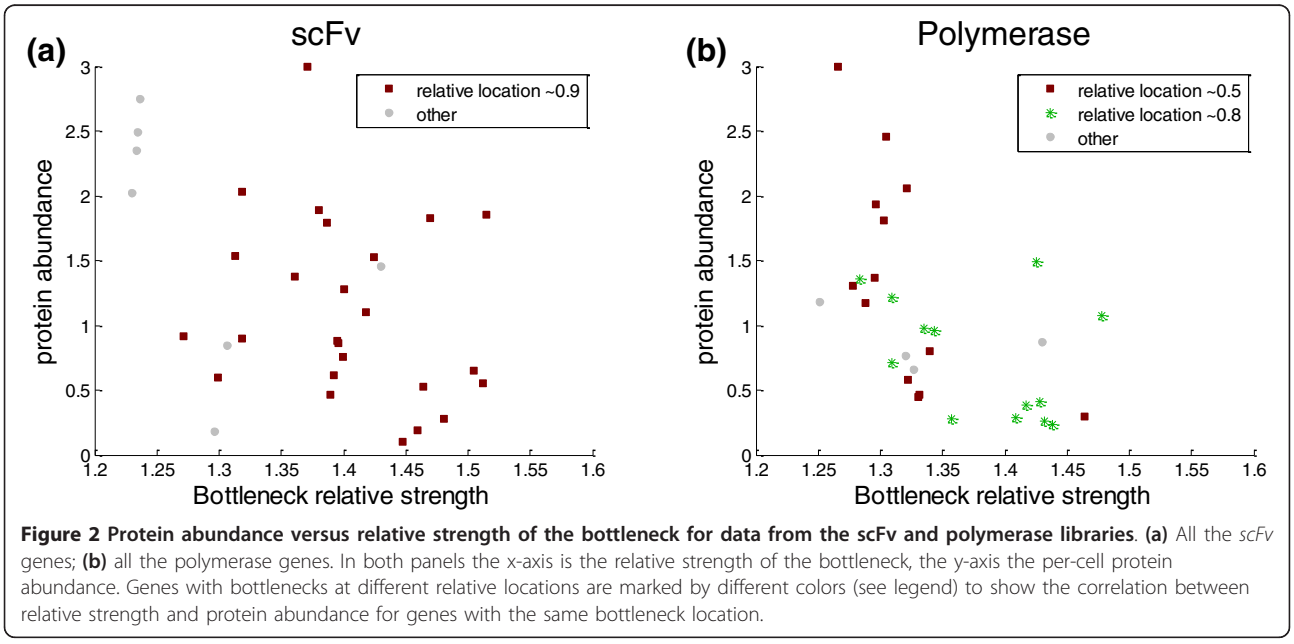

Figure 2 Protein abundance versus relative strength of the bottleneck for data from the scFv and polymerase libraries. **(a)** All the *scFv* genes; **(b)** all the polymerase genes. In both panels the x-axis is the relative strength of the bottleneck, the y-axis the per-cell protein abundance. Genes with bottlenecks at different relative locations are marked by different colors (see legend) to show the correlation between relative strength and protein abundance for genes with the same bottleneck location.

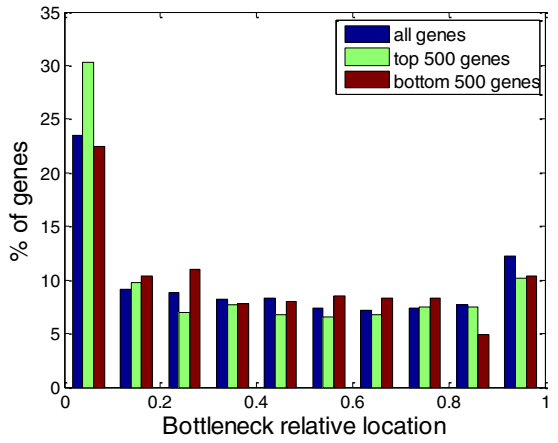

Figure 3 Distribution of bottleneck relative locations for *E. coli* genes. The distribution is shown for three groups of *E. coli* genes: all genes (blue); highly expressed genes (green); and lowly expressed genes (red). For all groups only genes longer than 100 codons are shown (this cutoff retains 90% of the *E. coli* genes). This resulted in 442 highly expressed genes (out of the top 500) and 473 lowly expressed genes (out of the bottom 500).

6.2×10^{-9}) and only 22% of these genes have the bottleneck located in the fourth quadrant, which is a significant depletion (hyper-geometric *P*-value 1×10^{-4}). Examining highly expressed genes separately (see Materials and methods; Figure S2b in Additional file 2), we also observe a depletion of a strong bottleneck in the fourth quadrant (18% of the genes, hyper-geometric *P*-value 0.02) and enrichment in the first quadrant (49%, *P*-value 0.005). In contrast, a separate examination of lowly expressed genes (Figure S2c Additional file 2) reveals no significant depletion or enrichment (depletion in the fourth quadrant 18% (*P*-value 0.39); enrichment in the first quadrant 41% (*P*-value 0.15)).

Kudla *et al.* [13] showed that the folding energy of the mRNA near the initiation site influences translation rate. It was suggested that a weak secondary structure enables the ribosome to bind more quickly to the mRNA, thus enabling a faster translation rate. These observations raised the possibility that the correlation we observe between bottleneck location and protein abundance in the GFP library is due to the confounding effects of mRNA secondary structure stability. We thus carried out correlation analysis to verify that the correlations we found still hold even when examining gene sets with similar mRNA folding energy. We calculated the partial correlation between bottleneck parameters and per-cell protein abundance while controlling for the folding energy. Both the relative location correlation (Pearson correlation -0.24, *P*-value 0.004; Spearman correlation -0.27, *P*-value 9.5×10^{-4}) and the relative strength at locations 0.16 to 0.28 (Figure 1) correlation (Pearson correlation 0.3, *P*-value 0.006; Spearman correlation, 0.24, *P*-value 0.024) remained significant even after controlling for the folding energy, indicating that bottleneck parameter correlations are significant on their own. Therefore, although in the GFP library the folding energy significantly affects the protein abundance, bottleneck location and strength also contribute to the changes in protein levels.

The cost of production

For efficient translation we are interested not only in the levels of expressed protein from a gene but also in the cost of expression. Considering the cost of production, we looked at how introducing a new gene into the host cell influenced cell fitness. The influence on fitness is, in general, a combination of the benefit the protein provides with the burden its production puts on the system. However, assuming that the genes from the heterologous libraries discussed here do not contribute to the fitness of the host cell, the fitness decline due to expression reflects only the pure cost of production.

Kudla *et al.* [13] showed that the measured optical density (OD), assumed to be proportional to the fitness of the host cell, is highly correlated with the CAI. Further analysis showed that the tAI is also correlated with OD (Pearson correlation 0.51, *P*-value 2.4×10^{-11}). These two similar measures describe the entire transcript and not a particular region within it. In contrast, we found that the bottleneck parameters that significantly correlate with protein abundance are not correlated with cell fitness. Thus, the factors that correlate with fitness and those correlating with protein abundance appear distinct in this library (Figure 4). It seems that while specific regions of the transcript affect protein abundance, the fitness is affected by the codon usage of the entire transcript.

Trying to understand the source for the correlation between the fitness and tAI or CAI, we examined the effect of individual codons on cell fitness. We analyzed the correlation between the usage frequency of each specific codon in the GFP sequence (number of copies of the codon in the sequence) and the fitness of the cell that was expressing that GFP variant (Figure 5). Interestingly, the extent of usage of some codons is negatively correlated with fitness, is positively correlated for others, and for the rest is not correlated with fitness. The cases of negative correlation may indicate a burden on fitness due to using particular codons. In contrast, since fitness can only decrease due to GFP expression, cases of positive correlation between codon usage in a gene and its host fitness likely reflect an artificial negative correlation of synonym codons; that is, the preference for not using its alternative codons rather than a preference for expressing the codon itself.

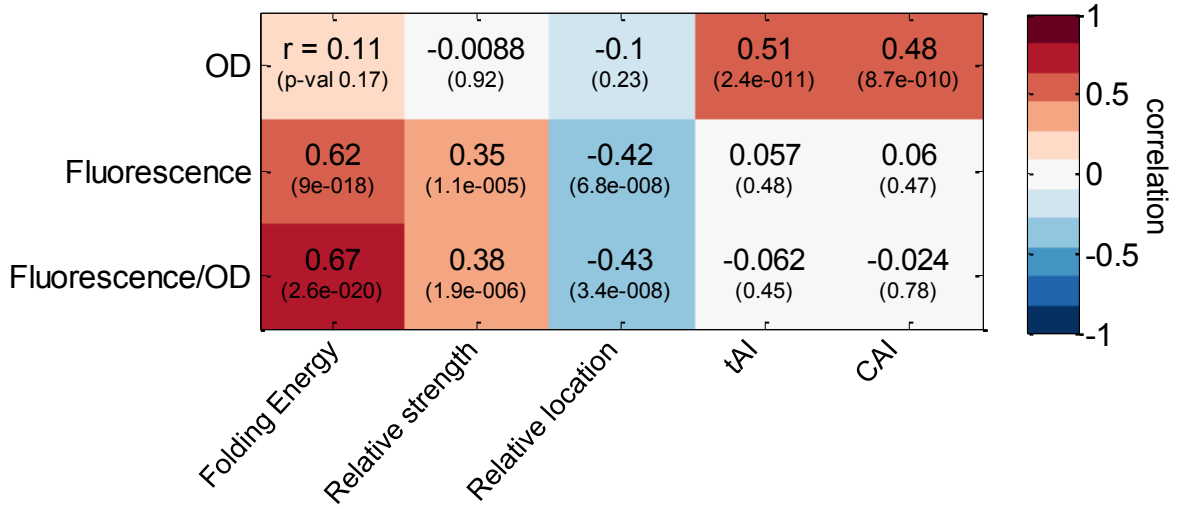

Figure 4 Correlation between the GFP experimental measurement and transcript calculated parameters. On the x-axis are different parameters that can be calculated from the transcript: folding energy of the initiation site calculated in Kudla *et al.* [13], bottleneck parameters, CAI and tAI. On the y-axis are the optical density (OD) measurement, protein abundance and per-cell protein abundance. The correlation value is indicated by both the color of the box and the number. The correlation *P*-value is given in parentheses.

Thus, focusing on the codons that correlate negatively with fitness, we detected three codons whose usage correlates most significantly: CAU (Pearson correlation -0.69, *P*-value < 10^{-324}); AAU (Pearson correlation -0.68, *P*-value < 10^{-324}); and UCA (Pearson correlation -0.67, *P*-value < 10^{-324}) (Figure 5; Table S2 in Additional file 1). Further examination reveals inter-dependencies between the usage of some of these codons; in particular, the frequencies of CAU and AAU are highly correlated (r = 0.92, *P*-value 10^{-64}) among themselves (the reasons for internal correlation may have to do with GFP construction methods; see Kudla *et al.* [13]). Using partial correlation analysis between the usage of each codon, we identified UCA and CAU as the main codons contributing to the decrease in the fitness (see Materials and methods).

The number of occurrences of the UCA codon, encoding serine, in a single gene varies between zero to three appearances. This codon is the rarest out of the six serine codons in the *E. coli* genome [Refseq: NC_012947], though it is not extremely rare (12.2% of all serine codons, and 0.7% of all 61 codons in the ORFs of the genome; Table S2 in Additional file 1). However, in the transcriptome (that is, the genome, weighted by the mRNA expression level from each gene; see Materials and methods) UCA is one of the rarest codons (8.7% of all serine codons and 0.45% of all 61 codons). The UCA codon is exclusively translated by the $tRNA_{UGA}$ [17]. The genome of *E. coli* has only one copy of this tRNA gene and, reassuringly, it was shown that a shortage of this tRNA decreases cell fitness [18]. The negative correlation between the copy number of the UCA codon and the fitness can thus imply that increased usage of the UCA codon causes a shortage of the corresponding tRNA, causing a decrease in fitness. Regarding codons CAU and AAU, they are negatively correlated with fitness (and with one another) yet we found no apparent reason for this.

Shortage of tRNAs explains some of the correlations between the usage of certain codons and fitness; however, it is not clear through which mechanism a shortage of tRNAs affects the fitness. The extensive usage of codons that correspond to rare tRNAs can affect the fitness in at least one of two alternative ways: by 'consuming' the tRNAs and sequestering them from participating in the translation of other transcripts; or through the unavailability of ribosomes that are delayed for longer times while searching for rare tRNAs. A simple means to distinguish between these two alternative options is to examine whether not only the number but also the location of such rare codons affects fitness. In particular, we expect that if the fitness-reducing effect of the rare codons is the jamming of ribosomes, then their utilization will be particularly harmful when located distally, closer to the 3' end of the transcript. In contrast, if the fitness-reducing effect is predominantly due to the consumption of rare tRNAs, then it is not expected to show such location dependence. In reality, we observed no correlation with the location (Figure S3 in Additional file 2), suggesting that it is the consumption of the rare tRNAs, in this case, that compromises fitness.

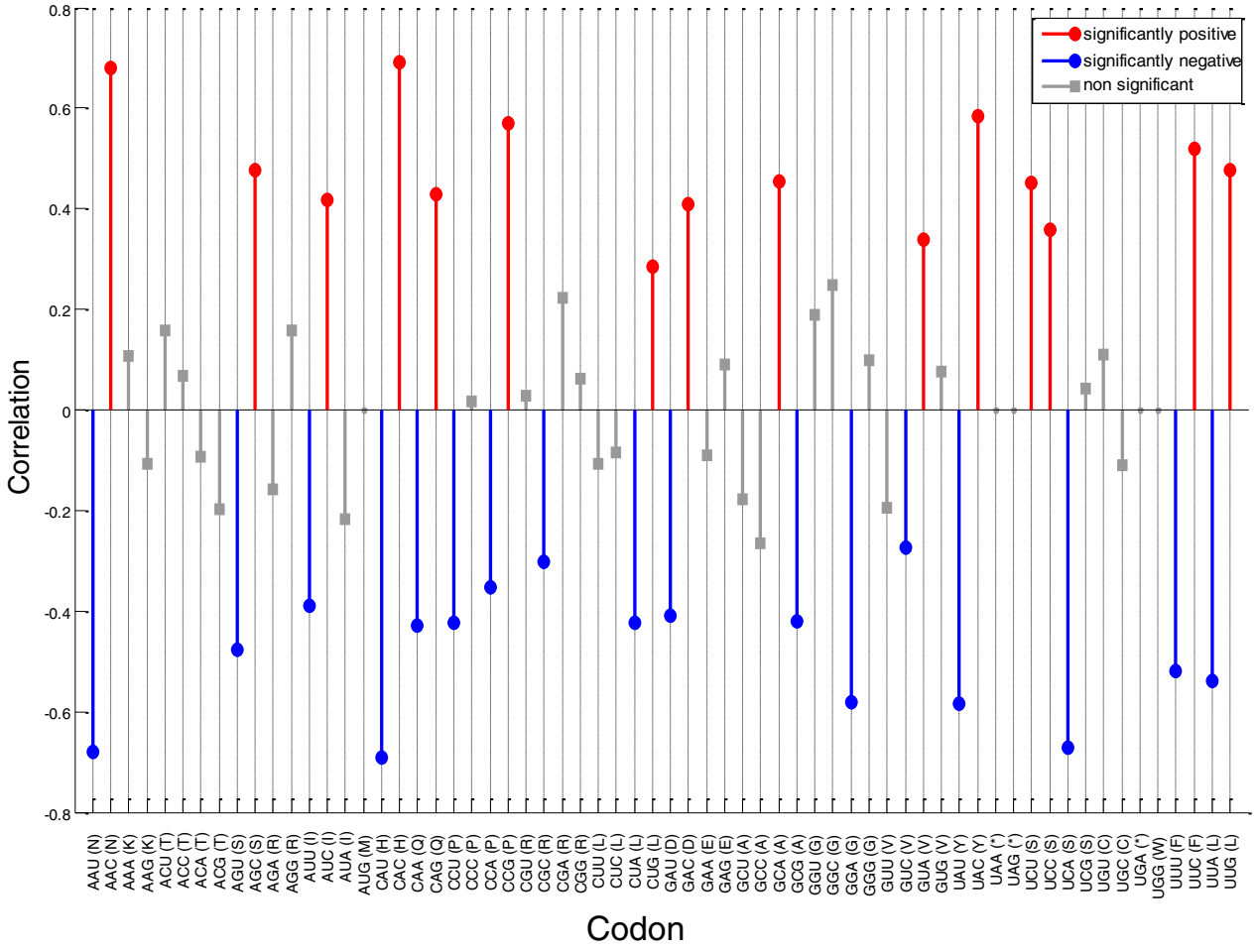

Figure 5 Correlation between codon usage in a transcript and fitness. The bar indicates the Pearson correlation value between codon frequency and OD. On the x-axis are listed all the codons in the format 'codon (amino acid)'. A correlation was determined to be significant if its *P*-value is below 0.05/61 (that is, alpha = 0.05 was corrected for the number of codons tested). Red bars represent codons for which there is a significantly positive correlation between their appearance and the OD. Blue bars represent codons that have a significant negative correlation. For codons with no significant correlation, grey squared bars are used. When no bar appears for a codon (for example AUG, UAA and so on) it means that the usage of that specific codon was constant for all genes, thus resulting in no correlation value. For usage of each amino acid in the GFP variant, see Table S3 in Additional file 1.

Conclusions

As shown, a proximal and strong bottleneck is correlated with an increase in protein abundance. A proximal bottleneck can reduce the number of jammed ribosomes on a transcript. Therefore, it can reduce both the number of occupied ribosomes and the number of delayed ribosomes. Delaying ribosomes on the mRNA might increase their abortion rate, thus causing early termination of the translation [19], reducing protein levels. For ribosomes to jam, a fast initiation rate is required. This is usually the case in highly expressed genes, in cases of heterologous gene expression, and in synthetic libraries such as discussed here where high protein levels are desired. Due to amino acid sequence constraints for some genes, a naïve approach, using only optimal codons, might result in an unintentional distal bottleneck.

While the bottleneck parameters are correlated with protein abundance, they are not correlated with fitness. This suggests that while the occupation of more ribosomes sequesters them from the cell's pool, for most genes in the GFP library it does not cause a shortage of ribosomes, enabling the cell to continue translating other transcripts. The decrease in fitness is correlated with the increased usage of codons UCA and CAU, suggesting a shortage of the complementary tRNAs.

Our results thus show that, along with mRNA stability, codon choice does affect translation efficiency, and that naïve averaged measures such as CAI and tAI do not capture this regulatory capacity. The results also

show that while codon choices do affect both translation efficiency and cell fitness, different aspects of codon selection affect differently the production capacity and costs. One direct conclusion from our results relates to the popular usage of 'His-tags', chains of histidine residues at carboxyl termini of genes in heterologous expression systems [20]. When using carboxy-terminal His-tags in bacterial expression systems it would be advantageous to encode histidine with CAC rather than with CAU for two reasons: first, because CAU appears to correlate negatively with fitness; and second, in order to avoid a bottleneck towards the end of the gene.

When trying to understand the cell system, one realizes its processes are regulated on many different levels. As shown in this paper, synthetic gene libraries enabled us to control for a significant portion of gene variability and focus on the effects of regions with less than optimal codons (the bottleneck). Identification of bottleneck effects in synthetic genes thus completes Tuller *et al.*'s [5] bioinformatics work that identified clustering of low efficient codons at the beginning of ORFs of natural genes. The results further demonstrate how correlative conclusions made from observations of natural gene sequences can be complemented by synthetic genes, allowing decoding of the sequence features governing the efficiency of translation and it costs.

It is our belief that through carefully designed synthetic libraries many other regulation processes can be understood, thus completing the first step towards understanding the regulation process as a whole.

Materials and methods

Defining the bottleneck

The bottleneck is a region on a gene where the harmonic mean of its codons' tAI values is minimal. For all codons except CGA, the tAI values were calculated using dos Reis *et al.*'s s-values [2]; for codon CGA the value 0.1333 was used. This codon is translated with $tRNA_{ACG}$; however, the s-value for this interaction is very high, resulting in a very low tAI value. This tAI value is smaller by at least an order of magnitude than the smallest tAI value, causing all other codons to have a relatively high tAI, disabling this analysis. Since CGA is actually translated by $tRNA_{ACG}$, we decided to change the s-value of this interaction to a more reasonable value, resulting in the above mentioned tAI value. Given the tRNA repertoire of *E. coli*, this change affects only the tAI value of codon CGA.

A codon tAI value is assumed to be proportional to the speed of the codon's translation [5]; higher tAI values correspond to high tRNA abundance and affinity, thus faster translation. A harmonic mean of speeds is simply an arithmetic mean of the corresponding times. Hence, looking for the region with the minimum harmonic mean of speed is equivalent to looking for the region that takes the longest time to translate.

For each region the harmonic mean of speed is:

$$\frac{n}{\sum_{c \in \mathrm{Re}\,gion} \frac{1}{tAI_c}}$$

where n is the region size, and c is the set of all the codons in the region (n codons).

To find the bottleneck, a sliding window of length n over the gene was used. The harmonic mean was calculated for each window and the window with the minimum value was identified. It should be noted that since we are averaging the translation time in a window, an incorrect window size might in some cases result in incorrect identification of the bottleneck. For example, if our estimated window size is too big, it might mask a cluster of a few slowly translated codons, of a more relevant size, that are surrounded by relatively rapidly translated codons. In most cases, however, the slow region is significant enough and its identification is not too sensitive to window size. Indeed, as mentioned in the Result and discussion section, our results did not change qualitatively for window sizes in the range $14 < n < 30$.

The bottleneck window size (n)

Under a maximal density scenario (fast initiation rate), the distance between two consecutive ribosomes will be minimal. In this case, when two ribosomes are translating the same mRNA simultaneously, the minimum possible distance between the two translated codons (one by each of the ribosomes) is one ribosome size (H codons) (Figure S4 in Additional file 2). At any given moment during the translation process, two adjacent ribosomes would have translated exactly the same codons apart from the last H codons - the first of the two ribosomes has already translated them, and the second is just about to start them. If the time it took the first ribosome to finish translating the nth codon, $T(n,1)$, is longer than the time it takes the second ribosome to translate the n-Hth codon, $T(n - H,2)$, the second ribosome will 'bump' into the first one. That is, if $T(n,1) > T(n - H,2)$, a traffic jam will be created. $T(n,1)$can be found by summing the time it takes the ribosome to assemble on the ATG (B) with the time it takes to translate the n codons:

$$T(n,\mathbf{1}) = B + \sum_{i=1}^{n} t(i)$$

where $t(i)$ is the time it takes to translate the ith codon. The second ribosome gains access to the ATG only when enough codons (minimum H) are cleared after being translated by the first ribosome. As a result a

traffic jam will be created if $Tw(k,H) > Tw(1,H)+B$, where $Tw(k,H)$ is the time to translate H consecutive codons starting from codon k:

$$Tw(k,H) = \sum_{i=k}^{k+H-1} t(i)$$

Therefore, the region of H codons with maximum translation time $\left(\underset{k=1:\text{mRNA length}-H}{\arg\max} \left(Tw(k,H) \right) \right)$ determines whether and where a traffic jam will be created (for a detailed calculation, see page 2 of Additional file 1). Choosing n in our bottleneck equation to be equal to H, it is easy to see that our bottleneck is related to this maximum.

As can be seen from this analysis, the minimal distance between two ribosomes should determine our window size. The footprint of the ribosome, which is the actual protection of the ribosome from RNA degradation, was determined quite accurately to be ten codons [21]. Due to the structure of the ribosomes, we assume that there should be some space between two consecutive 30S subunits. As a result, although only ten codons are protected, the minimal distance between the two ribosomes should be larger. Therefore, we chose to adopt the average ribosome-to-ribosome distance measured by Brandt *et al.* [22]. They measured the mean distance between the center of mass of two ribosomes on actual bacterial polysomes to be 21.6 nm [22], which is about 21 codons (0.34 nm per base). In this paper, n was set to be equal to H; that is n is set to 21 codons.

The bottleneck parameters

A bottleneck is characterized by two parameters: its 'location' and its 'strength'.

The 'location' of the bottleneck is defined as the location in the gene of the bottleneck's first codon (k codons from the ATG). The relative location of the bottleneck is defined as the location of the bottleneck divided by the number of possible windows; for example, $\frac{k}{l-n+1}$, where k is the location of the bottleneck, l is the length of the gene, and n is the window size.

The 'strength' of the bottleneck is defined as the arithmetic average of 1/tAI values for the codons in the region, for example, $\frac{1}{n}\sum_{c\in \text{Region}} \frac{1}{tAI_c}$ (the inverse of the harmonic mean). The relative strength of the bottleneck is defined as the strength of the bottleneck divided by the average 1/tAI for the entire gene, for example, $\frac{\frac{1}{n}\sum_{c\in bottleneck} \frac{1}{tAI_c}}{\frac{1}{l}\sum_{c=1}^{l} \frac{1}{tAI_c}}$; where l is the number of codons in the gene (excluding the stop codon).

Per-cell protein abundance

To get an estimate for protein expression per cell from the GFP library data [13], we normalized the measured protein abundance (measured by OD), which serves here as a proxy for the population size, the OD. The protein abundance levels for the data from Welch *et al.* [14] were measured while keeping the OD constant. Therefore, we can use this protein abundance as an already normalized protein level per cell.

Highly and lowly expressed genes of *E. coli*

The *E. coli* mRNA levels were taken from Lu *et al.* [23]. The highly expressed genes are the top 500 genes, and the lowly expressed genes are the bottom 500 genes (genes with no mRNA recorded were ignored). However, for both groups only genes that are longer than 100 codons were used.

Finding the main anti-correlated codons

We used partial correlation to find the codons that contribute the most to the decrease in cell fitness. The highest contributors were filtered according to the following steps. First, find codons that have a negative correlation to the OD (29 codons). We were looking for codons that caused a decrease in the fitness; hence, only anti-correlated codons. Second, for all codons left, we calculated the partial correlation matrix M(i,j) = Partial correlation (codon i, OD | codon j). Third, find the minimum absolute value of the partial correlation for each codon and rank the codons in a descending order accordingly. This gives us the codons with a correlation that cannot be explained by correlation to other codons (see Table S4 in Additional file 1 for a list of all codons with P-value < 0.1).

The codon at the top of the list is UCA, which is anti-correlated to the OD and its correlation cannot be explained by other codons. The second contributing codon is CAU, which has the highest partial correlation (-0.36, P-value 8.5×10^{-6}) when controlling for the UCA codon. This codon is also the second codon in the ranked list. All other codons have a partial correlation < 0.2 with a P-value ≥ 0.04 when controlling with one of the two codons (either UCA or CAU).

Calculating codon usage in the genome

The genome for *E. coli* strain B21 (which was used by Kudla *et al.* [13]) was downloaded from the NCBI ([Refseq:NC_012947], 11 January 2010)]. For each codon we counted its appearance in all the ORFs and normalized by the total number of codons.

Calculating codon usage in the transcriptome

mRNA levels were taken from Lu *et al.* [23]. If a gene did not have a measurement, it was assumed to have a

zero mRNA level. The measurements were done with *E. coli* strain K12 MG1655; thus, the sequence used for the calculation was different from that used for genome codon usage. The sequence was downloaded from NCBI ([Refseq: NC_000913], 1 April 2010). The contribution of each gene was calculated by multiplying the mRNA level measurements for the gene by the codon usage of the same gene. The contributions of all genes were summed for each codon and then divided by the total sum of all codons.

Additional material

Additional file 1: Supplementary methods. This file includes a discussion regarding codon translation speed, additional tables not included in the main text, and figure legends for the supplementary figures in Additional file 2.

Additional file 2: Supplementary figures. Additional figures not included in the main text.

Abbreviations

CAI: codon adaptation index; GFP: green fluorescence protein; OD: optical density; ORF: open reading frame; tAI: tRNA adaptation index.

Acknowledgements

We thank the 'Ideas' program of the European Research Council (ERC), and the Ben May Charitable Trust for grant support.

Authors' contributions

SN carried out all analyses. SN and YP conceived the work, analyzed the data and wrote the paper.

Received: 23 August 2010 Revised: 18 November 2010
Accepted: 1 February 2011 Published: 1 February 2011

References

1. Sharp PM, Li WH: **The codon Adaptation Index - a measure of directional synonymous codon usage bias, and its potential applications.** *Nucleic Acids Res* 1987, **15**:1281-1295.
2. dos Reis M, Savva R, Wernisch L: **Solving the riddle of codon usage preferences: a test for translational selection.** *Nucleic Acids Res* 2004, **32**:5036-5044.
3. Man O, Pilpel Y: **Differential translation efficiency of orthologous genes is involved in phenotypic divergence of yeast species.** *Nat Genet* 2007, **39**:415-421.
4. Sharp PM, Li WH: **An evolutionary perspective on synonymous codon usage in unicellular organisms.** *J Mol Evol* 1986, **24**:28-38.
5. Tuller T, Carmi A, Vestsigian K, Navon S, Dorfan Y, Zaborske J, Pan T, Dahan O, Furman I, Pilpel Y: **An evolutionarily conserved mechanism for controlling the efficiency of protein translation.** *Cell* 2010, **141**:344-354.
6. Clarke TFt, Clark PL: **Increased incidence of rare codon clusters at 5' and 3' gene termini:implications for function.** *BMC Genomics* 2010, **11**:118.
7. Bulmer M: **Codon usage and intragenic position.** *J Theor Biol* 1988, **133**:67-71.
8. Mitarai N, Sneppen K, Pedersen S: **Ribosome collisions and translation efficiency: optimization by codon usage and mRNA destabilization.** *J Mol Biol* 2008, **382**:236-245.
9. Romano MC, Thiel M, Stansfield I, Grebogi C: **Queueing phase transition: theory of translation.** *Phys Rev Lett* 2009, **102**:198104-198300.
10. Greulich : **Phase diagram and edge effects in the ASEP with bottlenecks.** *Physica A Stat Theor Phys* 2008, **387**:1972.
11. Dong : **Towards a model for protein production rates.** *J Stat Phys* 2007, **128**:21.
12. Shaw : **Local inhomogeneity in asymmetric simple exclusion processes with extended objects.** *J Phys A Mathematical General* 2004, **37**:2105.
13. Kudla G, Murray AW, Tollervey D, Plotkin JB: **Coding-sequence determinants of gene expression in *Escherichia coli*.** *Science* 2009, **324**:255-258.
14. Welch M, Govindarajan S, Ness JE, Villalobos A, Gurney A, Minshull J, Gustafsson C: **Design parameters to control synthetic gene expression in *Escherichia coli*.** *PLoS One* 2009, **4**:e7002.
15. Higgs PG, Ran W: **Coevolution of codon usage and tRNA genes leads to alternative stable states of biased codon usage.** *Mol Biol Evol* 2008, **25**:2279-2291.
16. Ran W, Higgs PG: **The influence of anticodon-codon interactions and modified bases on codon usage bias in bacteria.** *Mol Biol Evol* 2010, **27**:2129-2140.
17. Ishikura H, Yamada Y, Nishimura S: **Structure of serine tRNA from *Escherichia coli*. I. Purification of serine tRNA's with different codon responses.** *Biochim Biophys Acta* 1971, **228**:471-481.
18. Yamada Y, Matsugi J, Ishikura H: **tRNA1Ser(G34) with the anticodon GGA can recognize not only UCC and UCU codons but also UCA and UCG codons.** *Biochim Biophys Acta* 2003, **1626**:75-82.
19. Li X, Hirano R, Tagami H, Aiba H: **Protein tagging at rare codons is caused by tmRNA action at the 3' end of nonstop mRNA generated in response to ribosome stalling.** *Rna* 2006, **12**:248-255.
20. Hengen P: **Purification of His-Tag fusion proteins from *Escherichia coli*.** *Trends Biochem Sci* 1995, **20**:285-286.
21. Ingolia NT, Ghaemmaghami S, Newman JR, Weissman JS: **Genome-wide analysis in vivo of translation with nucleotide resolution using ribosome profiling.** *Science* 2009, **324**:218-223.
22. Brandt F, Etchells SA, Ortiz JO, Elcock AH, Hartl FU, Baumeister W: **The native 3D organization of bacterial polysomes.** *Cell* 2009, **136**:261-271.
23. Lu P, Vogel C, Wang R, Yao X, Marcotte EM: **Absolute protein expression profiling estimates the relative contributions of transcriptional and translational regulation.** *Nat Biotechnol* 2007, **25**:117-124.

doi:10.1186/gb-2011-12-2-r12
Cite this article as: Navon and Pilpel: The role of codon selection in regulation of translation efficiency deduced from synthetic libraries. *Genome Biology* 2011 **12**:R12.

Supplement Text

Codons translation speed

In this paper we used the tRNA adaptation index (tAI) developed by dos Reis [2] as an approximation for the codon translation speed. The tAI index was developed mainly based on optimizing the translation efficiency of highly express genes. Two recent papers [15, 16] used evolutionary selection for translation efficiency as a means to learn the efficiency and coefficients of codon-anticodon interactions. They found that some non-standard combinations seem to be selected for and hence deduced to be translated at high rates. One of the major difference between their conclusion to the tAI is the value of the U:U interaction (codon with wobble-U translated by a tRNA with a wobble- U) for amino acid in a 4-box. In the tAI calculations this interaction was assumed to be forbidden (sU:U=1) while based on selection it was suggested that this interaction is quite potent, which should result in a low sU:U in the tAI model.

To investigate the U:U interaction effects we manually added the sU:U interaction to the tAI calculations at 4-box cases and scanned the effects over the full possible range of values of sU:U, form 0 to 1. First we looked how adding sU:U changed the bottleneck parameters. Figure S5 shows the correlation between our original bottleneck parameters and the newly calculated one. As expected the correlation decreases as sU:U decreases. The correlation decreases from 1 for sU:U=1 (which is as in the original dos Reis tAI values) to 0.61 for sU:U=0, for the bottleneck relative location and 0.51 for the bottleneck relative strength.

Next we looked how the modified tAI predicts expression levels of the *E. coli* mRNA levels [26] for 3 different groups: all genes, highly expressed (top 250) and lowly

express (bottom 250). As can be seen in Figure S6 for all genes and the highly expressed ones the correlations increase with an introduction of the U:U interaction (sU:U<1). However it seems that the main contribution to the increase occurs merely by introducing the interaction, i.e. reducing sU:U from 1 to 0.7 results in half of the increase in the correlation. For this graph we find it hard to deduce what should be the optimal sU:U value, but the result indeed suggests a desired correction for the tAI. Finally we look at the two main correlations we find in the GFP library: the correlation with between the bottleneck relative location to the protein abundance and the correlation between the bottleneck relative strength for genes with the same relative location (between 0.16-0.28) and protein abundance. For both correlations we see (figure S7) that the introduction of sU:U actually reduces the correlations.

The bottleneck window size (*n*) - detailed calculation

The bottleneck is the region that will have the most slowing down effect on the ribosome. This region will only have a bottleneck effect if it slows the ribosomes enough to affect consecutive ribosome. As explained in the following the size of this region has to be about the minimum ribosome-to-ribosome distance (denoted below as *H*).

We make first the following definitions:

1. Traffic jam will be caused if the time it takes the first ribosome to finish translation of the nth codon is longer than the time it takes the second ribosome to finish translation of codon n-H. In this case the second ribosome will not be able to proceed to the (n-H+1)-th codon since it will collide with the first ribosome and hence will be delayed.

2. A ribosome can start assembling on the ATG when the first H codons (the minimum distance required between 2 ribosomes) are cleared from the preceding ribosome. Let B be the time it takes the ribosome to bind and assemble on the ATG.
3. If *t(i)* is the time it takes to translate codon *i*, and *T(n,j)* is the time it takes the jth ribosome to finish translation of the n^{th} codon, where *n* is the codon at the leading edge of the ribosome.

   then:

   a. The time it takes the first ribosome to reach the n^{th} codon:

   $$T(n,1) = B + \sum_{i=1}^{n} t(i)$$

   b. The time it takes the second ribosome to reach the (n-H)-th codon:

   $$T(n-H,2) = (\text{time until the assembly site is cleared}) + B + \sum_{i=1}^{n-H} t(i)$$

   $$\xrightarrow{yields} T(n-H,2) = B + \sum_{i=1}^{H} t(i) + B + \sum_{i=1}^{n-H} t(i)$$

4. For a traffic jam to be created, the time for the first ribosome to finish translation of the n^{th} codon should be longer than the time it takes the second ribosome to finish translation of the *n-H* codon :

   $$T(n,1) > T(n-H,2)$$

   $$\xrightarrow{yields} B + \sum_{i=1}^{n} t(i) > B + \sum_{i=1}^{H} t(i) + B + \sum_{i=1}^{n-H} t(i)$$

   $$\xrightarrow{yields} \sum_{i=n-H+1}^{n} t(i) > B + \sum_{i=1}^{H} t(i)$$

5. We define $Tw(k,H)$ is the time to translate H consecutive codons starting from codon k $\left(Tw(k,H)=\sum_{i=k}^{k+H-1}t(i)\right)$. Therefore, a traffic jam will be created if:

$$Tw\,(k,H) > B + Tw\,(1,H)$$

$$Tw\,(k,H) - Tw\,(1,H) > B$$

6. For any traffic jam to be created along the gene:

$$\underset{k=1:\text{mRNA length}-H}{\arg\max}\ \left(Tw(k,H)\right) - Tw(1,H) > B$$

Inspecting the slowest region (of H codons) for the specific gene (bottleneck strength), if the time to translate that region minus the time it takes to translate the first H codons is longer than the time to finish "assembling" the ribosome (B) than traffic jam will be created.

As can be seen from the equation the region size which determine whether two consecutive ribosomes will collide has the size of the minimum distance between 2 ribosomes.

Supplement Figures

Figure S1: protein abundance vs. bottleneck relative location of data from Welch *et al*.'s libraries.

In the left figure (A) plotted all the *scFv* genes and in the right figure (B) plotted all the Polymerase genes. In both figures the x-axis is the gene's relative location, the Y-axis is the per-cell protein abundance and the color is the gene's relative strength.

Figure S2: The distribution (2D histogram) of the bottleneck of the E. coli genes.

X-axis is the relative location, Y-axis the relative strength and the color is the % of genes having a bottleneck matching the parameters. **A** all *E. coli* genes longer than 100 (well above region size and still maintain 90% of the *E. coli* genes) codons were plotted. **B** only the highest expressed genes were plotted. The 500 genes which have the highest transcript levels were chosen and from these the genes with 100 codons or longer were taken, making a total of 442 genes. **C** only the lowest expressed genes were plotted. The 500 genes which have the lowest transcript levels were chosen and from these the genes with 100 or longer were taken, making a total of 473 genes.

Figure S3: location of first copy of a codon vs. the fitness.

Each point represents a gene in the GFP library. **A**, plotted is the location of the first CAU codon for each GFP variant vs. the variants' OD. In figure B, the location of the first UCA codon in the GFP variants is plotted vs. the variants' OD.

Figure S4: distances between two consecutive ribosomes

The figure illustrates two consecutive ribosomes, on the same mRNA, with the second one (left) currently being assembled on the ATG. The size of a ribosome in the figure is H codons. H_L is the distance from the ribosome A-site to the left end of the

ribosome, H_R is the distance from the A-site to the right end of the ribosome. The illustration shows that the minimum distance between two ribosomes' A-sites is *H* which is also “one ribosome size”. It can also be seen that in order for the second ribosome to start assembling on the ATG the first ribosome should have cleared the assembly area, e.g. translate *H* codons.

Figure S5: Correlation between the bottleneck parameters for different sU:U values

The correlation between the bottleneck relative location (**A),** and bottleneck relative strength **(B),** calculated once with the original dos-Reis tAI values and with alternative values of sU:U.

Figure S6: The gene expression prediction quality of the modified tAI values

For each sU:U value we calculated the correlation between the gene’s tAI value to the expression level. In the figure the correlation is plotted for three different groups: all the *E. coli* genes (blue), only the highly express ones, top 250 (green) and the lowly express ones, bottom 250 (red).

Figure S7: correlation between bottleneck parameters and the protein abundance for different sU:U values.

A Correlation between the bottleneck relative location and the protein abundance for all the GFP variants, for different sU:U values. The blue line is the correlation between the relative location and the abundance while the green line is the p-value of each correlation. **B** Correlation between the bottleneck relative strength and the protein abundance for the 86 GFP variants for which the bottleneck is located in between 0.16 to 0.28 (as done in the main text) for different sU:U values. The blue

line is the correlation between the relative location and the abundance while the green line is the p-value of each correlation.

Supplement Tables

Table S1. The correlations between the bottleneck relative strength to the protein abundance for the *scFv* and Polymerase libraries.

The relative location regions were chosen to incorporate many genes with the same relative location; the regions were chosen based on the plots in figure S1.

Protein	Relative location	Number of genes	Correlation with the bottleneck relative strength Pearson; Spearman	p-value Pearson; Spearman
scFv	0.9-1	25	-0.23; -0.32	0.27; 0.11
scFv	0-1 (All)	42	-0.43; -0.41	0.01; 0.02
Polymerase	0.48-0.52	13	-0.60; -0.67	0.03; 0.015
Polymerase	0.76-0.82	13	-0.38; -0.43	0.2; 0.14
Polymerase	0-1 (All)	39	-0.55;-0.67	0.0018; 7.1e-5

Table S2 – Codon parameters

For each codon the tables contains it amino acid, number of copies of complementary tRNA in the genome, its tAI value, the Pearson correlation with the OD measurements, the codon usage in the genome and the in the transcriptome. Except for the transcriptome all values are based on E. coli strain B, the transcriptome was calculated for *E. coli* K12 (see methods). When NaN (Not a Number) is listed it means that a correlation cannot be calculated due to a constant value of codons for all GFP variants

Amino acid	Codon	# tRNA Copies	tAI	correlation	p-value	Codon usage in genome %	Codon usage in transcriptome %
N	AAU	0	0.39	-0.68	<E-324	1.73	1.21
N	AAC	4	0.67	0.68	<E-324	2.16	2.69
K	AAA	6	1.00	0.11	1.96E-01	3.37	4.25
K	AAG	0	0.32	-0.11	1.96E-01	1.02	1.29
T	ACU	0	0.20	0.16	5.71E-02	0.89	1.30

T	ACC	2	0.33	0.07	4.09E-01	2.33	2.60
T	ACA	1	0.17	-0.09	2.57E-01	0.68	0.48
T	ACG	1	0.22	-0.20	1.64E-02	1.45	1.02
S	AGU	0	0.10	-0.48	8.13E-10	0.86	0.54
S	AGC	1	0.17	0.48	8.13E-10	1.61	1.34
R	AGA	1	0.17	-0.16	5.48E-02	0.18	0.10
R	AGG	1	0.22	0.16	5.48E-02	0.11	0.05
I	AUU	0	0.30	-0.39	9.18E-07	3.05	2.57
I	AUC	3	0.50	0.42	1.21E-07	2.52	3.26
I	AUA	0	0.055	-0.22	8.02E-03	0.41	0.19
M	AUG	7 (3.5, 3.5)*	0.58	NaN	NaN	2.81	2.73
H	CAU	0	0.10	-0.69	<E-324	1.28	0.95
H	CAC	1	0.17	0.69	<E-324	0.98	1.13
Q	CAA	2	0.33	-0.43	5.75E-08	1.53	1.15
Q	CAG	2	0.44	0.43	5.75E-08	2.89	2.93
P	CCU	0	0.10	-0.42	8.35E-08	0.69	0.57
P	CCC	1	0.17	0.02	8.45E-01	0.55	0.29
P	CCA	1	0.17	-0.35	1.08E-05	0.83	0.73
P	CCG	1	0.22	0.57	4.65E-14	2.35	2.54
R	CGU	4	0.67	0.03	7.23E-01	2.11	2.88
R	CGC	0	0.48	-0.30	1.92E-04	2.22	2.09
R	CGA	0	0.13	0.22	6.21E-03	0.35	0.17
R	CGG	1	0.17	0.06	4.53E-01	0.53	0.25
L	CUU	0	0.10	-0.11	1.95E-01	1.10	0.79
L	CUC	1	0.17	-0.08	3.08E-01	1.11	0.82
L	CUA	1	0.17	-0.42	7.56E-08	0.39	0.20
L	CUG	4	0.72	0.29	4.45E-04	5.33	5.80
D	GAU	0	0.30	-0.41	2.48E-07	3.20	2.97
D	GAC	3	0.50	0.41	2.48E-07	1.91	2.54
E	GAA	4	0.67	-0.09	2.79E-01	3.97	4.80
E	GAG	0	0.21	0.09	2.79E-01	1.77	1.80
A	GCU	0	0.20	-0.18	3.00E-02	1.54	2.31
A	GCC	2	0.33	-0.27	1.13E-03	2.57	2.09
A	GCA	3	0.50	0.46	6.25E-09	2.02	2.23
A	GCG	0	0.16	-0.42	9.49E-08	3.41	3.17
G	GGU	0	0.39	0.19	2.16E-02	2.48	3.39
G	GGC	4	0.67	0.25	2.44E-03	2.99	3.30
G	GGA	1	0.17	-0.58	8.66E-15	0.78	0.47

G	GGG	1	0.22	0.10	2.39E-01	1.10	0.71
V	GUU	0	0.20	-0.20	1.72E-02	1.83	2.66
V	GUC	2	0.33	-0.27	7.94E-04	1.52	1.29
V	GUA	5	0.83	0.34	2.50E-05	1.10	1.39
V	GUG	0	0.27	0.08	3.52E-01	2.64	2.36
Y	UAU	0	0.30	-0.58	7.11E-15	1.60	1.24
Y	UAC	3	0.50	0.58	7.11E-15	1.21	1.46
*	UAA	0	0.00	NaN	NaN	0.21	0.27
*	UAG	0	0.00	NaN	NaN	0.02	0.01
S	UCU	0	0.20	0.45	8.07E-09	0.84	1.19
S	UCC	2	0.33	0.36	7.79E-06	0.86	1.05
S	UCA	1	0.17	-0.67	<E-324	0.70	0.45
S	UCG	1	0.22	0.04	6.08E-01	0.90	0.60
C	UGU	0	0.10	0.11	1.84E-01	0.51	0.38
C	UGC	1	0.17	-0.11	1.84E-01	0.65	0.52
*	UGA	0	0.00	NaN	NaN	0.09	0.06
W	UGG	1	0.17	NaN	NaN	1.53	1.11
F	UUU	0	0.20	-0.52	1.22E-11	2.22	1.54
F	UUC	2	0.33	0.52	1.22E-11	1.65	2.05
L	UUA	1	0.17	-0.54	1.70E-12	1.38	0.79
L	UUG	1	0.22	0.48	9.38E-10	1.36	0.91

* Met is partly initiation tRNA and partly tRNA decoding regular Met codons. We assumed that about half of the Met tRNAs are used for initiation.

Table S3 Amino-acid usage in the GFP sequence

For each amino acid the table lists the number of times it is used in the GFP protein.

Amino acid	Copy number in GFP	Amino acid	Copy number in GFP	Amino acid	Copy number in GFP	Amino acid	Copy number in GFP	Amino acid	Copy number in GFP
A	8	C	2	H	9	M	6	T	16
R	6	Q	8	I	12	F	12	W	1
N	13	E	16	L	21	P	10	Y	11
D	18	G	22	K	20	S	10	V	18

Table S4. List of all codons which even after partial correlation still had a significant (p-value<0.1) correlation.

The codons with p-value <0.1 are:

Codon	Minimum negative partial correlation (p-value)	Controlling codon in the partial correlation
UCA	-0.29 (0.0004)	CAU
CAU	-0.24 (0.003)	AAU
AGU	-0.17 (0.04)	UCA
AAU	-0.156 (0.06)	CAU
GGA	-0.156 (0.06)	CAU
GUC	-0.15 (0.07)	UCA

Figure S1

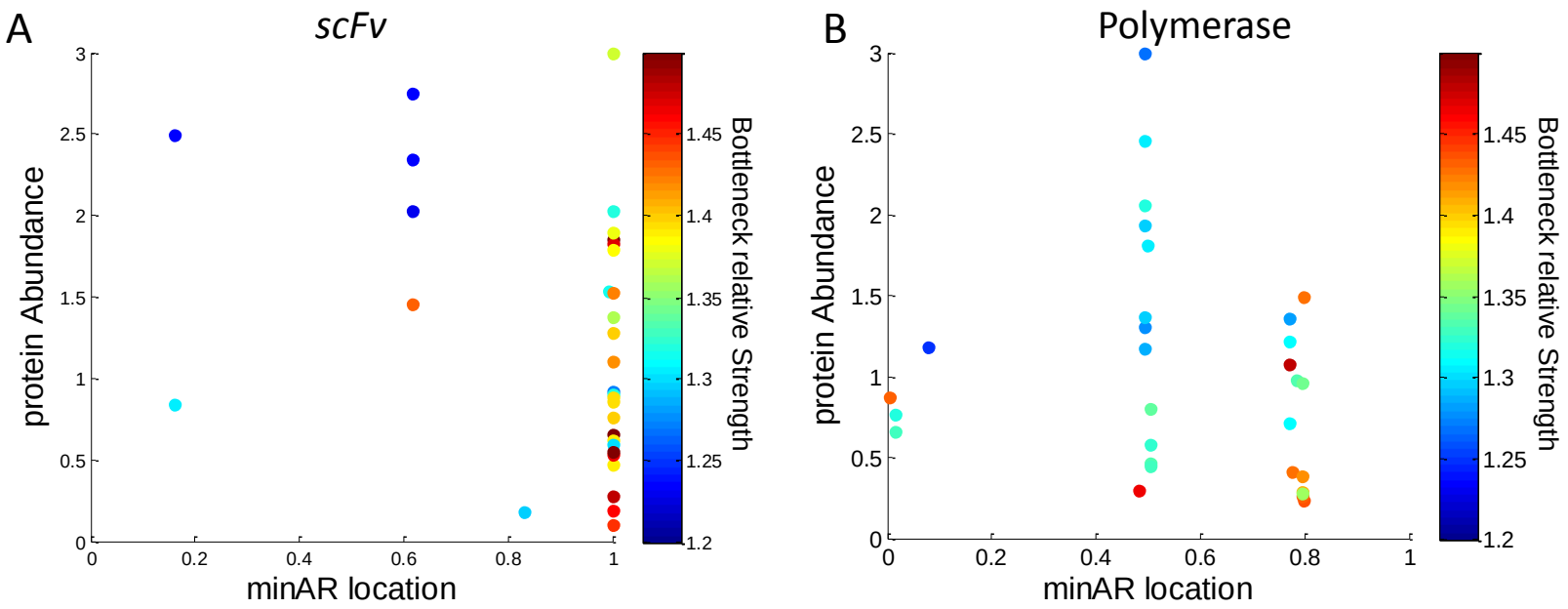
A
scFv
protein Abundance
minAR location
Bottleneck relative Strength
B
Polymerase
protein Abundance
minAR location
Bottleneck relative Strength

Figure S2

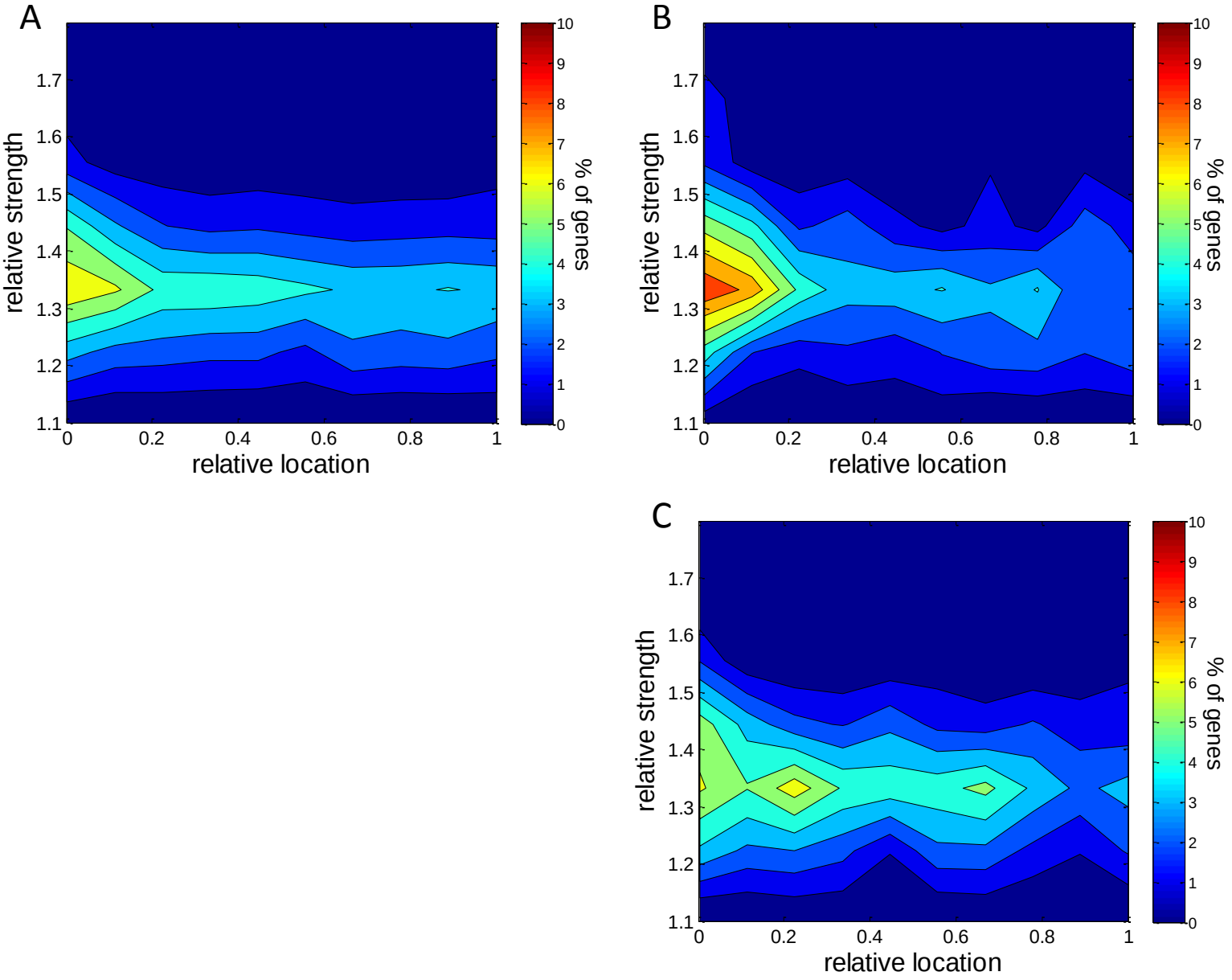
A
B
C
relative strength
relative location
% of genes
1.1
1.2
1.3
1.4
1.5
1.6
1.7
0
0.2
0.4
0.6
0.8
1
0
1
2
3
4
5
6
7
8
9
10

Figure S3

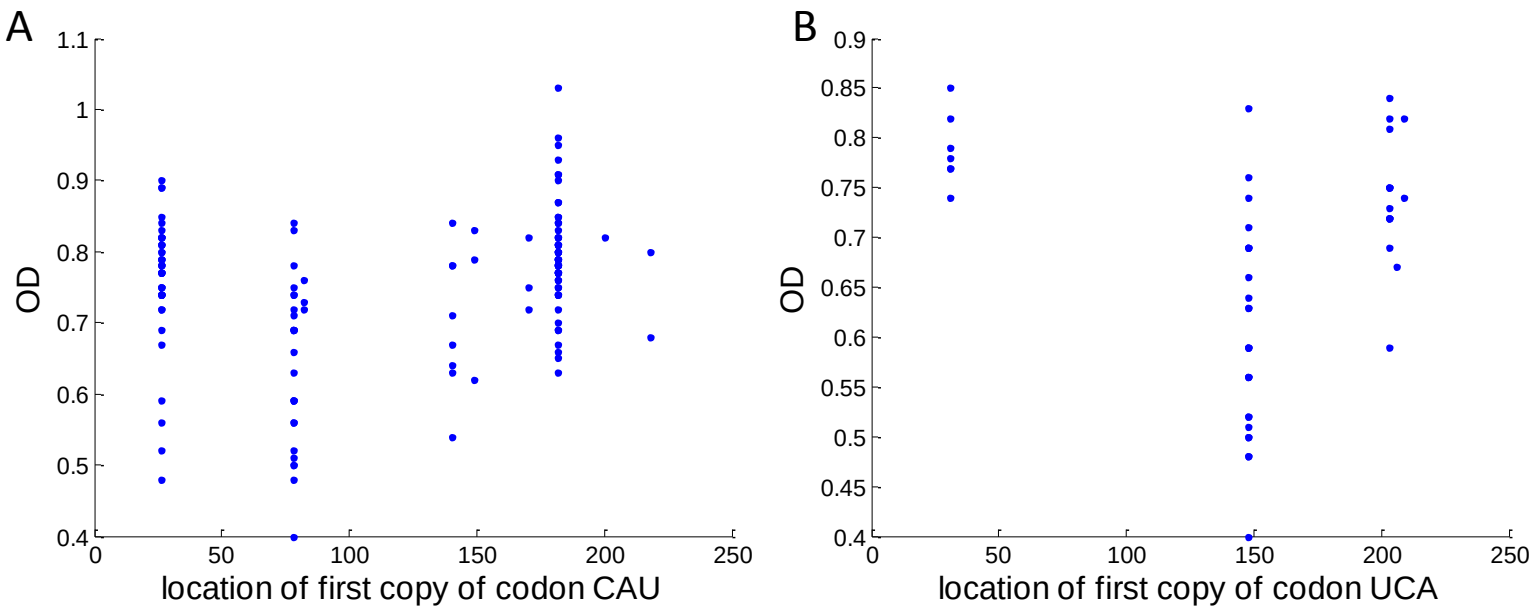
A
OD
location of first copy of codon CAU
B
OD
location of first copy of codon UCA

Figure S4

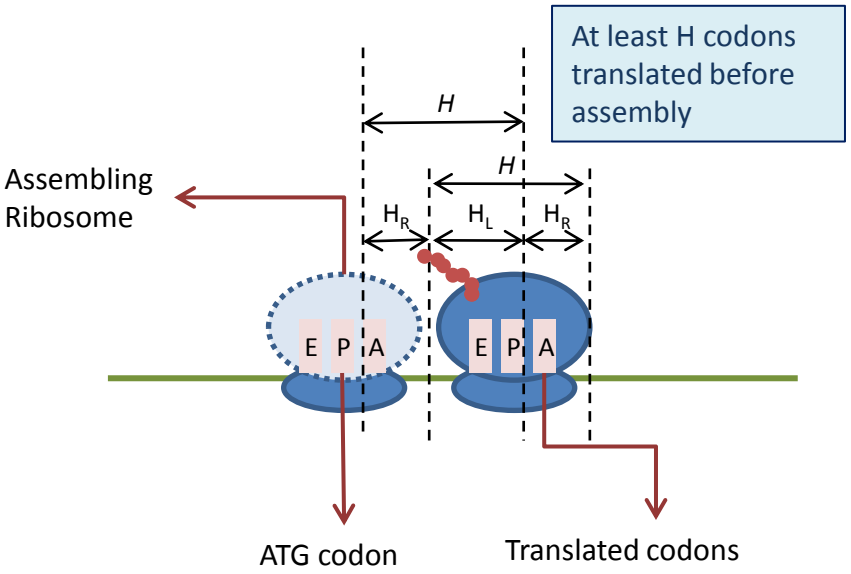
At least H codons translated before assembly
H
H
Assembling Ribosome
H_R
H_L
H_R
E P A
E P A
ATG codon
Translated codons

Figure S5

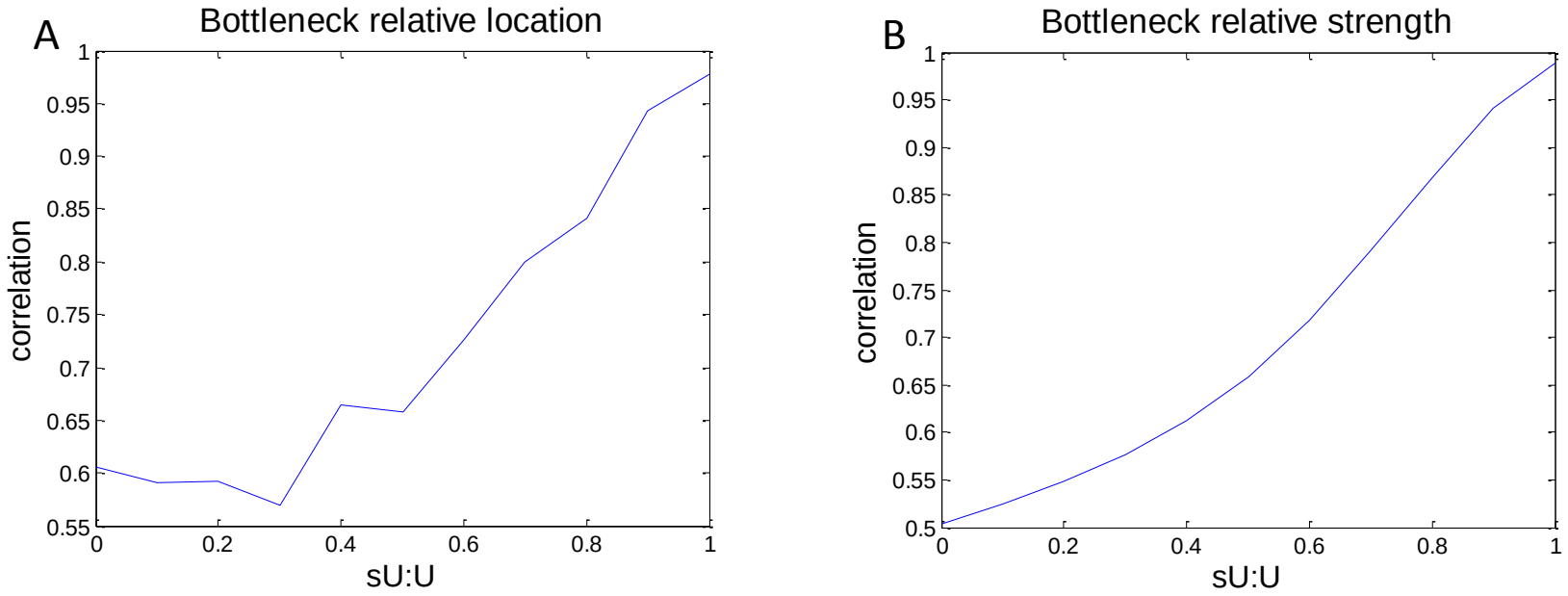
A
Bottleneck relative location
correlation
sU:U
1
0.95
0.9
0.85
0.8
0.75
0.7
0.65
0.6
0.55
0
0.2
0.4
0.6
0.8
1
B
Bottleneck relative strength
correlation
sU:U
1
0.95
0.9
0.85
0.8
0.75
0.7
0.65
0.6
0.55
0.5
0
0.2
0.4
0.6
0.8
1

Figure S6

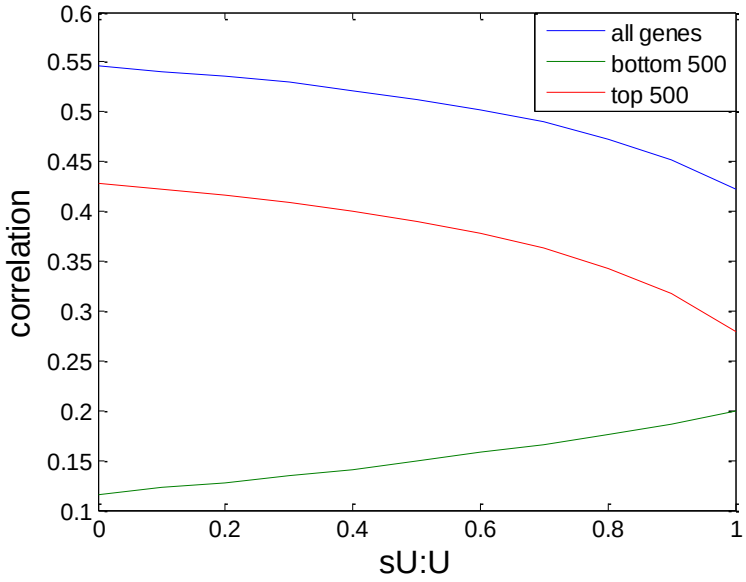
all genes
bottom 500
top 500
correlation
sU:U
0.6
0.55
0.5
0.45
0.4
0.35
0.3
0.25
0.2
0.15
0.1
0
0.2
0.4
0.6
0.8
1

Figure S7

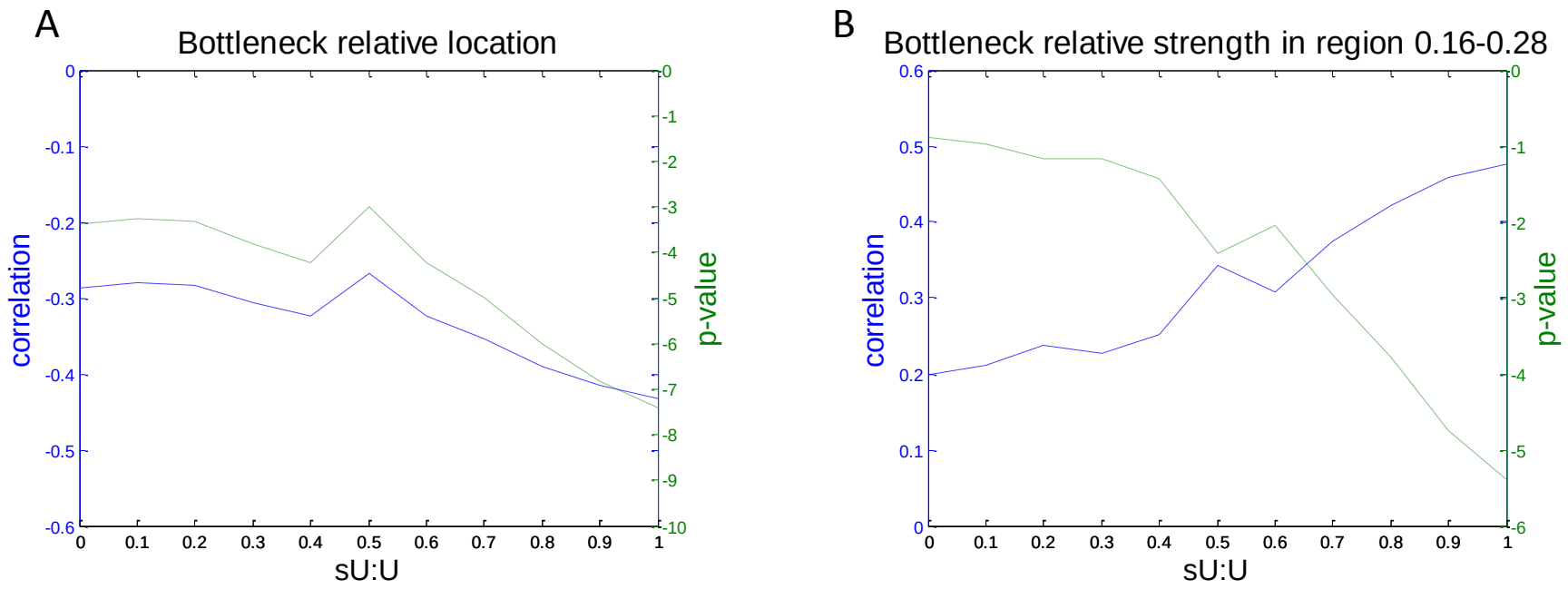
A
Bottleneck relative location
correlation
p-value
sU:U
0
-0.1
-0.2
-0.3
-0.4
-0.5
-0.6
-1
-2
-3
-4
-5
-6
-7
-8
-9
-10
0.1
0.2
0.3
0.4
0.5
0.6
0.7
0.8
0.9
1
B
Bottleneck relative strength in region 0.16-0.28
0.6
0.5
0.4
0.3
0.2
0.1

5.2 A Comprehensive tRNA deletion library unravels the genetic architecture of the tRNA pool

Researching the codon usage, we often refer to aspects such as the codons' translation speed or the ability of the cell to translate a codon. This ability is affected by the availability of the relevant tRNAs, namely the composition of the tRNA pool. In this project our aim was to study the tRNA pool of *S. cerevisiae* and gain a global understanding on the tRNA availability in cells. This project is a joint project between Dr. Zohar Bloom-Ackerman and me. I wrote all the analysis scripts and took part in designing the experiments and analyzing the data. The manuscript was accepted to PLOS Genetics.

To this aim, we created a comprehensive tRNA deletion library in *S. cerevisiae*, where in each strain a single genomic tRNA gene was deleted. Our tRNA deletion library includes 204 deletions, out of the 275 genomic tRNA genes identified in *S. cerevisiae*, covering all 20 amino acids and 40 out of the 42 anti-codon families. In addition the library consists of a selection of double, triple tRNA deletion mutants.

To assess the contribution of each tRNA gene to cellular growth, we set to accurately characterize the growth dynamics of each deletion strain. To this end we implemented a robotic method to screen and score growth phenotypes of all tRNA deletion strains in multiple conditions (for more details see Method0 4.2.1).

We screened the deletion library under a diverse set of growth conditions, including different metabolic challenges and stress-inducing reagents. In rich medium (YPD) only 13% of the library strains demonstrated a phenotype in growth rate and 27% showed a growth yield phenotype (Figure 2A-B). Most strains exhibited a phenotype only in one of the two parameters, which are extracted from distinct stages of the growth, resulting in no correlation between the two parameters (r=-0.02, p-value 0.8). Apart from the tRNAs who appear in only one copy in the cell (singletons) whose deletion strains are often dead or exhibit impaired growth, we could not explain the observed growth phenotypes, in either growth rate or yield, by either family size, or amino acid identity.

The percent of deletion strains exhibiting any growth phenotype varies between the different stresses (Figure 2C-D), indicating the demand for the different tRNA genes varies across conditions. In all stresses except proteotoxic stress most tRNA deletion strains do not exhibit any growth phenotype, indicating robustness to tRNA gene deletion. We showed that this robustness is enabled due to a wide spread backup between the different gene copies of the same tRNA family and between different families translating the same amino-acid.

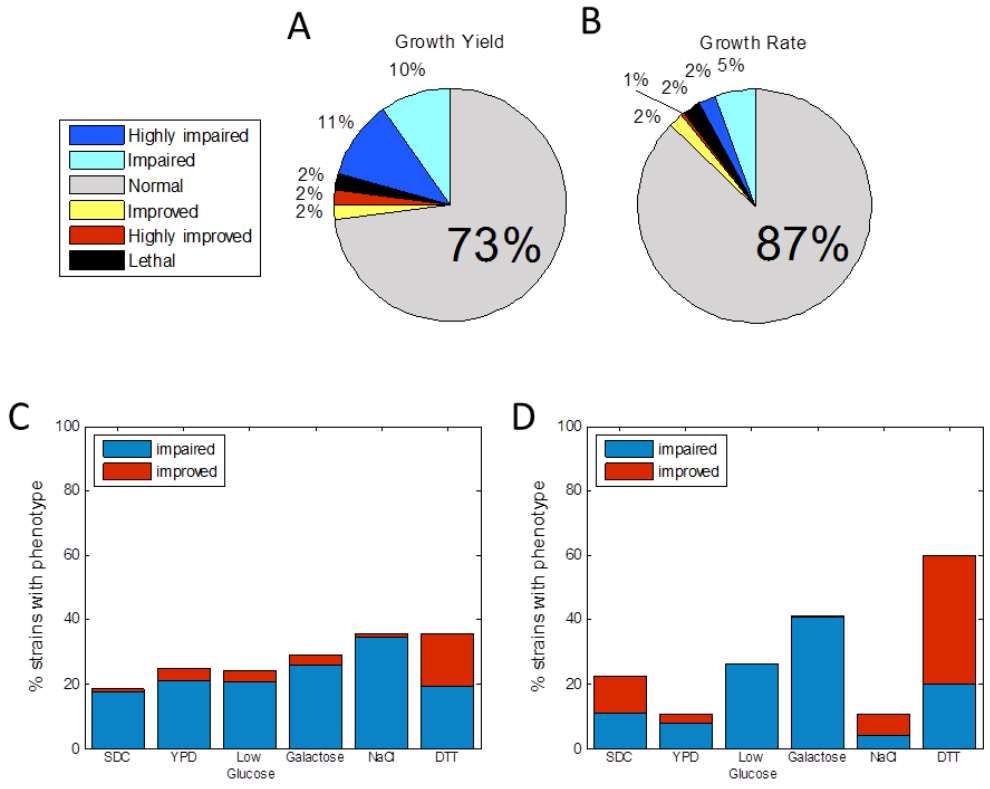

Figure 2. Deletion strain measurements in different conditions **(A-B)** Distribution of phenotypes for the tRNA deletion library on rich medium (YPD), according to two growth parameters: growth yield (A) growth rate (B). Deletion strains were assigned to categories according to their σ values. Thus, highly impaired for σ<-3, impaired for -2>σ>-3, improved for 2<σ<3, and highly improved for σ>3 for σ calculations see Method 4.2.1. **(C-D)** Percent of strains exhibiting a growth yield (C) phenotype and growth rate (D) phenotype in various conditions. The color indicates the type of phenotype: impaired (blue) or improved (red).

Although it is often implicitly assumed that all tRNA copies contribute similarly to the cellular tRNA pool, comparison of the growth parameters of tRNA deletions from the same family revealed marked differences between seemingly identical family members. In particular, under rich medium, we found that deletions from 21 out of the 32 examined, multi-copy families, span a broad range of at least 10% difference in growth yield (Figure 3A). Such differences

were also exposed in the growth rate parameter but were milder and we thus focus on the growth yield parameter in all further analysis. To further investigate these differences we focused on the *tR(UCU)* family that contains 11 identical copies in the genome, of which five are represented in our library. In rich medium two copies (*tR(UCU)E* and *tR(UCU)M2*) showed appreciable reduction in growth yield (termed Major copies), while deletions of the other three copies (*tR(UCU)M1*, *tR(UCU)G1* and *tR(UCU)K*) grow essentially as the wild-type (termed Minor copies). Further assessment of the Major and Minor copies across various stress conditions revealed that the hierarchy of Major and Minor is generally preserved (Figure 3B).

Since all family members have identical sequence, we hypothesized that differential contribution should be due to differences in their flanking regions. A complementation assay in which the different tRNAs from the UCU family were introduced to the *tR(UCU)M2* deletion strain revealed different degrees of complementation. The different constructs differ only in the region flanking the tRNA gene (200bp); thus the variation in complementation capability can be attributed to the different sequences flanking the tRNA. Next we turned to look which sequence features could govern differential expression of the family members and hence their differential contribution to fitness. For this purpose we used the data set created by Giuliodori *et al.* (Giuliodori et al., 2003) in which identified conserved sequence elements upstream of *S. cerevisiae* tRNA genes. In their study they identified four conserved sequence elements located at positions -53 (T-rich), -42(TATA-like), -30(T-rich) and -13 (pol III TSS) with respect to the first nucleotide of the mature tRNA. Our analysis revealed that only the two Major copies contain the conserved TATA-like motif at nucleotide -42. Examining the entire tRNA deletion library in rich medium, we found that strains exhibiting impairment in growth yield were enriched for the same TATA-like motif (hypergeometric test, p-value 0.0089). In addition, the TSS motif at position -13 was enriched in deletion strains that exhibit impairment in either in growth rate or growth yield (Figure 3C). To reinforce these observations we ran the MEME motif search algorithm (Bailey & Elkan, 1994) screening the upstream sequences of tRNA deletion strains exhibiting impaired growth yield for enriched motifs (see Methods). As can be seen in (Figure 3D),

we found two significant motifs that resemble those found by Giuliodori *et al.* both in sequence and location.

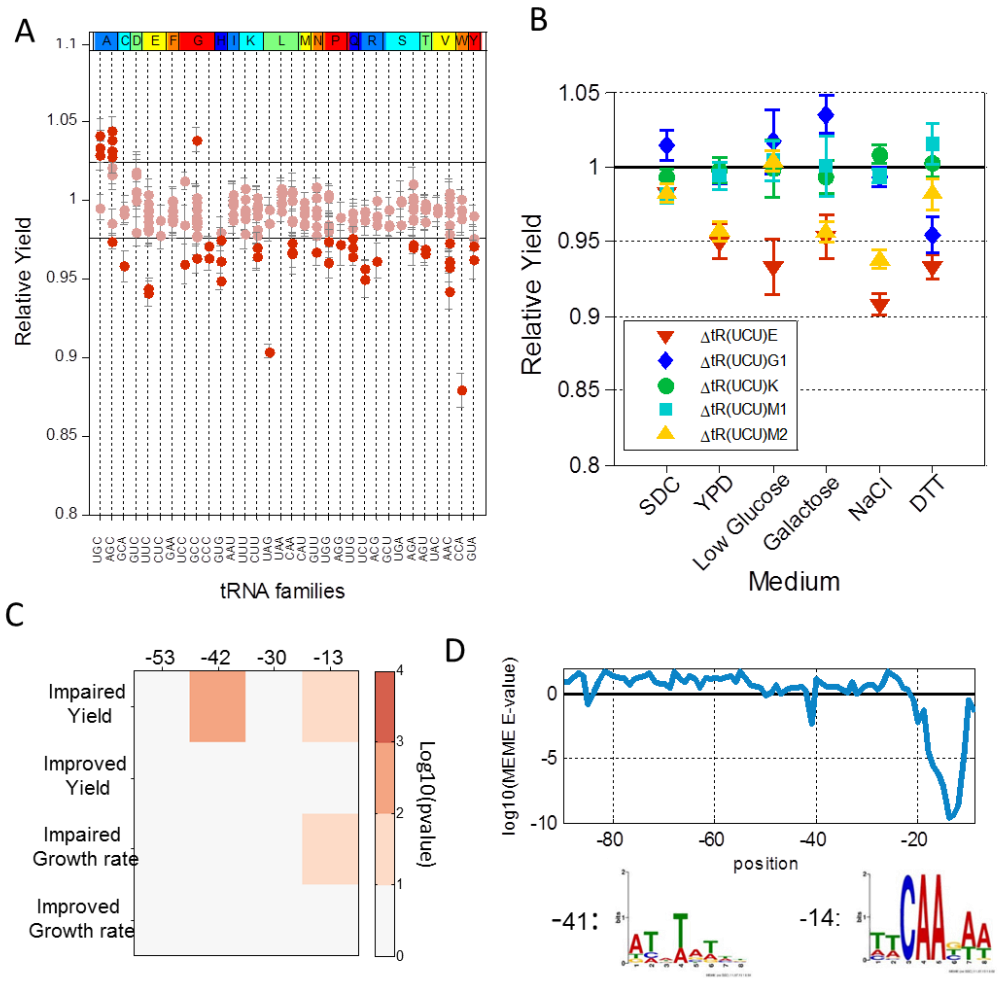

Figure 3. Different genes of the same tRNA family exhibit phenotype differences **(A)** Relative growth yield values of the tRNA deletion library strains in rich medium, sorted by anti-codon and amino-acid identity along the x-axis. Each dot along the vertical lines denotes the value (data are represented as mean of 3 biological repetitions +/- SEM) of a deletion strain of different tRNA gene of the respective family. The horizontal lines mark two standard deviations around the mean of the wild-type. Dots above or below these lines are considered non-normal phenotypes. **(B)** Relative growth yield of the five tR(UCU) members across different growth conditions, indicated on the x-axis. **(C)** Enrichment of conserved elements in tRNA genes divided according to phenotype observed in rich media for each growth parameter. Each column in the matrix denotes a conserved element as defined by (Giuliodori et al., 2003). Color bar indicates the -log10 of the hypergeometric p-value. **(D)** log10 E-value found by the MEME software for the most significant motif in a 9bp window starting from the position indicated by the x-axis. The LOGOs of the two significant motifs are displayed below, next to a number indicating its position. Position 0 is the first position of the mature tRNA.

Together these results indicate that the contribution to the tRNA pool and cellular fitness of different copies from the same tRNA family is far from equal. We provide one possible explanation, which can account for the observed

differences, implying that the sequences flanking tRNA genes play a role in determining their expression level.

To determine whether changes in the tRNA pool result in a distinct molecular signature, we examined five tRNA deletion strains using mRNA microarrays (see Methods). For each strain, we measured genome-wide changes in mRNA levels compared to the wild-type under rich growth conditions. The expression changes we exposed were modest and demonstrated a nice correspondence between the essentiality of the tRNA gene and the extent of changes in mRNA expression inflicted upon its loss. Clustering of the expression changes for all five deletion strains revealed that the strains could be divided into two groups: SC (the single copy family genes & initiator Methionine) and MC (the multi-copy family genes), Figure 4A. An example for this division can be found in the pronounced effect observed for the *COS8* gene. This gene was extremely up-regulated (about 16 fold) in the SC group while unchanged in the MC group (Figure 4B). This group division recapitulated a division found between the strains when exposed to proteotoxic stress (see full paper at the appendix for details). Thus, these results, suggest different molecular signatures for the two groups, which are also related to the proteotoxic stress response.

To expose what are the responses and underling molecular pathways that differentiate these two groups, we examined which KEGG pathways (Kanehisa & Goto, 2000, Kanehisa et al., 2012) differentiate between them. To this end we used Gene Set Enrichment Analysis (GSEA) software, which computationally determines whether pre-defined set of genes shows statistically significant difference in representation between two biological groups (Subramanian et al., 2005, Mootha et al., 2003). This analysis revealed a somewhat opposite signature between the two groups (Table 1). Pathways which are responsive to proteotoxic stress such as the “Proteasome” (FDR q-value <1E-5), and “Protein processing in endoplasmic reticulum” (FDR q-value 2E-3) are significantly induced in the SC group, relative to the MC group. While in the MC groups translation-related pathways such as “Ribosome biogenesis” (FDR q-value <1E-5) and “Ribosome” (FDR q-value 1E-4) are significantly induced compared to the SC group.

To further characterize these differences we focused on specific pathways. A more detailed examination of the expression changes observed for all the genes that constitute the proteasome complex revealed an up-regulation, to various extents in response to deletion of tRNAs from the SC group. The MC group demonstrated no change and even a slight down-regulation of these genes (Figure 4C), a trend which was further verified using RT-qPCR. These observations establish the notion that upon deletion of members of the SC group cells experience a proteotoxic stress. Another distinction between the groups was also observed in the RNA polymerase machinery pathway. Expression of genes that belong to this pathway were up-regulated only in the MC group (Table 1). Further examination revealed that this signal is due to the elevation of Pol III machinery (the polymerase responsible for tRNA gene transcription) and not Pol II machinery. The genes encoding for RNA Pol III machinery demonstrated up-regulation in the MC group and no change or even down regulation in the SC group (Figure 4D); further verified by RT-qPCR. This suggests a potential regulation of the tRNA pool by controlling the levels of the tRNA's transcribing polymerase.

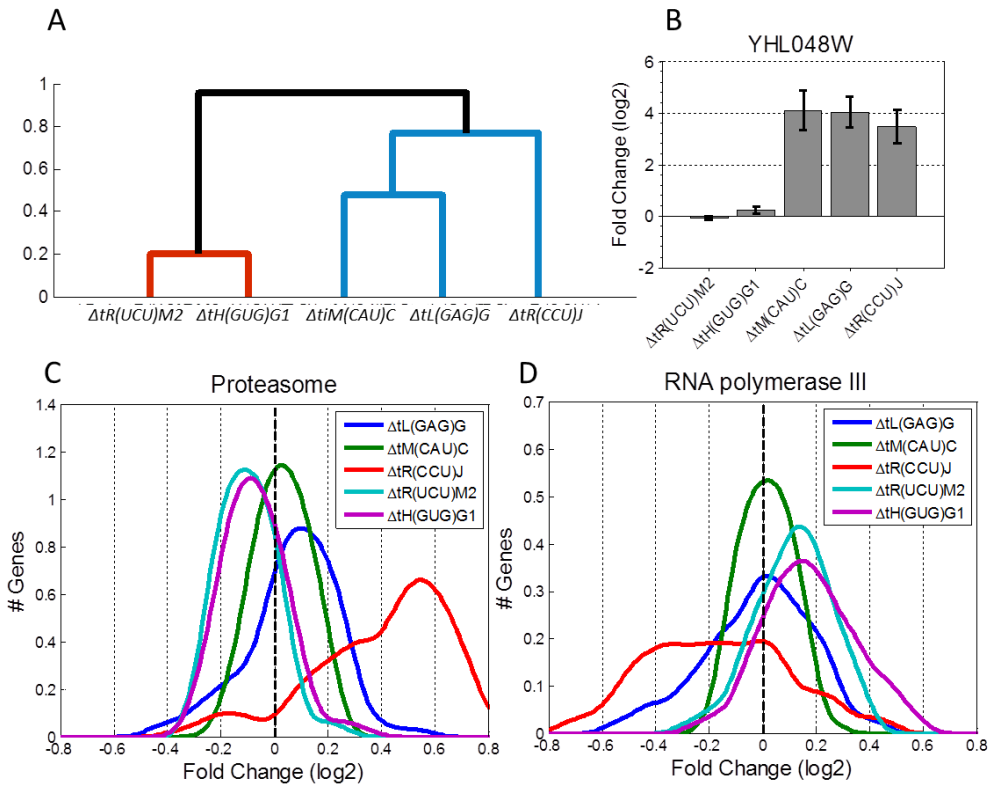

Figure 4. Molecular response to changes in the tRNA pool. **(A)** Dendrogram created by clustering changes in gene expression for five representative deletion strains. **(B)** Fold change of the *COS8*

(*YHL048W*) mRNA levels in each of the five deletion strains as measured by microarrays. **(C-D)** The fold change distribution of mRNA levels as measured by microarrays, of genes composing the Proteasome pathway **(C)** and the Pol III RNA Polymerase machinery module **(D)** as defined by the KEGG database. In both sub-figures values are plotted for the same five deletion strains: *tL(GAG)G* (blue), *tR(CCU)J* (red), *tiM(CAU)C* (green), *tH(GUG)G1* (magenta) and *tR(UCU)M2* (cyan).

To summarize, this work revealed additional levels of complexity within the tRNA pool including extensive backup interactions and differential contribution between tRNA copies. Combining these results with the fact that the essentiality of different tRNAs changes across conditions and the potential elevation of Pol III upon deletion all suggest the regulation of the pool is more complex than commonly accepted and perhaps even as complex as for mRNA genes.

The full results and conclusion are summarized in a paper, see appendix.

Table 1 KEGG pathways differentiating between tRNA deletion sets. KEGG pathways (Kanehisa & Goto, 2000, Kanehisa et al., 2012) for which changes in genes expression are significantly different between the two groups of tRNA deletion strains: MC (multi-copy) group *(Δ**tH(GUG)G1*** and Δ***tR(UCU)M2***) vs. SC (single-copy) group *(Δ**tL(GAG)G***, Δ***tR(CCU)J***, Δ***tiM(CAU)C***) calculated with GSEA (Subramanian et al., 2005, Mootha et al., 2003). In the first column are pathways, which are higher in SC vs. MC and vice versa in the second column. The values are corrected for multiple hypothesis and the FDR q-values are indicated next to each pathway.

Higher is SC than in MC	Higher is MC than in SC
Proteasome (<1E-5)	Ribosome biogenesis in eukaryotes (<1E-5)
Oxidative phosphorylation (<1E-5)	RNA polymerase (<1E-5)
Endocytosis(2E-3)	Phenylalanine, tyrosine and tryptophan biosynthesis (<1E-5)
SNARE interactions in vesicular transport (2E-3)	Pyrimidine metabolism (5E-5)
Protein processing in endoplasmic reticulum (2E-3)	Ribosome (1E-4)
Starch and sucrose metabolism (2E-3)	Lysine biosynthesis (1E-4)
Citrate cycle (TCA cycle) (0.01)	Histidine metabolism (4E-4)
Meiosis - yeast (0.01)	Cysteine and methionine metabolism (4E-4)
Homologous recombination (0.02)	Riboflavin metabolism (5E-3)
Mismatch Repair (0.02)	Arginine and proline metabolism (8E-3)
Cell cycle - yeast (0.02)	Valine, leucine and isoleucine biosynthesis (0.01)
MAPK signaling pathway - yeast (0.02)	Purine metabolism (0.03)
Fructose and mannose metabolism (0.02)	Sulfur metabolism (0.03)
Nitrogen Metabolism (0.02)	Tyrosine Metabolism (0.03)
Phagosome (0.03)	Folate biosynthesis (0.04)

5.3 Ribosome density governs patterns of mRNA cleavage in *Escherichia coli*

One of the main properties of an mRNA which can have a direct effect on the final gene expression is its stability. Changes in codon sequence were found to affects the mRNA levels and stability (Kudla et al., 2009, Sunohara et al., 2004, Petersen, 1987, Kolmsee & Hengge, 2011). In this project our aim was to study the interplay between degradation and translation in *Escherichia coli*. The manuscript is under revision in *Nucleic Acids Research.*

Ribosome density governs patterns of mRNA cleavage in *Escherichia coli*

Sivan Navon and Yitzhak Pilpel*

Department of Molecular Genetics, Weizmann Institute of Science, Rehovot, 76100 Israel

*To whom correspondence should be addressed. Tel:+972-8-9346058 ; Fax: :+972-8-9344108 ; Email: Pilpel@weizmann.ac.il

ABSTRACT

Recent developments in microbial genomics allow the study of ribosome profiling and RNA fragments in the cell. Analysing ribosome profiles it was discovered that Shine-Dalgarno-like motifs embedded within coding region cause ribosome pausing in bacteria. Yet, what are the potential functions of such ribosome pausing and attenuation sites remains unknown. Using these developments we set to unravel a regulatory relation between translation and mRNA degradation. We used genome-wide mapping of RNA fragments to identify the *Escherichia coli*'s mRNA cleavage sites and combined it with measurements of transcriptome-wide ribosome occupancy, exposing intricate relation between the two. We found a tendency to have a Shine-Dalgarno-like sequence and high ribosome occupancy downstream to cleavage sites, suggesting that the ribosome enhances degradation locally, immediately up-stream to its attenuation site. Conversely, genes with higher ribosome density around the start codon were often devoid of detectable cleavage points, suggesting that globally the ribosome protects the transcript. Our results expose for the first time on a genome-wide scale, a coupling between translation and mRNA degradation and ascribe the first functional role for ribosomal pausing in bacteria.

INTRODUCTION

The amount of protein synthesized in the cell is determined by two primary parameters: the mRNA levels of the genes and the rate of translation of this mRNA. mRNA levels in turn, are determined by both the rate of transcription and the rate of degradation. In bacteria the half-life of different transcripts varies significantly, from less than a minute to about an hour (reviewed in:1), thus allowing the stability of the mRNA to play a key role in regulating the transcriptome.

In *Escherichia coli* degradation of mRNA is initiated by endonucleolytic cleavage, the upstream fragments are degraded by 3'-to-5' exoribonucleases while the downstream fragments degrade through a series of successive endonucleolytic cleavages (2-4). Of the three site-specific endoribonucleases in *Escherichia coli*, RNase E is the main enzyme in mRNA decay (2,3). The common notion is that this enzyme cleaves at specific sites in single stranded regions of mRNAs that are typically AT-rich with no strong sequence specificity and with a stem&loop structure frequently found around the site (reviewed in: 2,3,5). For more on mRNA decay in bacteria, see reviews by (2,3,6).

The mRNA stability is tied to the translation process through two known stabilizing mechanisms: first, the ribosome can simply protect the mRNA by masking a potential cleavage site, namely the ribosome foot print protects the region from actually being cleaved (Reviewed in: 4) . The second mechanism that coordinates translation and mRNA decay is through the blocking of transcript's 5'. RNase E degradation pathway requires access to the 5'-end of the transcript and when this access is blocked the mRNA is

stabilized. For both mechanisms an efficient ribosome binding site (RBS) can have a stabilizing effect on the mRNA (4,7). Stalled ribosomes on the 5' end of the *ermC* were shown to stabilize the gene in *B. subtilis* (8). However not only the 5' UTR features can affect the mRNA stability but also properties of the ORF which affect the ribosome elongation, such as codon usage and Shine-Dalgarno like motifs (9 , see below). Rare codons in the *RpoS* gene were found to stabilize its transcript, potentially by concentrating the ribosome on the mRNA thus protecting it from RNase E attack (10). Earlier Petersen showed that altering codons immediately downstream to the ribosome binding site affect the transcript stability (11). It was suggested that these codons affect the transcript stability by changing the ribosome density on the gene (12). Though coupling between translation and the degradation was exposed for specific genes in the past, whether it is a genome wide phenomenon and what are the coupling mechanisms remain to be seen.

Until now, analysis of cleavage sites and their sequence properties was done by analyzing a handful of genes and different oligonucleotides. Here we set to analyze the cleavage sites of more than a thousand messenger RNAs in *Escherichia coli*. By analyzing 5' RNA sequencing reads mapped onto the genome (13,14) we identified mRNA cleavage sites. Combining this data with the recent data on transcriptome-wide ribosome occupancy (9) we explored the relation between translation efficiency and the mRNA cleavage and stability. We discovered a peak of higher ribosome density 25 bps downstream to the cleavage sites potentially due to higher anti-Shine-Dalgarno (aSD) affinity of the region. This suggests that accumulation of ribosomes at an attenuation site enhance local mRNA cleavage immediately up-stream to them. On the other hand, higher ribosome density at the 5' termini of genes was found to be associated with more stable mRNAs, suggesting that globally the ribosome exerts a protective effect on the transcript. Thus, by analyzing cleavage sites of many genes this work sheds light on the potential modes of coordination between translation and degradation.

MATERIAL AND METHODS

Identification of RNA cleavage sites from RNA deep sequencing data

We used data derived from a modified RNA deep sequencing protocol (15) to deduce location of endonucleolytic cleavage sites. The Mapping of *E. coli* 5'-end monophosphorylated RNA fragments were taken from the Quax paper (13) which were downloaded from http://www.weizmann.ac.il/molgen/Sorek/Navon_data.fasta.gz. Analyzing the data we noticed that the 5'-end of tens of thousands of fragments was identified to be inside coding regions. Fragments inside ORF are less likely to be transcription start site, suggesting that these fragments represent the downstream residue of an endonucleolytic cleavage site. Since *E. coli* does not have a 5'-to-3' exoribonuclease and endonucleolytic cleavage is a main step in the RNA degradation pathway, such data can be used to deduce the genome wide features of cleavage sites that cause mRNA degradation.

Analyzing only coding regions, the data consists of 13,926 unique potential cleavage sites in the genome, which represent mapping of unique RNA fragments (we set a quality threshold such that each unique location had to appear at least in two independent reads in the data to be considered) . These 13,926 cleavage sites distributed over 2218 mRNAs of the *Escherichia coli* reference genome NC_000913, implying that the rest of the 1923 annotated ORFs do not show even a single cleavage point in our final dataset. After filtering of sites that less not likely to represent cleavage sites (see Materials and Methods) we focused on 4157 high quality sites.

Filtering cleavage sites

For both the *E. coli* and the *P. aeruginosa* all identified sites were clustered into groups (clusters) based on the distance between consecutive sites, two sites which were separated by less than 5 nucleotides were clustered together. As a result different clusters had at least 5 nucleotides between their closest sites.

Filtering the *Escherichia coli* data: For a *site* to be considered as a cleavage site it should fulfill three criteria: (i) It needs to be the site with highest number of reads in its cluster, (ii) it needs to have at least three reads and no more than 50, (iii) it needs to be at least 10 nucleotides upstream or downstream from a known transcription start site (based on the EcoCyc database (16)).

Filtering the *Pseudomonas aeruginosa* data: sites that appeared in either the 37ºC sample or the 28ºC sample were considered, (as long as the site appeared in both the Tap+ and Tap-). For a site to be considered a cleavage site if it fulfilled three criteria: (i) It needs to be the site with highest number of reads in its cluster, (ii) it needs to have more than two reads and no more than 50 (averaging the Tap+ and Tap- reads), (iii) it needs to be at least 10 nucleotides upstream or downstream from the transcription start sites identified by Wurtzel *et al*. (14).

As Li *et al.* did in their kinematic analysis, for the analysis of the ribosome density around the cleavage sites we avoided regions with known changes in the ribosomes density. In particular we excluded sites which were close (up to 50 bases) to the start or the stop codon, since it is known that the ribosome dwells longer on these particular codons (17). By analyzing only sites in the middle of the gene, where the ribosome density should be relatively constant and there are no known causes for SD-like sequence to exist there, the observed changes can be associated to cleavage sites.

mRNA folding energy and unpairing score calculations

We used a sliding window of 20 nucleotides to create a folding energy and pairing score profiles for all mRNAs. Each window of 20 nucleotides was folded using Vienna RNAfold package (18). The free energy of the window was assigned to the 11^{th} nucleotide in the window. The unpairing score for each nucleotide was calculated by counting the number of times it was unpaired over it total number of appearances (20

appearances for nucleotides far from the edges of the transcript). The secondary structure analysis was run with different window sizes (in the range of 10 to 100 nucleotides) with no significant differences in the results (not shown).

Calculating the genes' ribosome density

Using data deposited in GSE35641 (9) we constructed the genes' ribosome occupancy. The ribosome occupancy for each gene was normalized to the sum of the ribosome occupancy over all the mRNA including its UTRs, to include 50 nucleotides upstream and downstream to it. We chose 50 nucleotides since the average distance of the main TSS site identified in the E. coli 5' data is 49 nucleotides. Then the ribosome density profile was average between the two repeats to get the final ribosome density of a gene.

Defining expressed, cleaved and not-cleaved genes

For the expression level of the genes we used the average mRNA in supplement database 2 in Lu *et al.* paper (19), which averages three different mRNA level papers. After ignoring all the genes which had no mRNA level reads and genes which are shorter than 200 bases, we ended up with 2025 genes, we took the top 50% of these genes which had the highest mRNA levels ending up with 1012 which we defined as expressed genes.

From these 1028 genes were constructed two set of genes. The first set included only genes which had no cleavage site at all, a total of 246 genes. The second set included genes which had at least one cleavage site after filtering a total of 541 genes. The rest of the expressed genes had cleavage site which did not pass the filter (see filtering cleavage sites).

RESULTS

Sequence information is found around cleavage sites

Examining the sequence content around the cleavage site some consensus emerges, mainly in nucleotides -1 to 1 ("0" is defined to be the first nucleotide position immediately downstream to the cleavage site, i.e. the first nucleotide in the RNA fragment detected). Reassuringly we noticed that indeed just around the cleavage site there is an AT-rich region, about 70% of nucleotides are either A or T for all three sites (-1 to 1), see Supplement Figure 1. Clustering the sites based on their sequence (using the Jukes-Cantor distance (20)) revealed two potential motif groups. The first motif, [G/A]N↑[A/T]TT (↑ denotes the cleavage site, Supplement Figure 1B) includes the core consensus sequence ATT suggested by Ehretsmann *et al.* (21) that was obtained from a handful of data points, while the first [C/A]T↑ (Supplement Figure 1C) was not detected before, to the best of our knowledge .

High ribosome occupancy downstream of cleavage sites

A relation between the presence and density of ribosomes and mRNA degradation was repeatedly suggested (4,7,10,12), particularly due to the potential of the ribosome to protect the mRNA from degradation (reviewed in: 4). Recent profiling of ribosome density along mRNAs in *Escherichia coli* (9) allows us to examine potential relation between the ribosome density along transcripts and cleavage sites.

First we examined the ribosome occupancy around the cleavage sites, Figure 1A. We worked throughout with ribosome occupancy profiles that are normalized for each gene individually, thus depicting relative changes in occupancy along a gene, and ignoring absolute differences between genes. As can be seen in the figure, around 12 bases downstream to the cleavage site there is a deep in the ribosome density profile (Wilcoxon rank sum test $p<1e-27$ compared to the density of all 100 bases around the cleavage site) and around 24 bases downstream there is a peak in the ribosome density profile (Wilcoxon rank sum test $p<1e-31$ compare to the density of all sites 100 bases around the cleavage site). The differences in the ribosome density could not be explained by codon bias (see supplement Figure 2).

Following Li *et al.*'s (9) work we examined whether Shine-Dalgarno (SD) like sequences drive ribosomes pausing downstream to our candidate cleavage points. Using the same method as in Li *et al*. we constructed the anti-Shine-Dalgarno (aSD) affinity profile of genes (the affinity to bind to the complementary sequence of the Shine-Dalgarno, which is at the 3' end of the 16S rRNA) profile around each cleavage site. We found a high aSD affinity about 13 bases downstream to the cleavage site (Wilcoxon rank sum test $p<1e-12$), see Figure 1B; this peak in the aSD affinity is located 11 bases upstream to the peak of the ribosome occupancy. Since the ribosome occupancy data are aligned to the A-site, the peak in the aSD affinity is 8 nucleotides upstream to the P-site which is in range for an effective SD (22).

To further examine the relation between cleavage sites and SD-like sequences we turned to another bacterial species, *Pseudomonas aeruginosa*. Using 5'-end mapping of RNA fragments published by Wurtzel *et al.* in this specie (14) we calculated the aSD affinity around the *P. aeruginosa* cleavage sites (see Materials and Methods). As in *E. coli* we find a high aSD affinity about 13 bases downstream to the cleavage site (Wilcoxon rank sum test $p<1e-4$), see Figure 1C.

High ribosome occupancy downstream potentially increases cleavage probability by keeping the region upstream to it free of secondary structure, as required by RNase E. To further investigate the connection between cleavage and the structure of the RNA we computed predicted mRNA secondary structure around the cleavage sites. We examined the averaged free energy profile around the cleavage sites and searched for significant differences in free energy and potential pairing of the nucleotides (see Material and Methods). For comparison we examined profiles of randomly permutated sequences around cleavage sites and sequence without cleavage sites. Reassuringly we found differences in the free energy around the cleavage site (Figure 2A). While around the cleavage site the energy is 60% higher

(looser structure), the structure becomes tight (low free energy values) further upstream and downstream from the cleavage site. In addition, from Figure 2C we notice there is a significant difference between the amounts of base pairing of some nucleotide position around the cleavage site, mainly base 0 and base -6 (Wilcoxon rank sum test compared to background p=3e-21, p=2e-54 respectively). Similar figures were obtained for folding *P. aeruginosa*, see figures 2B and 2D

Ribosomes stabilize transcripts

While so far we revealed that ribosomes can affect locally degradation by enhancing cleavage immediately up-stream, here we turned to examine more global effect of ribosomes on stability of their harboring transcripts. As mentioned above, we identified one or more cleavage sites in only about a half of the *E. coli* genes; for the rest of the genes no such site was seen in the data. To further investigate why some genes show cleavage sites and others do not, we examined the ribosome density of cleaved and non-cleaved genes. For this analysis we avoided genes with low expression levels (see Material and methods) as these are unlikely to show cleavage events. The expressed genes were divided into two sets: without any observed cleavage site, and genes with at least one cleavage site (see Material and Methods). As can be seen in Figure 3A, expressed genes without cleavage sites have significantly higher ribosome density around their start codon. This observation might suggest that high ribosome density close to the 5' UTR exerts a global protecting effect on RNAs from cleavage.

To further check the relationship between the ribosome density around the start codon and the gene cleavage we divided all of the *E. coli* genes into 3 equal groups based on their relative ribosome density in nucleotide positions -6 to +4 relative to the ATG. For each group we checked the fraction of expressed genes which had cleavage sites, Figure 3B. The set of genes with low relative density had significantly higher fraction of genes with cleavage sites than expected (hyper-geometric probability 0.0015) and the set of genes with high density had significantly lower fraction of genes with cleavage sites than expected (hyper-geometric probability 0.0028). To conclude, genes with low relative ribosome density around the start codon are more likely to have cleavage sites which suggest that stalled ribosomes around the ATG protect the transcript from cleavage.

DISCUSSION

The modified RNA deep sequencing protocol (15) enables, as far as we know for the first time, to analyze cleavage sites of bacteria on a single nucleotide resolution on a genome-wide scale. This genome-wide analysis reinforces the notion that the mRNAs are cleaved in AT-rich regions that have a relatively loose structure.

An important aspect of cleavage control that is analyzed here is the coupling between translation and degradation. Coupling between layers of gene expression regulation is a common theme (23) and here

we provide one such mode of coupling. We notice high relative ribosome occupancy about 25 bases downstream to the cleavage site suggesting the ribosome enhances degradation locally. Due to the ribosome size (foot-printing of 25-42 nucleotides (9)) a cleavage site which is 25 bases upstream to the ribosome A-site will most likely be free of the ribosome but very close to it, thus with limited ability to refold. The single stranded requirement of the RNase E is thought to be maintained by the RNA secondary structure; however here we suggest an additional mechanism. We suggest that the ribosomes take an active role in keeping the cleavage sites single stranded by dwelling a bit longer just downstream of the cleavage sites.

While the ribosome enhances degradation locally, we found that globally it exerts global protection to the transcript. On a genome-wide scale we notice that high ribosome occupancy around the start codon may stabilize the transcript. Such ribosomes have the potential to mask essential cleavage sites and jam other ribosomes on the 5' UTR, thus blocking it from the degradation machinery which requires access to the 5' end of the transcript.

In the future it will be interesting to repeat this analysis on data from different bacteria, on mutants which have different RNases knock down and in different stress conditions, which could activate additional degradation pathways (24) and modify the ribosome patterns genome wide (9). Such data can shed more light on the degradation process, its coupling to the translation process and its different enzymes.

SUPPLEMENTARY DATA

Supplementary Data are available at NAR online.

ACKNOWLEDGEMENT

We acknowledge grant support from the European Research Council and the Ben-May Charitable Trust. YP is the incumbent of the Ben-May Professorial Chair. Special thanks to Omri Wurtzel a former PhD. Student at Rotem Sorek's lab for extensive assistance throughout. We also thank Gene-Wei Li from Jonathan Weissman's lab for his help with the ribosome profiling data and analysis.

FUNDING

This work was supported by the European Research Council (through grant number 205199-ERNBPTC); and the Ben-May Charitable Trust. Funding for open access charge: the European Research Council.

REFERENCES

1. Richards, J., Sundermeier, T., Svetlanov, A. and Karzai, A.W. (2008) Quality control of bacterial mRNA decoding and decay. *Biochim Biophys Acta*, **1779**, 574-582.
2. Steege, D.A. (2000) Emerging features of mRNA decay in bacteria. *Rna*, **6**, 1079-1090.
3. Regnier, P. and Arraiano, C.M. (2000) Degradation of mRNA in bacteria: emergence of ubiquitous features. *Bioessays*, **22**, 235-244.
4. Deana, A. and Belasco, J.G. (2005) Lost in translation: the influence of ribosomes on bacterial mRNA decay. *Genes Dev*, **19**, 2526-2533.
5. Carpousis, A.J., Luisi, B.F. and McDowall, K.J. (2009) Endonucleolytic initiation of mRNA decay in Escherichia coli. *Prog Mol Biol Transl Sci*, **85**, 91-135.
6. Deutscher, M.P. (2006) Degradation of RNA in bacteria: comparison of mRNA and stable RNA. *Nucleic Acids Res*, **34**, 659-666.
7. Kaberdin, V.R. and Blasi, U. (2006) Translation initiation and the fate of bacterial mRNAs. *FEMS Microbiol Rev*, **30**, 967-979.
8. Bechhofer, D.H. and Zen, K.H. (1989) Mechanism of erythromycin-induced ermC mRNA stability in Bacillus subtilis. *J Bacteriol*, **171**, 5803-5811.
9. Li, G.W., Oh, E. and Weissman, J.S. (2012) The anti-Shine-Dalgarno sequence drives translational pausing and codon choice in bacteria. *Nature*, **484**, 538-541.
10. Kolmsee, T. and Hengge, R. (2011) Rare codons play a positive role in the expression of the stationary phase sigma factor RpoS (sigmaS) in Escherichia coli. *RNA Biol*, **8**.
11. Petersen, C. (1987) The functional stability of the lacZ transcript is sensitive towards sequence alterations immediately downstream of the ribosome binding site. *Mol Gen Genet*, **209**, 179-187.
12. Pedersen, M., Nissen, S., Mitarai, N., Lo Svenningsen, S., Sneppen, K. and Pedersen, S. (2011) The functional half-life of an mRNA depends on the ribosome spacing in an early coding region. *J Mol Biol*, **407**, 35-44.
13. Quax, T.E., Wolf, Y.I., Koehorst, J.J., Wurtzel, O., van der Oost, R., Ran, W., Blombach, F., Makarova, K.S., Brouns, S.J., Forster, A.C. *et al.* (2013) Differential Translation Tunes Uneven Production of Operon-Encoded Proteins. *Cell Reports*, **4**.
14. Wurtzel, O., Yoder-Himes, D.R., Han, K., Dandekar, A.A., Edelheit, S., Greenberg, E.P., Sorek, R. and Lory, S. (2012) The single-nucleotide resolution transcriptome of Pseudomonas aeruginosa grown in body temperature. *PLoS Pathog*, **8**, e1002945.
15. Wurtzel, O., Sapra, R., Chen, F., Zhu, Y., Simmons, B.A. and Sorek, R. (2010) A single-base resolution map of an archival transcriptome. *Genome Res*, **20**, 133-141.
16. Kessler, I.M., Mackie, A., Peralta-Gil, M., Santos-Zavala, A., Gama-Castro, S., Benavidez-Martinez, C., Filcher, C., Huerta, A.M., Kothari, A., Krummenacker, M. *et al.* (2013) EcoCyc: fusing model organism databases with systems biology. *Nucleic Acids Res*, **41**, D605-612.
17. Oh, E., Becker, A.H., Sandikci, A., Huber, D., Chaba, R., Gloge, F., Nichols, R.J., Typas, A., Gross, C.A., Kramer, G. *et al.* (2011) Selective ribosome profiling reveals the cotranslational chaperone action of trigger factor in vivo. *Cell*, **147**, 1295-1308.
18. Lorenz, R., Bernhart, S.H., Honer Zu Siederdissen, C., Tafer, H., Flamm, C., Stadler, P.F. and Hofacker, I.L. (2011) ViennaRNA Package 2.0. *Algorithms Mol Biol*, **6**, 26.
19. Lu, P., Vogel, C., Wang, R., Yao, X. and Marcotte, E.M. (2007) Absolute protein expression profiling estimates the relative contributions of transcriptional and translational regulation. *Nat Biotechnol*, **25**, 117-124.
20. Jukes, T.H. and Cantor, C.R. (1969) In Munro, H. N. (ed.), *Mammalian Protein Metabolism*. Academic Press, New York, pp. 21-132.

21. Ehretsmann, C.P., Carpousis, A.J. and Krisch, H.M. (1992) Specificity of Escherichia coli endoribonuclease RNase E: in vivo and in vitro analysis of mutants in a bacteriophage T4 mRNA processing site. *Genes Dev*, **6**, 149-159.
22. Chen, H., Bjerknes, M., Kumar, R. and Jay, E. (1994) Determination of the optimal aligned spacing between the Shine-Dalgarno sequence and the translation initiation codon of Escherichia coli mRNAs. *Nucleic Acids Res*, **22**, 4953-4957.
23. Dahan, O., Gingold, H. and Pilpel, Y. (2011) Regulatory mechanisms and networks couple the different phases of gene expression. *Trends Genet*, **27**, 316-322.
24. Yamaguchi, Y. and Inouye, M. (2009) mRNA interferases, sequence-specific endoribonucleases from the toxin-antitoxin systems. *Prog Mol Biol Transl Sci*, **85**, 467-500.

TABLE AND FIGURES LEGENDS

Figure 1. Ribosome Occupancy and SD-like sequences around the cleavage site
(**A**) For each base aligned around the cleavage site the median of the ribosome density profile in *E. coli* is plotted. The confidence intervals plotted by thin lines were found using bootstrapping. The black line is the median of all the bases between -50 to 50 around the cleavage site regardless to their location. (**B-C**) mean aSD affinity profile around the cleavage site for the *E. coli* sites (B) and the *P. aeruginosa* (C). The profile was calculated by averaging the aSD binding affinity (as calculated by Li *et al* (9)) for each base over all cleavage sites. The confidence intervals (thin lines) were calculated using bootstrapping. The plot was smoothed with a moving average of 3 bases to reduce frame effects. The black line is the average of all point in the ±50 region. As can be seen there about 11 nucleotides upstream of the high ribosome occupancy there is a high aSD affinity which could explain the ribosome occupancy.

Figure 2. Secondary structure features around the cleavage site
In the figure are plotted the mRNA secondary structure properties around the *E. coli* (A&C) and *P. aeruginosa* (B&D) cleavages sites calculated as describe in the Material and Methods. (**A, B**) The free energy aligned around the cleavage site averaged over the cleavage site sequences; *E. coli* (A) and *P. aeruginosa* (B). (**C, D**) The unpairing score profile aligned around the cleavage site averaged over all the sites; *E. coli* (C) and *P. aeruginosa* (D). In each subplot in addition to the profile for all cleavage sites (solid blue line) are plotted two additional controls: (i) after randomly permutating the sequences of the cleavage site (line-dot black), and (ii) sequences without cleavage sites (dashed gray).

Figure 3. Ribosome Density of genes with and without cleavage sites
(**A**) From the express genes were two groups were constructed: (i) expressed genes with at least one cleavage site (red) (ii) expressed genes without any site, even ones that didn't pass our filter (blue). For each group the median of the ribosome density is plotted when the genes are all aligned to the start codon (starting with nucleotide 0). It is important to notice that while the ribosome is assembled on the "P site", the ribosome's location is mapped to its "A" site in the ribosome data. Therefore high ribosome occupancy on the ATG is shifted toward the second codon. The error bars are the standard deviation for nucleotide three calculated using bootstrapping. (**B**) The genes in subplot (A) were divided into 3 groups

depending on their level of ribosome density in nucleotides -6 to 4 (thresholds were set to have 3 equal size groups when analyzing all genes). For each group of genes the fraction of cleaved genes is plotted. The error bars (red) are the standard deviation calculated using bootstrapping. * indicates that the level of the cleaved genes is significantly different than expected. The ‘low’ occupancy group has more cleaved genes than expected (hyper-geometric probability 0.0015) while the ‘high’ occupancy group has less than expected (hyper-geometric probability 0.0028)

Figure 1

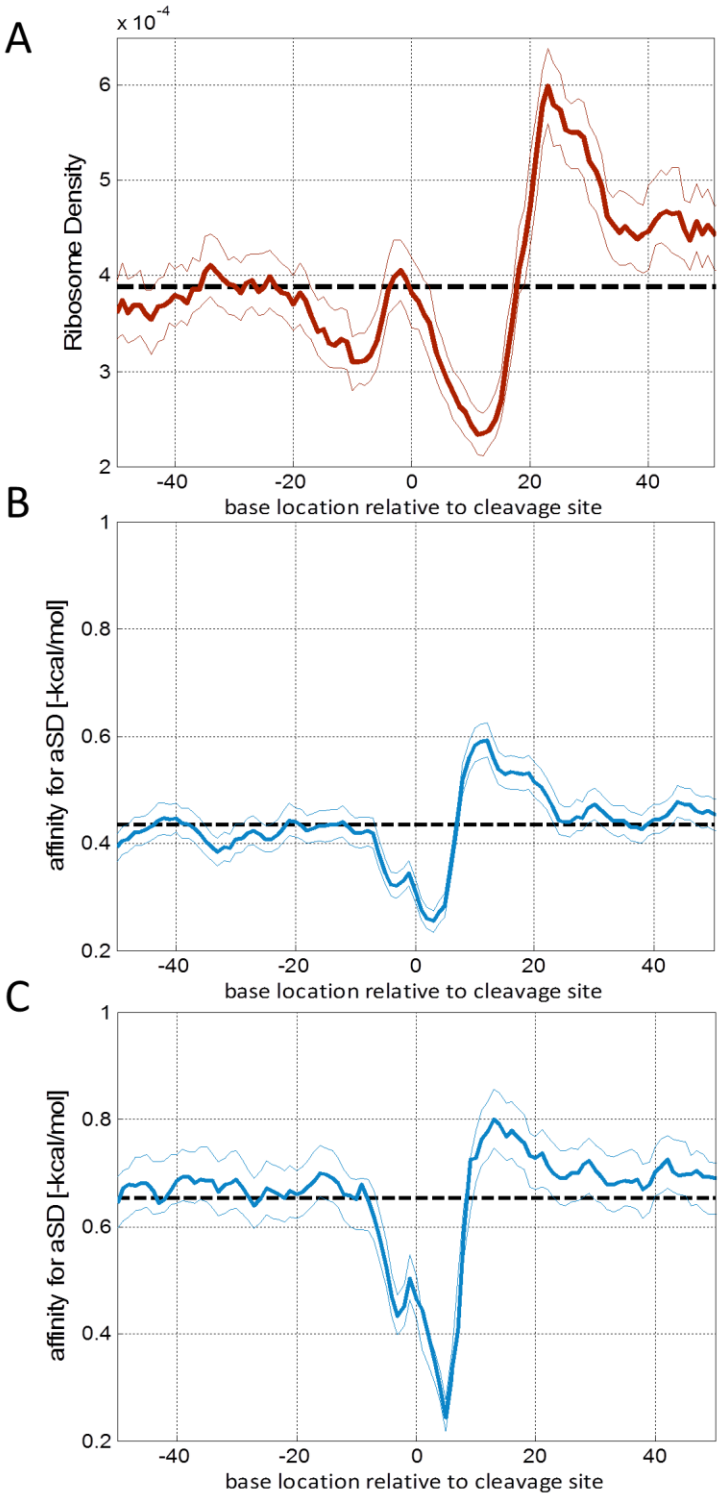
A
x 10^-4
Ribosome Density
6
5
4
3
2
-40
-20
0
20
40
base location relative to cleavage site
B
affinity for aSD [-kcal/mol]
1
0.8
0.6
0.4
0.2
-40
-20
0
20
40
base location relative to cleavage site
C
affinity for aSD [-kcal/mol]
1
0.8
0.6
0.4
0.2
-40
-20
0
20
40
base location relative to cleavage site

Figure 2

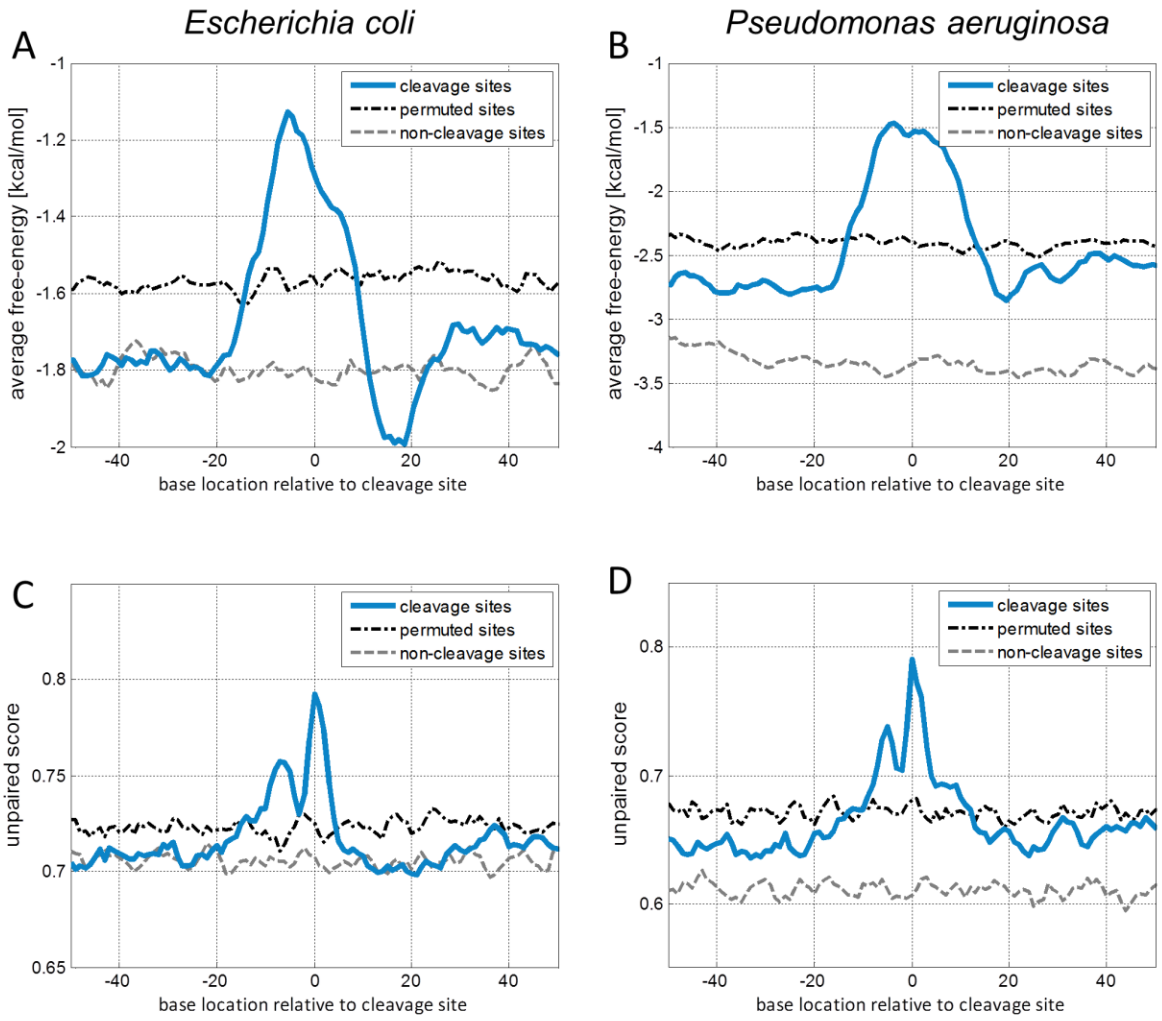
A
Escherichia coli
B
Pseudomonas aeruginosa
C
D
cleavage sites
permuted sites
non-cleavage sites
average free-energy [kcal/mol]
unpaired score
base location relative to cleavage site

Figure 3

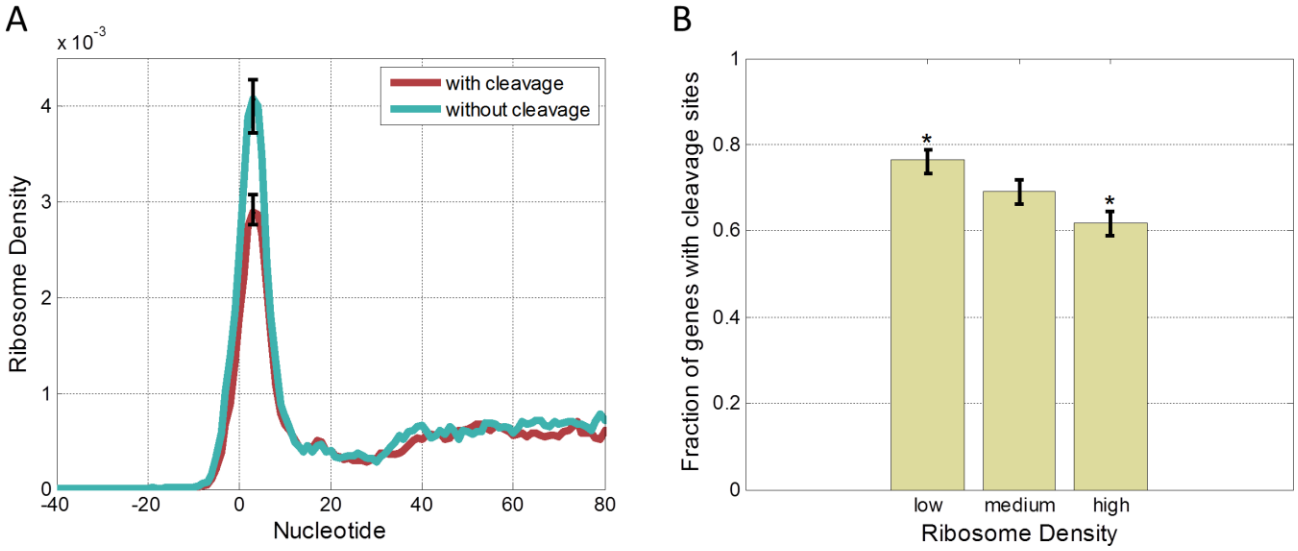
A
x 10^-3
with cleavage
without cleavage
Ribosome Density
Nucleotide
B
Fraction of genes with cleavage sites
low
medium
high
Ribosome Density

Supplementary Figures

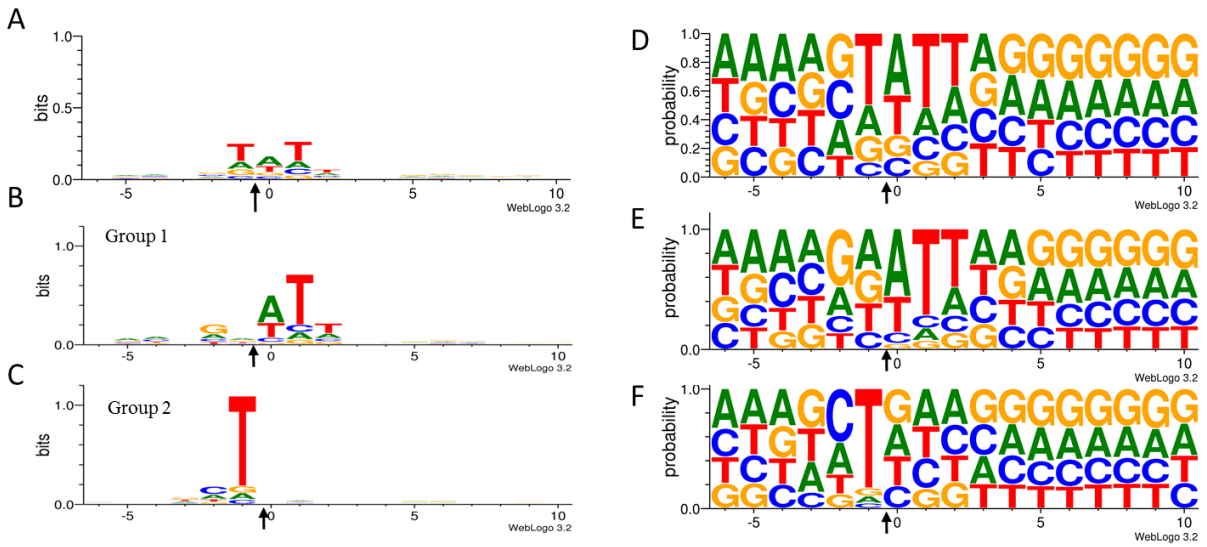

Supplement Figure 1. Sequence information of the cleavage sites

(**A**) Sequence logo (Crooks *et al.*, 2004) of 4157 cleavage sites. After clustering we get two groups of genes: (**B**) Sequence logo of the first group of genes (2321 genes), (**C**) Sequence logo of the second group of genes (1836). In all subplots base 0 is the first nucleotide just after the cleavage site (the cleavage is between base -1 to base 0). (**D-F**) is the probability logo of: all 4157 cleavage sites (D), first group of genes (E), second group of genes (F).

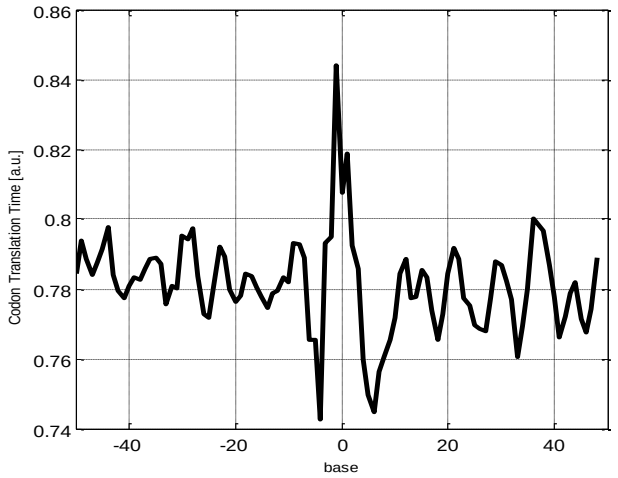

Supplement Figure 2. Codon's translation time around the cleavage sites.

The figure shows the mean time it takes to translate the region around the cleavage site. One over the codon adaptiveness index from the tAI definition (dos Reis *et al.*, 2004; Tuller *et al.*, 2010) was used as a proxy for the time it take to translate each codon. We constructed a translation time profile for each gene by dividing the time it takes to translate the codon evenly between its 3 nucleotides. Then we aligned these profiles around the reliable cleavage sites to get the mean translation time around the cleavage sites.

6 Discussion

The ability to predict final protein levels based on the nucleotide sequence is a major challenge for proteomics, computational biology and biotechnology. During the translation process the codon sequence is decoded into amino acids by tRNAs. Most amino acids are coded by more than one codon. Though resulting with the same polypeptide the levels of protein were found to change by up to 100 fold just by changing the codon sequence which in turns changes the mRNA secondary structure and the translation rates (Kudla et al., 2009, Welch et al., 2009, Subramaniam et al., 2013). To predict these changes we need to understand which additional information is coded by the codons in addition to the amino-acid sequence.

During the years a few indices were developed to try to predict protein levels based on the codon sequence. The two famous indices are the CAI (Sharp & Li, 1986) and the tAI (dos Reis et al., 2004). Both indices score a gene according to the adaptation of its codon sequence to the cellular translation capabilities. Though these indices were shown to correlate with protein levels in different organisms, they failed to predict protein levels in synthetic experiments in which the same protein was expressed with different codon combinations.

The basic assumption that underlines these indices and their weakness point is that they only look at the gene's codon composition regardless to the codon's location. In an earlier work we realized that in many organisms across the three domains of life the codons are not distributed evenly across the gene. We found that the first codons tend to be "slow codons", i.e. codons which takes longer to be translated (Tuller et al., 2010a). In the work that followed this initial publication we focused on the single gene level and examined how regions of "slow codons" affect protein expression. We found that localizing the slowest codons in the 5' end is correlated with higher protein levels, while localizing them in the 3' end correlates with lower protein levels. In addition, we found that the time it takes to translate these codons affected the protein levels, if the slowest codons are indeed located at the 5' end, then the slower region the higher will the protein levels be. In contrast if the slowest region is closer to the 3' end of the transcript then the slower that region is the lower, on average, is the expression

level. By analyzing the codons of a given gene and locating the slowest region we believe that we can improve the prediction of protein levels and improve the design of synthetic genes.

In the past few years, much work was done to in the field trying to settle whether different codon usage for the same protein results in different expression level is due to secondary structure changes in the mRNA or due to translation efficiency of different codons. The main focus was on the N-terminal codons which are enriched with codons corresponding to rare tRNAs (Tuller et al., 2010a). As first showed on a small library by Kudla et al. (Kudla et al., 2009) and recently, on a much larger library, by Goodman et al. (Goodman et al., 2013) a reduced RNA structure at the 5'-end and not codon rarity itself is responsible for expression increases. This goes along with findings by Li *et al.* (Li et al., 2012) which showed by ribosome occupancy data that on rich medium the rate of translation of all codons in *E. coli* is the same. While the secondary structure seems to be the dominate factor for the N-terminal these results do not explain how codons far from the N-terminal also affect the expression level (Welch et al., 2009). In addition it was recently shown that in amino-acid starvation condition changes in protein expression were due to limited availability of tRNAs (Subramaniam et al., 2013). These limitations should also be taken into account when trying to express proteins in extremely high levels since in that case the synthetic protein codon usage might cause by itself a tRNA shortage in the cell, as suggested by our analysis of the Kudla library (Navon & Pilpel, 2011). Thus, although currently secondary structure is the leading answer I believe that as in many field in biology the answer is not secondary structure or codon translation efficiency but both. Only by understanding both mechanisms and their limitation we will be able to predict when each mechanism will dominate and improve our protein level predictions.

As found in our analysis of the Kudla's library (Kudla et al., 2009) and also shown by Li *et al.* and Subramaniam *et al.* shortage is tRNAs can affect the cell's fitness and protein levels. Thus, to better predict the protein levels we need to gain a better understanding of the tRNA pool. Since measuring the tRNA concentrations in the cell is far from trivial, we would like to learn about it regulation, thus enabling us to predict their levels just from the genomic sequence.

To study the tRNA pool we created a comprehensive tRNA deletion library in *S. cerevisiae*. When deleting the tRNA genes we found that there is extensive backup between the different tRNAs, resulting in robustness to deletion of most tRNA genes. This suggests that either the tRNAs usually transcribed in higher amounts than required for growth in rich medium or that the transcription rate of the remaining genes increases. The idea that decrease in tRNA levels can be sensed by the cell and result is increased transcription rate of related tRNAs is very intriguing and resembles the backup mechanism found between paralog mRNA genes (Kafri *et al.*, 2006).

The tRNA genes are transcribed by RNA polymerase III which binds to internal promoters inside the tRNA sequence. Since many tRNA genes have identical sequences or at least identical internal promoter it is reasonable to expect that those tRNA will have the same transcription rate. Yet, in our study we discovered that even identical tRNA contribute differently to the tRNA pool. The results prove the tRNA surrounding may affect its transcription. We found that upstream motifs maybe the source for the identified differences between the tRNAs. Upstream motifs were shown to affect the tRNA transcription by facilitating the binding of RNA polymerase III (Giuliodori et al., 2003, Parthasarthy & Gopinathan, 2005). This again reminds regulation mechanisms of mRNA transcription by RNA polymerase II and suggests the tRNA transcription is more complex than previously assumed and might be as complex as mRNA transcription. This conclusion is reinforced by our results from microarray analysis of a few tRNA deletion strains where we found up-regulation of RNA polymerase III genes in some deletion strains indicating the ability to regulate of the tRNA transcription.

While mRNA transcription rates is studied and modeled thoroughly (Sharon *et al.*, 2012) the tRNA transcription is neglected. Our work showed the complexity of the tRNA pool and took the first step toward understanding the underling mechanisms that regulate it. Nevertheless, since the tRNA pool may affect the cell's fitness (Navon & Pilpel, 2011) and the protein levels (Subramaniam et al., 2013), it is clear that for better predictions of protein levels we need better predictions of tRNA levels in the cell.

Researching the information coded by the codons it is clear that the most direct question is how the codon usage influences the translation process through the regulation of the ribosome elongation rates. However, codon usage was shown to also affect the mRNA stability (Sunohara et al., 2004, Petersen, 1987, Kolmsee & Hengge, 2011), the protein folding (Pechmann & Frydman, 2013) and even the host fitness, upon expressing the protein (Kudla et al., 2009). The codons affect these properties of the transcript either through the coupling between the mRNA degradation/folding process with the translation process or through additional levels of information overlaid on the codon sequence. For example, different combination of codons result in different nucleotide sequences thus creating/eliminating overlaid information as sequence motifs.

During my research we encountered twice a coupling between the different processes. One of the results of the tRNA deletion library is that some deletion strains have more misfolded proteins and an elevated protein quality control pathway. This result suggests that reduced levels of a specific tRNA in the pool resulted in a reduced translation efficiency of the related codon(s), which in turn changed the ribosome elongation rate and hampered the correct folding of the protein. A coupling between codon usage and folding was also found by others (Pechmann & Frydman, 2013). However, the exact mechanisms are still unclear and our ability to predict which codons are essential for correct folding is still lacking. A unique feature of our approach is that we disrupted translation-folding coupling without manipulating the translated mRNA directly, but only by modifying the tRNA supply.

The second coupling we explored in my research is the coupling between codon usage and mRNA stability. The work by Kudla *et al.* who created a synthetic library of the same GFP protein coded with many different codon combinations revealed that codon usage can affect mRNA level even by 6 fold. Understanding this coupling is essential for synthetic biology in which the promoters are used to optimize transcript levels and codons are used to optimize translation efficiency. In my research I focused on mRNA degradation in *E. coli* and its coupling to the translation process. In bacteria, the mRNA degradation process consists of a series of endonucleolytic cleavages. By combining cleavage site information with ribosome profiling data we found that the ribosomes play a dual role: locally their

accumulation at strategic locations enhances mRNA cleavage immediately upstream, globally their high density on the transcript 5' termini is associated with a tendency to be protected from degradation.

Surprisingly, the ribosome accumulation which enhances the degradation is not caused by slow codons but rather by the affinity of the downstream sequence to the anti-Shine-Dalgarno (aSD) sequence. This result goes along with the discovery by Li *et al.* (Li *et al.*, 2012) who showed that in bacteria ribosome pausing is caused mainly by Shine-Dalgarno like sequences. In addition to the Shine-Dalgarno sequence, which was found to affect the ribosome elongation and mRNA stability, we also found that the cleavage sites themselves are not random and that they occur in locations with specific sequence information. However, not only the sequence is important for cleavage but also the transcript secondary structure, which is required to be single-stranded for cleavage. Thus, the secondary structure is another layer of information that causes indirect coupling between the codons and other cell process.

The work described in this thesis exposes four levels of dependencies between codons and gene expression that should be taken into consideration when designing proteins or trying to predict their expression: The first is the ability of the cell to translate the chosen codons based on the availability of the tRNAs. The second is the order of the codons and the load it exerts on the ribosomes. The third are the motifs and the secondary structure which are the results of specific codon choices. The four and perhaps the most complicated of all is the coupling between the different processes such as translation and degradation or folding. The done work here, from the point of view of the gene expression, was mainly done on *E. coli* while the work on the tRNA pool was done in *S. cereviease*. Due to the many difference between the translation, degradation, maturation and coupling between the different processes in eukaryotes vs. prokaryotes additional work is required in all domain of life.

All together, these studies expand our understanding of the basic processes of gene expression, showing some of the less obvious effect of codon selection and putting forth the extensive coupling between the translation and degradation processes in prokaryotes.

7 Literature

7.1 References

Agris, P. F., (1991) Wobble position modified nucleosides evolved to select transfer RNA codon recognition: a modified-wobble hypothesis. *Biochimie* **73**: 1345-1349.

Agris, P. F., (2004) Decoding the genome: a modified view. *Nucleic Acids Res* **32**: 223-238.

Bailey, T. L. & C. Elkan, (1994) Fitting a mixture model by expectation maximization to discover motifs in biopolymers. *Proc Int Conf Intell Syst Mol Biol* **2**: 28-36.

Bechhofer, D. H. & K. H. Zen, (1989) Mechanism of erythromycin-induced ermC mRNA stability in Bacillus subtilis. *J Bacteriol* **171**: 5803-5811.

Bernstein, J. A., A. B. Khodursky, P. H. Lin, S. Lin-Chao & S. N. Cohen, (2002) Global analysis of mRNA decay and abundance in Escherichia coli at single-gene resolution using two-color fluorescent DNA microarrays. *Proc Natl Acad Sci U S A* **99**: 9697-9702.

Brandt, F., S. A. Etchells, J. O. Ortiz, A. H. Elcock, F. U. Hartl & W. Baumeister, (2009) The native 3D organization of bacterial polysomes. *Cell* **136**: 261-271.

Braun, F., E. Hajnsdorf & P. Regnier, (1996) Polynucleotide phosphorylase is required for the rapid degradation of the RNase E-processed rpsO mRNA of Escherichia coli devoid of its 3' hairpin. *Mol Microbiol* **19**: 997-1005.

Canella, D., V. Praz, J. H. Reina, P. Cousin & N. Hernandez, (2010) Defining the RNA polymerase III transcriptome: Genome-wide localization of the RNA polymerase III transcription machinery in human cells. *Genome Res* **20**: 710-721.

Chan, P. P. & T. M. Lowe, (2009) GtRNAdb: a database of transfer RNA genes detected in genomic sequence. *Nucleic Acids Res* **37**: D93-97.

Cormack, R. S. & G. A. Mackie, (1992) Structural requirements for the processing of Escherichia coli 5 S ribosomal RNA by RNase E in vitro. *J Mol Biol* **228**: 1078-1090.

Crick, F. H., (1966) Codon--anticodon pairing: the wobble hypothesis. *J Mol Biol* **19**: 548-555.

Deana, A. & J. G. Belasco, (2005) Lost in translation: the influence of ribosomes on bacterial mRNA decay. *Genes Dev* **19**: 2526-2533.

Dittmar, K. A., J. M. Goodenbour & T. Pan, (2006) Tissue-specific differences in human transfer RNA expression. *PLoS Genet* **2**: e221.

Dittmar, K. A., M. A. Sorensen, J. Elf, M. Ehrenberg & T. Pan, (2005) Selective charging of tRNA isoacceptors induced by amino-acid starvation. *EMBO Rep* **6**: 151-157.

dos Reis, M., R. Savva & L. Wernisch, (2004) Solving the riddle of codon usage preferences: a test for translational selection. *Nucleic Acids Res* **32**: 5036-5044.

Dreyfus, M., (2009) Killer and protective ribosomes. *Prog Mol Biol Transl Sci* **85**: 423-466.

Duret, L., (2000) tRNA gene number and codon usage in the C. elegans genome are co-adapted for optimal translation of highly expressed genes. *Trends Genet* **16**: 287-289.

Ehretsmann, C. P., A. J. Carpousis & H. M. Krisch, (1992) Specificity of Escherichia coli endoribonuclease RNase E: in vivo and in vitro analysis of mutants in a bacteriophage T4 mRNA processing site. *Genes Dev* **6**: 149-159.

Giuliodori, S., R. Percudani, P. Braglia, R. Ferrari, E. Guffanti, S. Ottonello & G. Dieci, (2003) A composite upstream sequence motif potentiates tRNA gene transcription in yeast. *J Mol Biol* **333**: 1-20.

Goodman, D. B., G. M. Church & S. Kosuri, (2013) Causes and Effects of N-Terminal Codon Bias in Bacterial Genes. *Science*.

Gu, W., T. Zhou & C. O. Wilke, (2010) A universal trend of reduced mRNA stability near the translation-initiation site in prokaryotes and eukaryotes. *PLoS Comput Biol* **6**: e1000664.

Hayes, C. S. & R. T. Sauer, (2003) Cleavage of the A site mRNA codon during ribosome pausing provides a mechanism for translational quality control. *Mol Cell* **12**: 903-911.

Ikemura, T., (1981) Correlation between the abundance of Escherichia coli transfer RNAs and the occurrence of the respective codons in its protein genes. *J Mol Biol* **146**: 1-21.

Ikemura, T., (1982) Correlation between the abundance of yeast transfer RNAs and the occurrence of the respective codons in protein genes. Differences in synonymous codon choice patterns of yeast and Escherichia coli with reference to the abundance of isoaccepting transfer RNAs. *J Mol Biol* **158**: 573-597.

Ikemura, T., (1985) Codon usage and tRNA content in unicellular and multicellular organisms. *Mol Biol Evol* **2**: 13-34.

Kafri, R., M. Levy & Y. Pilpel, (2006) The regulatory utilization of genetic redundancy through responsive backup circuits. *Proc Natl Acad Sci U S A* **103**: 11653-11658.

Kanaya, S., Y. Yamada, Y. Kudo & T. Ikemura, (1999) Studies of codon usage and tRNA genes of 18 unicellular organisms and quantification of Bacillus subtilis tRNAs: gene expression level and species-specific diversity of codon usage based on multivariate analysis. *Gene* **238**: 143-155.

Kanehisa, M. & S. Goto, (2000) KEGG: kyoto encyclopedia of genes and genomes. *Nucleic Acids Res* **28**: 27-30.

Kanehisa, M., S. Goto, Y. Sato, M. Furumichi & M. Tanabe, (2012) KEGG for integration and interpretation of large-scale molecular data sets. *Nucleic Acids Res* **40**: D109-114.

Kolmsee, T. & R. Hengge, (2011) Rare codons play a positive role in the expression of the stationary phase sigma factor RpoS (sigmaS) in Escherichia coli. *RNA Biol* **8**.

Kudla, G., A. W. Murray, D. Tollervey & J. B. Plotkin, (2009) Coding-sequence determinants of gene expression in Escherichia coli. *Science* **324**: 255-258.

Kutter, C., G. D. Brown, A. Goncalves, M. D. Wilson, S. Watt, A. Brazma, R. J. White & D. T. Odom, (2011) Pol III binding in six mammals shows conservation among amino acid isotypes despite divergence among tRNA genes. *Nat Genet* **43**: 948-955.

Li, G. W., E. Oh & J. S. Weissman, (2012) The anti-Shine-Dalgarno sequence drives translational pausing and codon choice in bacteria. *Nature* **484**: 538-541.

Lorenz, R., S. H. Bernhart, C. Honer Zu Siederdissen, H. Tafer, C. Flamm, P. F. Stadler & I. L. Hofacker, (2011) ViennaRNA Package 2.0. *Algorithms Mol Biol* **6**: 26.

Lu, P., C. Vogel, R. Wang, X. Yao & E. M. Marcotte, (2007) Absolute protein expression profiling estimates the relative contributions of transcriptional and translational regulation. *Nat Biotechnol* **25**: 117-124.

Man, O. & Y. Pilpel, (2007) Differential translation efficiency of orthologous genes is involved in phenotypic divergence of yeast species. *Nat Genet* **39**: 415-421.

McDowall, K. J., S. Lin-Chao & S. N. Cohen, (1994) A+U content rather than a particular nucleotide order determines the specificity of RNase E cleavage. *J Biol Chem* **269**: 10790-10796.

Mootha, V. K., C. M. Lindgren, K. F. Eriksson, A. Subramanian, S. Sihag, J. Lehar, P. Puigserver, E. Carlsson, M. Ridderstrale, E. Laurila, N. Houstis, M. J. Daly, N. Patterson, J. P. Mesirov, T. R. Golub, P. Tamayo, B. Spiegelman, E. S. Lander, J. N. Hirschhorn, D. Altshuler & L. C. Groop, (2003) PGC-1alpha-responsive genes involved in oxidative phosphorylation are coordinately downregulated in human diabetes. *Nat Genet* **34**: 267-273.

Navon, S. & Y. Pilpel, (2011) The role of codon selection in regulation of translation efficiency deduced from synthetic libraries. *Genome Biol* **12**: R12.

Parthasarthy, A. & K. P. Gopinathan, (2005) Transcription of individual tRNA1Gly genes from within a multigene family is regulated by transcription factor TFIIIB. *FEBS J* **272**: 5191-5205.

Parthasarthy, A. & K. P. Gopinathan, (2006) Transcriptional activation of a moderately expressed tRNA gene by a positioned nucleosome. *Biochem J* **396**: 439-447.

Paule, M. R. & R. J. White, (2000) Survey and summary: transcription by RNA polymerases I and III. *Nucleic Acids Res* **28**: 1283-1298.

Pechmann, S. & J. Frydman, (2013) Evolutionary conservation of codon optimality reveals hidden signatures of cotranslational folding. *Nat Struct Mol Biol* **20**: 237-243.

Percudani, R., A. Pavesi & S. Ottonello, (1997) Transfer RNA gene redundancy and translational selection in Saccharomyces cerevisiae. *J Mol Biol* **268**: 322-330.

Petersen, C., (1987) The functional stability of the lacZ transcript is sensitive towards sequence alterations immediately downstream of the ribosome binding site. *Mol Gen Genet* **209**: 179-187.

Quax, T. E., Y. I. Wolf, J. J. Koehorst, O. Wurtzel, R. van der Oost, W. Ran, F. Blombach, K. S. Makarova, S. J. Brouns, A. C. Forster, E. G. Wagner, R. Sorek, E. V. Koonin & J. van der Oost, (2013) Differential translation tunes uneven production of operon-encoded proteins. *Cell Rep* **4**: 938-944.

Sharon, E., Y. Kalma, A. Sharp, T. Raveh-Sadka, M. Levo, D. Zeevi, L. Keren, Z. Yakhini, A. Weinberger & E. Segal, (2012) Inferring gene regulatory logic from high-throughput measurements of thousands of systematically designed promoters. *Nat Biotechnol* **30**: 521-530.

Sharp, P. M. & W. H. Li, (1986) An evolutionary perspective on synonymous codon usage in unicellular organisms. *J Mol Evol* **24**: 28-38.

Sharp, P. M. & W. H. Li, (1987) The codon Adaptation Index--a measure of directional synonymous codon usage bias, and its potential applications. *Nucleic Acids Res* **15**: 1281-1295.

Subramaniam, A. R., T. Pan & P. Cluzel, (2013) Environmental perturbations lift the degeneracy of the genetic code to regulate protein levels in bacteria. *Proc Natl Acad Sci U S A* **110**: 2419-2424.

Subramanian, A., P. Tamayo, V. K. Mootha, S. Mukherjee, B. L. Ebert, M. A. Gillette, A. Paulovich, S. L. Pomeroy, T. R. Golub, E. S. Lander & J. P. Mesirov, (2005) Gene set enrichment analysis: a knowledge-based approach for interpreting genome-wide expression profiles. *Proc Natl Acad Sci U S A* **102**: 15545-15550.

Sunohara, T., K. Jojima, H. Tagami, T. Inada & H. Aiba, (2004) Ribosome stalling during translation elongation induces cleavage of mRNA being translated in Escherichia coli. *J Biol Chem* **279**: 15368-15375.

Tuller, T., A. Carmi, K. Vestsigian, S. Navon, Y. Dorfan, J. Zaborske, T. Pan, O. Dahan, I. Furman & Y. Pilpel, (2010a) An evolutionarily conserved mechanism for controlling the efficiency of protein translation. *Cell* **141**: 344-354.

Tuller, T., Y. Y. Waldman, M. Kupiec & E. Ruppin, (2010b) Translation efficiency is determined by both codon bias and folding energy. *Proc Natl Acad Sci U S A* **107**: 3645-3650.

Varenne, S., J. Buc, R. Lloubes & C. Lazdunski, (1984) Translation is a non-uniform process. Effect of tRNA availability on the rate of elongation of nascent polypeptide chains. *J Mol Biol* **180**: 549-576.

Welch, M., S. Govindarajan, J. E. Ness, A. Villalobos, A. Gurney, J. Minshull & C. Gustafsson, (2009) Design parameters to control synthetic gene expression in Escherichia coli. *PLoS One* **4**: e7002.

Wurtzel, O., R. Sapra, F. Chen, Y. Zhu, B. A. Simmons & R. Sorek, (2010) A single-base resolution map of an archaeal transcriptome. *Genome Res* **20**: 133-141.

Wurtzel, O., D. R. Yoder-Himes, K. Han, A. A. Dandekar, S. Edelheit, E. P. Greenberg, R. Sorek & S. Lory, (2012) The single-nucleotide resolution transcriptome of Pseudomonas aeruginosa grown in body temperature. *PLoS Pathog* **8**: e1002945.

Yarian, C., H. Townsend, W. Czestkowski, E. Sochacka, A. J. Malkiewicz, R. Guenther, A. Miskiewicz & P. F. Agris, (2002) Accurate translation of the genetic code depends on tRNA modified nucleosides. *J Biol Chem* **277**: 16391-16395.

Yarus, M., (1982) Translational efficiency of transfer RNA's: uses of an extended anticodon. *Science* **218**: 646-652.

Zaborske, J. M., J. Narasimhan, L. Jiang, S. A. Wek, K. A. Dittmar, F. Freimoser, T. Pan & R. C. Wek, (2009) Genome-wide analysis of tRNA charging and activation of the eIF2 kinase Gcn2p. *J Biol Chem* **284**: 25254-25267.

7.2 List of publications

1. Sivan Navon and Yitzhak Pilpel. Ribosome density governs patterns of mRNA cleavage in *Escherichia Coli*. ***Nucleic Acids Research*** under revision
2. Zohar Bloom-Ackermann, Sivan Navon, Hila Gingold, Ruth Towers, Yitzhak Pilpel and Orna Dahan. Unraveling the Genetic Architecture of the tRNA Pool Using a Comprehensive Deletion Library**.** accepted, **PLOS Genetics**
3. Sivan Navon and Yitzhak Pilpel. The Role of Codon Selection in Regulation of Translation Efficiency Deduced from Synthetic Libraries. **Genome Biology**, Feb. 2011, Volume 12
4. Tamir Tuller, Asaf Carmi, Kalin Vestsigian, Sivan Navon, Yuval Dorfan, John Zaborske, Tao Pan, Orna Dahan, Itay Furman, & Yitzhak Pilpel. An Evolutionarily Conserved Mechanism for Controlling the Efficiency of Protein Translation. **Cell** April 2010; Volume 141, 344-354.

8 Declaration

I hereby declare that this thesis summarizes my independent efforts under the supervision of Yitzhak Pilpel.

The only project performed in collaboration was the tRNA deletion library project. This project was performed in collaboration with Dr. Zohar Bloom-Ackerman which was a fellow PhD student, from Yitzhak Pilpel's laboratory at Weizmann Institute of Science who did all the experimental work. I wrote all the analysis scripts, did the bioinformatics analysis and took part in designing the experiments and analyzing the data.

9 Appendix

9.1 A Comprehensive tRNA deletion library unravels the genetic architecture of the tRNA pool (Bloom-Ackerman *et al.*)

Accepted to Plos Genetic

A Comprehensive tRNA deletion library unravels the genetic architecture of the tRNA pool

Zohar Bloom-Ackermann, Sivan Navon, Hila Gingold, Ruth Towers, Yitzhak Pilpel* and Orna Dahan

Department of Molecular Genetics

Weizmann Institute of science

Rehovot, 76100 Israel

*corresponding author, Pilpel@weizmann.ac.il

November 9, 2013

Abstract

Deciphering the architecture of the tRNA pool is a prime challenge in translation research, as tRNAs govern the efficiency and accuracy of the process. Towards this challenge, we created a systematic tRNA deletion library in *S. cerevisiae*, aimed at dissecting the specific contribution of each tRNA gene to the tRNA pool and to the cell's fitness. By harnessing this resource, we observed that the majority of tRNA deletions show no appreciable phenotype in rich medium, yet under more challenging conditions, additional phenotypes were observed. Robustness to tRNA gene deletion was often facilitated through extensive backup compensation within and between tRNA families. Interestingly, we found that within tRNA families, genes carrying identical anti-codons can contribute differently to the cellular fitness, suggesting the importance of the genomic surrounding to tRNA expression. Characterization of the transcriptome response to deletions of tRNA genes exposed two disparate patterns: in single-copy families, deletions elicited a stress response; in deletions of genes from multi-copy families, expression of the translation machinery increased. Our results uncover the complex architecture of the tRNA pool and pave the way towards complete understanding of their role in cell physiology.

Author Summery

Transfer RNAs are an important component of the translation machinery. Despite extensive biochemical investigations, a systems-level investigation of tRNAs' functional roles in physiology, and genetic interactions among them, are lacking. We created a comprehensive tRNA deletion library in yeast and assessed the essentiality of each tRNA gene in multiple conditions. The majority of tRNA deletions show no appreciable fitness defect when such strains were grown on rich medium. More challenging environmental conditions however revealed a richer set of specific-tRNA phenotypic defects. Co-deletion of tRNA combinations revealed that tRNAs with essential function can be compensated by members of the same or different anti-codon families. Often times, we saw that identical tRNA gene copies contribute deferentially to fitness, suggesting that the genomic context of each gene can affect function. Genome-wide expression changes in response to tRNA deletions revealed two distinct responses. When a deleted tRNA belongs to a family which contain multiple genes with the same anti-codon, the affected cells responded by up-regulating the translation machinery; but upon deletion of singleton tRNAs, the cellular response resembled that of proteotoxic stress. Our tRNA deletion library is a unique resource that offers a way towards fully characterizing the tRNA pool and their important role in cell physiology.

Introduction

Messenger RNA translation is a central molecular process in any living cell and is among the most complicated and highly regulated of cellular processes [1,2]. The tRNA pool is a fundamental component in that process, serving as the physical link between the nucleotide sequence of mRNAs and the amino acid sequence of proteins. In the cycle of translation elongation, tRNA selection is considered the rate-limiting step [3], therefore tRNA availability is one of the major factors that govern translation-efficiency and accuracy of genes [4,5].

Previous studies have established that efficient translation can increase protein levels and provide a global fitness benefit by elevating the cellular concentrations of free ribosomes [6,7], while accurate translation benefits the cell by reducing the metabolic cost of mis-incorporation events [8].

The tRNA pool is composed of various tRNA isoacceptor families, each family carries a different anti-codon sequence that decodes the relevant codon by Watson-Crick base pairing, or codons with non-perfect base pairing of the third nucleotide by the wobble interaction. tRNA families are further classified to isotypes if they carry the same amino acid. In all eukaryotic genomes, each tRNA family can be encoded by a single or multiple gene copies [9,10]. It was previously shown for several organisms that the concentrations of various tRNA isoacceptors positively correlates with the tRNA family's gene copy-number [11,12]. These observations along with detailed analysis of the relationship between gene copy-number of tRNA families and codon-usage, established the notion that the multiplicity of tRNA genes in yeast is not functionally redundant. Such multiplicity might establish the correct balance between tRNA

concentrations and the codon usage in protein-coding genes [13], thus justifying the use of the tRNA gene copy-number as a proxy for actual tRNA amounts [12,14,15].

The transcription of tRNA genes is catalyzed by RNA polymerase III (pol III), promoted by highly conserved sequence elements located within the transcribed region [16]. A genome wide analysis of pol III occupancy in yeast revealed that virtually all tRNA genes are occupied by the pol III machinery [17–19], and are thus considered to be genuinely transcribed. This observation, combined with the fact that tRNA genes within a family are highly similar, led to the notion that all copies within a family contribute equally to the total expression level and hence to the tRNA pool.

Although tRNAs have been extensively studied, until very recently many of the studies were performed on individual genes at the biochemical level. Only in recent years systematic genome-wide approaches started to complement the biochemical approach. These studies reveal a much more complex picture in which pol III occupancy, a proxy for tRNA transcription, varies within families and between tissues [17,20–22]. Expression however does not equal function, and so far no systematic study has been carried out to decipher the specific contribution of each tRNA gene to the tRNA pool and to the cell's fitness.

To study the role of individual tRNAs and the architecture of the entire tRNA pool, we created a comprehensive tRNA deletion library in the yeast *S. cerevisiae.* The library includes 204 deletions of nuclear-encoded tRNA genes out of the total 275 present in the yeast genome. In addition, we created double deletions of selected tRNA gene combinations and of specific tRNAs with a tRNA modifying enzyme. We developed a robotic method to screen and score various fitness

parameters for these deletion strains, and applied it across various growth conditions. This systematic deletion library revealed an architecture of genetic interactions that feature extensive backup-compensations within and between tRNA families. Such compensation capacity endows the organism with robustness to environmental changes and to genetic mutations. We found that different copies within a tRNA family contribute differently to the organism's fitness, revealing a higher level of complexity in the tRNA pool's architecture, possibly at the regulatory level. Finally, we observed two distinct molecular signatures that underlie the cellular response to changes in the tRNA pool. First, the deletion of non-essential single-copy tRNA genes invoked proteotoxic stress responses, indicating a connection between aberrant tRNA availability and protein misfolding. Second, the deletion of representative tRNAs from multi-copy families triggered milder responses by up-regulating genes that are involved in the translation process. Together our results uncover the complex architecture of the tRNA pool reviling a profound effect on cellular fitness and physiology.

Results

Generation of a tRNA deletion library in S. cerevisiae

To gain a better understanding of the functional role of individual tRNA genes and their contribution to the tRNA pool, we created a comprehensive tRNA deletion library in *S. cerevisiae*, where in each strain a single nuclear–encoded tRNA gene was deleted. This methodology is based on recombining a selective marker into the genome at the expense of the deleted gene, as was done in the creation of the yeast ORF deletion library [23] (Figure 1A). A particular challenge in targeting specific tRNA genes for deletion by such a method stems from the high degree of sequence similarity within tRNA families, which can share 100% sequence identity. Consequently, in order to create specific gene deletions, we relied on unique sequences that overlap or flank the tRNA genes (see Supplemental text S1). Our tRNA deletion library contained 204 deletions out of the 275 nuclear-encoded tRNA genes identified in *S. cerevisiae* (see Materials and Methods). These deletions covered all 20 amino acids and 40 of the 42 anti-codon families. The remaining 71 tRNA genes were not deleted due to their complex genomic surrounding, since such deletions might affect neighboring potential features in their genomic vicinities. The library also consisted of 50 strains that represent various combinations of tRNA deletions, and co-deletions of selected tRNAs with the *TRM9* gene which codes for an enzyme that post-transcriptionally modifies tRNA molecules.

Although the majority of tRNA families contain multiple gene copies, there are six single-copy tRNA families in the *S. cerevisiae* genome. Out of these singleton families, four (*tS(CGA)*, *tR(CCG)*, *tQ(CAG) tT(CGU)*) were found to be essential in

our analysis, which confirms previous reports [24–26](see Supplemental text S1). The remaining two singleton families (*tR(CCU)*, *tL(GAG)*) were identified as non-essential upon deletion. All the tRNA genes that belong to multi-copy families were non-essential upon deletion.

Cells were robust to tRNA gene deletions in rich medium but reveal sensitivity in challenging conditions

To assess the contribution of each tRNA gene to cellular growth, we attempted to accurately characterize the growth dynamics of each deletion strain by implementing a robotic method to screen and score growth phenotypes of all tRNA deletion strains in a given growth condition. This fitness measurement approach allowed us to differentiate between physiological effects of the deletion under different growth phases, unlike the competition approaches for fitness measurement [27] that typically integrated all growth phases. We characterized each deletion strain by two growth parameters: growth rate and growth yield, the latter is defined as the size of the population upon entering stationary phase (Figure 1B and Supplemental figure S1A).

We began the characterization of the tRNA deletion library by growing the strains in rich medium. Under this condition, 13% of the deletion strains demonstrated a phenotype in growth rate and 27% showed a growth yield phenotype (Figure 1C-D and Supplemental figure S1B). Most strains exhibited a notable phenotype only in one of the two parameters. Strains that showed altered phenotypes in both growth rate and yield were rare (Supplemental figure S1B). Overall, most tRNA deletion strains did not exhibit any altered growth phenotype in rich medium, indicating robustness to tRNA gene deletion. Seven

percent of the tRNA deletion strains resulted in growth improvement, suggesting that for some genes the cost of retaining them in the genome and/or expressing them may exceed their benefit in this condition. Similar observations were also made on a selection of protein-coding genes in this species [28]. Apart from the singletons whose deletion strains were often dead or exhibit impaired growth, we could not explain the observed growth phenotypes in growth rate or yield by either tRNA family size or amino acid identity (Supplemental figure S2). To further examine the phenotypes of the tRNA deletion strains, we calculated the correlation to the mRNA expression level of adjacent genes and found none (see, Supplemental table S1 figure S3 and Supplemental text S1).

Given that yeast cells are constantly exposed to varying environmental conditions, their tRNA repertoire should differentially accommodate growth in various environments. We next examine whether stressful conditions would retain the robustness observed in rich medium or reveal another set of condition-dependent growth phenotypes. We screened the deletion library under a diverse set of growth conditions including different metabolic challenges and stress-inducing reagents reported in previous studies [29–31]. The fact that the production of tRNA molecules is considered energetically costly [32] prompted us to explore the effect of carbon limitation, alternative carbon sources and minimal medium on tRNA essentiality.

Growing the tRNA deletion library under stressful conditions revealed condition-specific phenotypes (Figure 2A-D, Supplemental table S2). In all but one of the examined conditions (Dithiothreitol-DTT, a reducing agent that also inflicts a general protein-unfolding stress), robustness to tRNA gene deletion was maintained. In the DTT condition, the phenotypes were surprising: while

158 multiple tRNA deletions exhibited impaired growth rates, many also
159 demonstrated growth rate improvements (Figure 2B, 2D). As in the rich medium
160 condition, we could not explain the observed growth phenotypes by either the
161 family size, or the amino acid identity in all of the examined stress conditions.

162 ***Extensive redundancy underlies robustness to tRNA gene deletion***

163 Our observations of robustness to tRNA gene deletions in rich medium, as well as
164 several stressful growth conditions, prompted us to further explore the genetic
165 architecture conferring this phenotype. Given that most tRNA families contain
166 multiple gene copies, we hypothesized that at least part of the observed
167 robustness might be the outcome of compensation provided by the remaining
168 genes in the family. In addition, due to wobble-interactions, robustness may also
169 be the outcome of compensation between families of the same isotype. Focusing
170 on rich medium conditions, we generated selected combinations of multiple
171 tRNA deletions. To examine the first possibility we created deletions of entire
172 two-member and three-member tRNA families. As shown in figure 3A such
173 family deletions resulted in either lethality (indicating a loss of the family's
174 function), or viability with growth impairment (indicating a partial
175 compensation of the family's function by other families).

176 We then turned to examine in more detail the interactions within these essential
177 three-gene families by examining the growth of various double deletion strains.
178 Contrary to the common notion that suggests little or no functional redundancy
179 between tRNA gene copies [13], we observed that in each of these families any
180 one family member can sustain normal or near-normal fitness (Figure 3A,
181 Supplemental figure S4A-B and Supplemental table S3). Similar observations

were made for essential two-gene families upon one member's deletion (Figure 3A). Such results can either imply that yeast cells carry more tRNA copies than are actually needed to sustain growth under optimal growth conditions, or that a responsive backup mechanism might be at work, one that provides compensation by increasing the transcription of the remaining copies, as was previously observed in protein-coding genes [33–35]. We thus decided to investigate the expression levels of certain tRNA families, using RT-qPCR (Figure S5). For each deletion, we compared the expression level of the remaining copies belonging to the designated family to that of a wild-type strain. We observed in most strains an expected reduction in expression of the respective family. These findings suggest that in these families, tRNA supply exceeds the demand under rich medium conditions (Figure S5A). However in some cases there were no such decreases in expression, there were even observable increases, demonstrating that a responsive backup mechanism may have been at work, inducing the expression of the remaining family members following deletion of a certain member (Figure S5B).

Next, we turned to examine the surprising cases in which the deletion of an entire tRNA gene family resulted in a viable strain. We reasoned that in these cases a different type of compensation, which is based on wobble interactions across iso-acceptor families, came into play. To decipher this compensation mechanism we focused on the genetic interactions involving the two non-essential singleton families, *tL(GAG)* and *tR(CCU)* (Figure 3A).

In the absence of *tL(GAG)*, the members of the *tL(UAG)* family represent the sole tRNA that can decode the CUN Leucine codons, and might be a candidate for providing compensation upon deletion of *tL(GAG)* even though such decoding

does not match the classic wobble rules [36]. Co-deletion of *tL(GAG)* with one of the *tL(UAG)* gene copies resulted in growth aggravation and negative epistasis. Deletion of the *tL(GAG)* together with two copies of the *tL(UAG)* family was lethal despite the fact that one copy of *tL(UAG)* still remained in the genome, indicating that a single *tL(UAG)* gene was insufficient to compensate for the loss of *tL(GAG)* (Figure 3B). The genetic interaction between *tL(UAG)* and *tL(GAG)* appeared specific, since co-deleting one copy of the *tL(UAG)* family together with two additional tRNA genes (*tL(CAA)G3* and *tW(CCA)G1*) did not generate observable epistasis in either case (Figure 3B). We thus concluded that the *tL(UAG)* family is partially redundant to the *tL(GAG)* family, yet such redundancy was not sufficient to completely compensate for the loss of *tL(GAG)*.

Similarly, the viability of the *tR(CCU)* deletion strain could be due to compensation provided by the 11 copies of the *tR(UCU)* family. Indeed the wobble rules are consistent with this assumption, but such interaction was never functionally demonstrated. Formally, demonstrating that the *tR(UCU)* family can compensate for the loss of the singleton *tR(CCU)* would amount to co-deleting all 12 tRNA genes. Looking for simpler means, we decided on a more economic, albeit indirect way. We co-deleted the singleton *tR(CCU)* with the Trm9 enzyme, which is responsible for methylating the third anticodon position of *tR(UCU)* and *tE(UUC)* [37]. It was previously shown that such methylation is needed for supporting the wobble interaction between *tR(UCU)* tRNAs and the AGG codon (the cognate codon of the CCU anti-codon)[37]. The *tR(CCU)–trm9* double deletion strain was viable, but exhibited an appreciable aggravation of growth yield (Figure 3A and 3C). Thus our results confirm that the methylated *tR(UCU)* family can partially compensate for the loss of *tR(CCU).* We attempted to define a

more general role for the Trm9 modification enzyme in modulating the compensation mechanism between tRNA families. To this end we created 10 additional double deletions of the enzyme along with each of 10 tRNA genes from two glutamic acid families, one that is modified by the enzyme and one that is reportedly not modified by the enzyme [38] (see Supplemental figure S6). No epistasis was detected between the enzyme and any of these 10 tRNAs and hence, the data cannot support or exclude a putative similar role of the enzyme beyond the *tR(UCU)* family.

We thus conclude that there are two mechanisms that can account for the observed robustness for tRNA deletions under favorable growth conditions. The first is redundancy within a family, and its efficiency appears to be independent of the number of remaining tRNA gene copies. The second is compensation between families, which operates via wobble interactions.

Identical tRNA genes contributed differentially to cellular fitness

We then asked whether all copies within a family contribute equally to the tRNA pool. It is often implicitly assumed that all tRNA copies contribute similarly to the cellular tRNA pool. However, comparison of the growth parameters of tRNA deletions from the same family revealed marked differences between seemingly identical family members. In particular, under rich medium, 21 out of the 32 deletions examined from multi-copy families showed growth yield differences spanning a broad range of at least 10% (Figure 4A). Such differences were also detected in the growth rate parameter (Supplemental figure S7A) although they were less pronounced. We thus focus on the growth yield parameter in all further analysis. The phenomenon of differential contribution to fitness by

256 different family members was further enhanced when we grew the deletion
257 strains on more challenging conditions such as low glucose (Figure 4B and
258 Supplemental figure S7B). To further investigate the genetic interactions
259 between differentially contributing tRNA copies within a given family, we
260 focused on the *tR(UCU)* family.
261 The *tR(UCU)* family contains 11 identical copies in the genome, 5 of which were
262 represented in our library. In rich medium, two copies (*tR(UCU)E* and
263 *tR(UCU)M2*) showed appreciable reduction in growth yield (termed Major
264 copies), while deletions of the other three copies (*tR(UCU)M1*, *tR(UCU)G1* and
265 *tR(UCU)K*) grew essentially as the wild-type (termed Minor copies). Introducing
266 a plasmid with the appropriate tRNA gene copy complemented the growth of all
267 deleted copies (Supplemental figure S7C). To further assert the separation
268 between the Major and Minor copies, we examined various pair-wise deletion
269 combinations of these members. All pairs that included at least one Major
270 member exhibited growth impairment upon deletion, while pairs that consisted
271 of only Minor copies demonstrated either a slight growth defect or none at all
272 (Figure 4C). Further analysis of genetic interactions of these family members
273 with either the *TRM9* gene, or with the above mentioned *tR(CCU)* gene that
274 belongs to a different Arginine family, revealed a similar effect (Figure 4C). These
275 results indicate that the loss of different *tR(UCU)* genes in the same genetic
276 background does not affect the phenotype equally, Major copies are more
277 essential than Minor copies and as such are also more essential in providing
278 compensation within the family.
279 We next turned to examine whether the hierarchy of Major and Minor copies is
280 preserved across various stress conditions (Figure 4D). Examining essentiality in

281 several conditions, we observed the same phenomenon in which Major copies
282 demonstrated a stronger effect on growth compared to Minor copies in most
283 stress conditions. We also noted that the Minor copies showed a diverse
284 response ranging from slight growth improvement, wild-type level growth to
285 observable growth impairment. A potential scenario may be one in which the
286 Major copies always actively contribute to the pool, while the Minor copies might
287 be recruited at times of need to maintain efficient translation. Thus, the loss of a
288 Major copy could only be partially compensated by the remaining copies.
289 Following these observations, we turned to examine possible genetic elements
290 that might promote the phenomenon of differential contribution. Since all family
291 members have identical sequence, we hypothesized that differential contribution
292 should be due to differences in the vicinity of tRNA genes. To demonstrate this
293 notion we performed a complementation assay, introducing different tRNAs
294 from the UCU family, along with 200bp of their flanking sequences, to the
295 *tR(UCU)M2* deletion strain. We observed different degrees of complementation.
296 Given that different constructs differ only in the region flanking the tRNA gene,
297 the variation in complementation capability can be attributed to the different
298 sequences flanking the tRNA (Supplemental figure S7D). The effect of sequences
299 that flank tRNA genes on their transcription was reported in multiple
300 studies[39–42]. In one such study Giuliodori *et al*. [42] preformed an analysis of
301 conserved sequence elements upstream of *S. cerevisiae* tRNA genes. They
302 identified four conserved sequence elements located at positions -53 (T-rich), -
303 42(TATA-like), -30(T-rich) and -13 (pol III TSS) with respect to the first
304 nucleotide of the mature tRNA. We used these results to examine the entire tRNA
305 deletion library and checked whether tRNA deletions that exhibited or that did

not exhibit altered phenotype in rich medium revealed enrichment for any particular motif (Figure 4E). We found that deletions exhibiting phenotypes of growth impairment were significantly enriched for the presence of specific motifs. In particular, deleted strains that exhibited impairment in growth yield had an enrichment for the TATA-like motif at position -42. In addition, the TSS motif at position -13 was enriched in deletion strains that exhibited impairment in both growth rate and yield. To reinforce these observations, we ran the MEME motif search algorithm [43] to screen the upstream sequences of tRNA deleted strains exhibiting impaired growth yield for enriched motifs (see Materials and Methods). Two significant motifs were found that resemble those reported by Giuliodori *et al*. in both sequence and location (Figure 4F).

Together these results indicate that the contribution to the tRNA pool and cellular fitness of different copies of the same tRNA family are far from equal. We provide one possible explanation, which can account for the differential essentiality, implying that the sequences flanking tRNA genes play a role in determining their expression level.

Physiological effects of tRNA gene deletions on protein folding

As mentioned above, screening the tRNA deletion library in the presence of the reducing agent Dithiothreitol (DTT), a drug that exerts a proteotoxic stress in the cell, showed severe phenotypic defect in many deletion mutants (Figure 2A, B). Yet, many of the strains that demonstrated growth reduction in other conditions were less sensitive than wild-type to this drug (Figure 2C, D). These findings point towards a connection between tRNA functionality and the protein folding state in the cells. To further explore this connection, we turned to thoroughly

characterize a selection of tRNA deletions in the presence of various proteotoxic agents. We chose two deletion mutants that exhibited either impaired or wild-type growth under DTT, namely (*tR(UCU)M2 and tH(GUG)G1),* both members of multi-copy families designated the MC group. In addition to the two viable single gene deletions (*tR(CCU)J* and *tL(GAG)G*), the initiator methionine *tiM(CAU)C* also demonstrated improved growth; we thus designated these three strains the SC group.

The various strains were treated with either DTT, Azetidine 2 carboxylic acid (AZC)- a toxic analog of proline [44], or Tunicamycin- a drug used to induce the unfolded protein response (UPR) in the endoplasmic reticulum (ER) [45]. The growth of each strain was characterized under each proteotoxic agent applied at several concentrations. The strains in the MC group demonstrated either growth impairment or wild-type growth under all examined conditions. However, the deletions of single-copy tRNAs and to some extent the imitator methionine demonstrated reduced sensitivity to all three proteotoxic agents (Figure 5A-C). The differences in relative growth for all the examined strains were apparent even at low concentrations and were consistent upon increase in the concentrations of these proteotoxic agents (Figure 5A-C).

The fact that the tRNA deletion strains from the SC group are resistant to proteotoxic agents led us to hypothesize that deleting these genes might inflict intrinsic and chronic misfolding stress, even at the absence of the drug. This stress results in the activation of relevant cellular response that protects cells from the aggravating effect of extrinsic proteotoxic stress. Such an effect is reminiscent of the cross protection effect observed between environmental

stressors [46], yet here it is manifested between a genetic perturbation and an environmental stress.

To directly examine whether changes in the tRNA pool induce proteotoxic stress in these strains, we examined the state of the protein quality control machinery using the naturally unstructured human protein VHL as a proteotoxic stress reporter [47]. In this system, the VHL protein can be destined to one of two cellular localizations. If the cell experiences protein-folding stress, the heterologous protein VHL will aggregate in inclusions (or puncta) due to saturation of the protein quality control machinery. In contrast, under normal conditions, the quality control machinery is available to properly deal with this naturally unfolded heterologous protein, thus it remains soluble in the cytoplasm and no inclusions are formed. For each of the five deletion strains, we quantified the number of VHL inclusions (puncta) in populations of yeast cells. This analysis revealed that indeed the tRNA deletions in the SC group exhibited a significant increase in the number puncta containing cells relative to the wild-type (Figure 5D and 5F), indicating saturation of the quality control machinery caused by intrinsic proteotoxic stress. The MC group did not exhibit inherent proteotoxic stress; their puncta containing cells count resembled that of the wild-type.

The inherent chronic proteotoxic stress observed for the SC deletions might provide them with the capacity to respond better to an additional external proteotoxic stress. To further explore this possibility we examined the state of the protein quality control machinery upon extrinsic proteotoxic stress induced by treatment with AZC. Treating the wild-type cells with AZC resulted in a rapid accumulation of the VHL protein in stress foci, indicated by increase in the occurrence of multiple inclusions [48]. As anticipated, the behavior of the SC

group demonstrated a significant increase in the presence of a single punctum upon AZC treatment, however the appearance of stress foci (multi-puncta) was significantly lower compared to the wild-type and to the MC group (Figure 5E and 5G). As in the previous experiment, the deletions of the MC group responded in a similar manner to that of the wild-type, displaying increased number of stress foci.

These results thus indicate that the deletion of some tRNA genes induced an inherent proteotoxic stress in the cell, demonstrating a physiological role of proper tRNA supply in protein folding by an undetermined mechanism. Such physiological response renders these cells relatively less sensitive, compared to other tRNA deletion strains and the wild-type, from the otherwise harmful effect of proteotoxic drugs.

Different molecular responses to deletions of tRNAs from single and multiple copy families

To determine whether changes in the tRNA pool result in a distinct molecular signature, we examined the same set of tRNA deletions (SC and MC groups) using mRNA microarrays. For each strain, we measured genome-wide changes in mRNA levels compared to the wild-type, under rich growth conditions. The expression changes we observed were modest and demonstrated a correlation between the essentiality of the tRNA gene and the extent of changes in mRNA expression upon its loss. Hierarchical clustering of the strains according to similarity in expression changes (Fig 6A and supplemental figure S8), revealed that the strains could be divided into two groups recapitulating the division to the SC and MC groups. An example for this division can be found in the

pronounced effect observed for the *COS8* gene. This gene was extremely up-regulated (about 16 fold) in the SC group while unchanged in the MC group (Figure 6B). These results suggest different molecular signatures for the two groups, which are also related to the proteotoxic stress response.

To determine the responses and the underling molecular pathways that differentiate these two groups, we examined which KEGG pathways [49,50] differentiate between them. We used Gene Set Enrichment Analysis (GSEA), a computational software which determines whether a defined set of genes shows statistically significant differences between two biological states [51,52]. This analysis revealed a somewhat opposite signature between the two groups (Table 1 and supplemental figure S8). Pathways which are responsive to proteotoxic stress such as the Proteasome (FDR q-value <1E-5) and Protein processing in endoplasmic reticulum (FDR q-value 2E-3) were significantly induced in the SC group relative to the MC group. While in the MC groups, translation-related pathways such as Ribosome biogenesis (FDR q-value <1E-5) and Ribosome (FDR q-value 1E-4) were significantly induced compared to the SC group.

To further characterize these differences we focused on specific pathways. A more detailed examination of the expression changes observed for all the genes that constitute the proteasome complex revealed an up-regulation to various extents in response to deletion of tRNAs from the SC group. The MC group demonstrated no change and even a slight down-regulation of these genes (Figure 6C), a trend which was further verified using RT-qPCR (Figure 6D). These observations establish the notion that cells experience proteotoxic stress upon deletion of members of the SC group. A further indication of proteotoxic stress in these deletion strains is the up regulation of *COS8*. The exact biological

function of this gene is still unclear, it was however found to interacts with *IRE1*, which is a hallmark regulator of the unfolding stress response [53].

An interesting distinction between the groups was also observed in the pathway consisting of the RNA polymerase machinery. Expression of genes that belong to this pathway were up-regulated only in the MC group (Table 1). Separating the RNA polymerase genes into modules corresponding to the different polymerases, revealed an interesting pattern. While the genes that encode RNA Pol II subunits did not change in any of the tRNA deletion strains (Supplemental figure S9), the genes encoding RNA Pol III machinery (the polymerase responsible for tRNA gene transcription) demonstrated up-regulation in the MC group and no change or even down regulation in the SC group (Figure 6E). These results were further verified by RT-qPCR (Figure 6F). Up-regulation of the pol III machinery for the MC group may suggest that in some MC deletion strains, the transcription of the remaining tRNA genes could increase, thus providing a possible molecular mechanism for backup compensation within families. Such response to deletions of tRNAs from the MC group could indicate the presence of a negative feedback loop, allowing the cell to respond to changes in the tRNA pool in the attempt to regain steady state levels.

Discussion

In this study, we investigated the genetic architecture of the tRNA pool and its effect on cellular fitness using a comprehensive tRNA deletion library. We found extensive dispensability of many tRNA genes, especially under optimal growth conditions. Such lack of essentiality has been studied in protein-coding genes, and is often interpreted to reveal a role for partially redundant genes and pathways providing backup compensation for the deleted gene [33,34,54–56]. Similar design principles are displayed in the architecture of tRNA genes, which exhibited significant gene redundancy and compensation (either partial or complete) among family members. An additional reason for apparent lack of essentiality of genes is the limited set of examined environmental challenges, and it was indeed shown for protein-coding genes that challenging gene deletion libraries to less favorable conditions exposes more essentiality [57,58]. We showed that a similar situation holds for tRNA genes. We found condition-specific functional roles for tRNAs, demonstrating increased demand for certain tRNA genes under certain defined conditions. This implies that the compensation within tRNA families changes across conditions. Such changes in the essentiality of tRNA genes can imply that the tRNA pool is dynamic and changes across conditions to accommodate cellular needs, as was recently suggested [59].

Further, we have discovered interesting architecture within families, which questions the prior notion that all tRNA gene copies contribute equally to the pool. Previous work has shown that Pol III transcription machinery displays different occupancy levels at various copies of the same tRNAs in the genome [21,22,60]. However, the potential phenotypic consequences of such

transcriptional differences have not been previously explored. We report that the flanking sequences around each tRNA gene contains motifs that are predictive of the deletion phenotypic consequences, potentially affecting pol III transcription machinery.

We further speculate that some tRNA genes, i.e. the Major copies, might be active across all conditions and with only partial functional redundancy, thus their loss cannot be fully compensated. Minor copies on the other hand are either not transcribed or have a modest contribution to the tRNA pool, with complete functional redundancy by other copies, thus their loss can be fully compensated. Such architecture could provide the cell with means to respond in a dynamic manner to changes in the environment, by transcribing varying portions of the members of each tRNA family depending on demand. As such, differential contribution within tRNA families exposed an additional novel mean to regulate the tRNA pool and as a consequence to regulate the translation process.

An interesting finding was that changes in the tRNA pool elicit molecular changes in the cells even when no severe phenotype is detected. Our results demonstrated two distinct molecular signatures which can be attributed to the family architecture and the severity of the changes in the pool. Upon deletion of the two viable single copy tRNAs, and also upon deletion of one of the initiator tRNA methionine copies, the cell exhibited a response reminiscent of a proteotoxic stress. We were able to identify such a stress in these mutant cells. Although the exact mechanisms by which changes in the tRNA pool induces proteotoxic stress remains to be determined, we hypothesize that the elimination or reduction in these tRNAs may lead to events of amino acid misincorporation, ribosome frame-shifting or stalled protein synthesis

terminations. Such events would have a clear impact on the protein quality control machinery of the cell by titrating chaperons to deal with misfolded or misassembled proteins. Translation errors such as incorrect tRNA selection and incorrect tRNA aminoacylation have been shown to induce proteotoxic stress in yeast [61,62]. Given that cells exploit chaperon availability as a sensing mechanism to induce a stress response [63,64], translation errors may lead to the onset such a response. On the other hand, deletions of tRNAs from multi-copy families results in milder effects on the tRNA pool due to the extensive redundancy or backup-compensation, and they indeed elicit a different cellular response from the one invoked upon deletion of single-member families. In the response to deletion of members from multi-gene families, the pol III transcription machinery seems to be up regulated. Such up-regulation would bring about induced transcription of tRNAs, this would act as a feedback mechanism to bring the tRNA pool closer to its normal state [65]. At least in one case (Supplemental figure S5) our results suggest the existence of such responsive backup among tRNA genes from the same family. Yet, a clearer relationship between changes in the tRNA pool, pol III activation, and tRNA transcription is still lacking. Regardless of the actual mechanism that determines the exact cellular response to tRNA deletions, the fact that such a response wiring exists may be beneficial for maintaining cellular robustness upon environmental changes and mutations.

This work provides for the first time a systemic tool to study the functional role of individual tRNA genes. Using this deletion library, we discovered a much more complex picture than was previously known. We anticipate that a high throughput mapping of all genetic interactions between pairs of tRNA genes (as

done for protein-coding genes) [66,67] would reveal the full genetic network. In addition, it might reexamine and potentially refine the wobble interaction rules from a genetic, rather than the traditional biochemical/structural perspective. The design principles defined in this study, consisting of massive gene redundancy as well as differential contribution of gene copies may provide cellular plasticity and allow the tRNA pool to accommodate various growth conditions and developmental planes. Deciphering the effects of tRNA variations as is found in some diseases such as cancer [68] and Huntington [69] can provide possible routes for future treatment. We provide this novel set of minimalist genetic perturbations in the translation machinery as a resource to the yeast community towards further characterization of this highly complex process as well as additional cellular processes.

Materials and Methods

Creation of tRNA deletion library

The complete tRNA pool of *S. cerevisiae* was obtained from the tRNA genomic database [70], where 286 tRNA genes are annotated. 13 tRNA genes are encoded by the mitochondrial genome and the remaining are nuclear-encoded. Here we focused on the nuclear-encoded tRNAs. Two tRNA genes that are annotated in this database as not determined, belong to the *tS(GCU)* family. Thus, the *tS(GCU)* family contains two additional members, *tS(GCU)L* and *tS(GCU)D* , both verified by PCR, bringing the total number of nuclear encoded tRNA genes to 275. Deletion strains were constructed using a PCR-based gene deletion [71,72], in the genetic background of the Y5565 strain (*MATα, can1Δ::MFA1pr-HIS3, mfα1Δ::MFα1pr-LEU2, lyp1Δ, ura3Δ0, leu2Δ0*). The *S. cerevisiae* strain S288C reference genome sequence R57-1-1 downloaded from the Saccharomyces Genome Database was used for primer design. Each deletion construct contained 45 bp flanking or overlapping a tRNA sequence for specific recombination event, a unique barcode and the HPH antibiotics 'cassette', conferring resistance to the antibiotic hygromycin B, [73]. PCR products were transformed into yeast cells and single colonies were verified by PCR. Three colonies from each strain were used to verify phenotypes in growth analysis. A wild-type strain in which the same antibiotic marker was integrated 200bp upstream of the *tL(CAA)L3* locus was created as a control and was used in all analyses as wild-type. A complete list of all plasmids, yeast strains and PCR fragments can be found in Supplemental text S1 and Supplemental table S5.

555 ***Measurements of growth using OD reads***

556 Strains were grown for two days at 30^{o}C in YPD (1% yeast extract, 2% peptone,
557 2% glucose), diluted (1:50) into the appropriate medium in U-bottom 96-well
558 plates and grown at 30^{o}C (using TECAN Freedom EVO robot). The OD of the
559 population in each plate was monitored every 30 minutes using a
560 spectrophotometer at 600 nm (INFINITE200-TECAN). Each plate contained a
561 wild-type strain to which the growth parameters of the deletions strains were
562 normalized. The OD reads served for growth analysis and extraction of growth
563 parameters. At least 3 biological repeats and 36 technical repeats were
564 performed for each strain in each condition. Complete description of analysis and
565 normalization procedures are provided in the Supplemental text S1.

566 ***Yeast growth conditions***

567 Library strains were screened in the following growth conditions: YPD, SCD
568 (0.67% Bacto-yeast nitrogen base w/o amino acids 2% glucose supplemented
569 with amono acids), YP supplemented with 0.025% glucose, YP supplemented
570 with 1% galactose, YPD supplemented with 0.5M NaCl, SCD supplemented with
571 1.5mM DTT. Growth measurements were also performed on YPD supplemented
572 with increasing concentrations of the proteotoxic agents DTT, AZC and
573 Tunicamycin.

574 ***Motif Analysis***

575 A sequence motif analysis was performed using the MEME online software [43].
576 The motif search was done on the upstream sequence of tRNA genes which
577 exhibited a yield impairment phenotype in rich medium upon deletion (42
578 genes) versus the upstream sequence of tRNA genes which exhibited a

phenotype in no more than two out of the six conditions (99 genes). To apply location constrains on the motifs, the MEME analysis was done in windows of size 9bp, looking for motifs of 4-8bp in length.

Analysis of protein quality control using VHL-CHFP reporter

Wild-type and tRNA deletion strains harboring the pGAL-VHL-mCherry (CHFP) fusion were grown overnight on SCD+2% raffinose, diluted into SCD+2% galactose and grown at 30°C for 6 hours. Cells were visualized using an Olympus IX71 microscope controlled by Delta Vision SoftWoRx 3.5.1 software, with X60 oil lens. Images were captured by a Photometrics Coolsnap HQ camera with excitation at 555/28 nm and emission at 617/73 nm (mCherry). Images were scored using the ImageJan Image Processing and Analysis software. The percentage of cells harboring VHL-CHFP foci was determined by counting at least 500 cells for each strain in three biological repetitions. Protein un-folding stress was induced with AZC at a concentration of 2.5 mM AZC (Sigma) following induction with galactose.

Analysis of genome wide expression changes

Cultures were grown in YPD medium at 30°C to a cell concentration of $1.5*10^7$ cells/ml. Cells were then harvested, frozen in liquid nitrogen, and RNA was extracted using MasterPure™ (EPICENTER Biotechnologies). The quality of the RNA was assessed using the BIOANALYZER 2100 platform (AGILENT); samples were then processed and hybridized to Affymetrix yeast 2.0 microarrays using the Affymetrix GeneChip system according to manufacturer's instructions. The background adjustment was done using the Robust Multi-array Average (RMA) procedure followed by quintile normalization.

For each strain, the fold change in expression for all genes was calculated by comparing the wild-type measurement in the same batch and averaged over two biological repeats.

Microarray analysis

The cluster tree is based on the correlation between the mRNA fold change of the different strains. For the clustering we used the top 50% of the sorted genes based by the gene variance across the strains.

Microarray data access

The data from this study have been submitted to the NCBI Gene Expression Omnibus (GEO) under accession number GSE47050. A list of the measured fold changes for all genes in each strain can be found in Supplemental table S4.

RT-qPCR measurements

Cultures were grown in YPD medium at 30°C to a cell concentration of $1*10^7$ cells/ml. RNA was extracted using MasterPure™ (EPICENTER Biotechnologies), and used as a template for quantitative RT–PCR using light cycler 480 SYBR I master (Roche)(LightCycler 480 system) according to the manufacture instructions. A list of the primers can be found in Supplemental table S6.

Acknowledgments:

We thank all the members of the Pilpel lab for many fruitful discussions. We thank Daniel Kaganovich for providing the VHL-CHFP yeast plasmids. We thank Sebastian Leidel and Refael Ackermann for critical reading of the manuscript. We thank Ilya Soifer for assistance with the Robotic system. We thank Ofer Moldovsky, Yifat Cohen and Tslil Ast for their assistance with the VHL-CHFP system and the microscope analysis. We thank Nir fluman for assistance with the protein measurements.

References

1. Kozak M (2005) Regulation of translation via mRNA structure in prokaryotes and eukaryotes. Gene 361: 13–37. doi:10.1016/j.gene.2005.06.037.
2. Jackson RJ, Hellen CUT, Pestova T V (2010) The mechanism of eukaryotic translation initiation and principles of its regulation. Nature reviews Molecular cell biology 11: 113–127. doi:10.1038/nrm2838.
3. Varenne S, Buc J, Lloubes R, Lazdunski C (1984) Translation is a non-uniform process. Effect of tRNA availability on the rate of elongation of nascent polypeptide chains. Journal of molecular biology 180: 549–576.
4. Kudla G, Murray AW, Tollervey D, Plotkin JB (2009) Coding-sequence determinants of gene expression in Escherichia coli. Science (New York, NY) 324: 255–258. doi:10.1126/science.1170160.
5. Stoletzki N, Eyre-Walker A (2007) Synonymous codon usage in Escherichia coli: selection for translational accuracy. Molecular biology and evolution 24: 374–381. doi:10.1093/molbev/msl166.
6. Plotkin JB, Kudla G (2011) Synonymous but not the same: the causes and consequences of codon bias. Nature reviews Genetics 12: 32–42. doi:10.1038/nrg2899.
7. Gingold H, Pilpel Y (2011) Determinants of translation efficiency and accuracy. Molecular systems biology 7: 481. doi:10.1038/msb.2011.14.
8. Drummond DA, Wilke COC (2008) Mistranslation-induced protein misfolding as a dominant constraint on coding-sequence evolution. Cell 134: 341–352. doi:10.1016/j.cell.2008.05.042.
9. Bermudez-Santana C, Attolini CS-O, Kirsten T, Engelhardt J, Prohaska SJ, et al. (2010) Genomic organization of eukaryotic tRNAs. BMC genomics 11: 270. doi:10.1186/1471-2164-11-270.
10. Goodenbour JM, Pan T (2006) Diversity of tRNA genes in eukaryotes. Nucleic acids research 34: 6137–6146. doi:10.1093/nar/gkl725.
11. Kanaya S, Yamada Y, Kinouchi M, Kudo Y, Ikemura T (2001) Codon usage and tRNA genes in eukaryotes: correlation of codon usage diversity with translation efficiency and with CG-dinucleotide usage as assessed by multivariate analysis. Journal of molecular evolution 53: 290–298. doi:10.1007/s002390010219.
12. Tuller T, Carmi A, Vestsigian K, Navon S, Dorfan Y, et al. (2010) An evolutionarily conserved mechanism for controlling the efficiency of protein translation. Cell 141: 344–354. doi:10.1016/j.cell.2010.03.031.
13. Percudani R, Pavesi A, Ottonello S (1997) Transfer RNA gene redundancy and translational selection in Saccharomyces cerevisiae. Journal of molecular biology 268: 322–330. doi:10.1006/jmbi.1997.0942.
14. Man O, Pilpel Y (2007) Differential translation efficiency of orthologous genes is involved in phenotypic divergence of yeast species. Nature genetics 39: 415–421. doi:10.1038/ng1967.
15. Pechmann S, Frydman J (2012) Evolutionary conservation of codon optimality reveals hidden signatures of cotranslational folding. Nature structural & molecular biology advance on. doi:10.1038/nsmb.2466.

16. Dieci G, Fiorino G, Castelnuovo M, Teichmann M, Pagano A (2007) The expanding RNA polymerase III transcriptome. Trends in genetics : TIG 23: 614–622. doi:10.1016/j.tig.2007.09.001.
17. Canella D, Praz V, Reina JH, Cousin P, Hernandez N (2010) Defining the RNA polymerase III transcriptome: Genome-wide localization of the RNA polymerase III transcription machinery in human cells. Genome research 20: 710–721. doi:10.1101/gr.101337.109.
18. Roberts DN, Stewart AJ, Huff JT, Cairns BR (2003) The RNA polymerase III transcriptome revealed by genome-wide localization and activity-occupancy relationships. Proceedings of the National Academy of Sciences of the United States of America 100: 14695–14700. doi:10.1073/pnas.2435566100.
19. Moqtaderi Z, Struhl K (2004) Genome-wide occupancy profile of the RNA polymerase III machinery in Saccharomyces cerevisiae reveals loci with incomplete transcription complexes. Molecular and cellular biology 24: 4118–4127. doi:10.1128/MCB.24.10.4118.
20. Dittmar KA, Goodenbour JM, Pan T (2006) Tissue-specific differences in human transfer RNA expression. PLoS genetics 2: e221. doi:10.1371/journal.pgen.0020221.
21. Raha D, Wang Z, Moqtaderi Z, Wu L, Zhong G, et al. (2010) Close association of RNA polymerase II and many transcription factors with Pol III genes. Proceedings of the National Academy of Sciences of the United States of America 107: 3639–3644. doi:10.1073/pnas.0911315106.
22. Kutter C, Brown GD, Gonçalves A, Wilson MD, Watt S, et al. (2011) Pol III binding in six mammals shows conservation among amino acid isotypes despite divergence among tRNA genes. Nature genetics 43: 948–955. doi:10.1038/ng.906.
23. Brachmann CB, Davies A, Cost GJ, Caputo E, Li J, et al. (1998) Designer deletion strains derived from Saccharomyces cerevisiae S288C: a useful set of strains and plasmids for PCR-mediated gene disruption and other applications. Yeast (Chichester, England) 14: 115–132. doi:10.1002/(SICI)1097-0061(19980130)14:2<115::AID-YEA204>3.0.CO;2-2.
24. Chakshusmathi G, Kim S Do, Rubinson DA, Wolin SL (2003) A La protein requirement for efficient pre-tRNA folding. The EMBO journal 22: 6562–6572. doi:10.1093/emboj/cdg625.
25. Weiss WA, Friedberg EC (1986) Normal yeast tRNA(CAGGln) can suppress amber codons and is encoded by an essential gene. Journal of molecular biology 192: 725–735.
26. Johansson MJO, Esberg A, Huang B, Björk GR, Byström AS (2008) Eukaryotic wobble uridine modifications promote a functionally redundant decoding system. Molecular and cellular biology 28: 3301–3312. doi:10.1128/MCB.01542-07.
27. Breslow DK, Cameron DM, Collins SR, Schuldiner M, Stewart-Ornstein J, et al. (2008) A comprehensive strategy enabling high-resolution functional analysis of the yeast genome. Nature methods 5: 711–718. doi:10.1038/nmeth.1234.
28. Delneri D, Hoyle DC, Gkargkas K, Cross EJM, Rash B, et al. (2008) Identification and characterization of high-flux-control genes of yeast

through competition analyses in continuous cultures. Nature genetics 40: 113–117. doi:10.1038/ng.2007.49.
29. Causton HC, Ren B, Koh SS, Harbison CT, Kanin E, et al. (2001) Remodeling of Yeast Genome Expression in Response to Environmental Changes. Mol Biol Cell 12: 323–337.
30. Gasch AP, Spellman PT, Kao CM, Carmel-Harel O, Eisen MB, et al. (2000) Genomic Expression Programs in the Response of Yeast Cells to Environmental Changes. Mol Biol Cell 11: 4241–4257.
31. Gasch AP, Werner-Washburne M (2002) The genomics of yeast responses to environmental stress and starvation. Functional & integrative genomics 2: 181–192. doi:10.1007/s10142-002-0058-2.
32. Stoebel DM, Dean AM, Dykhuizen DE (2008) The cost of expression of Escherichia coli lac operon proteins is in the process, not in the products. Genetics 178: 1653–1660. doi:10.1534/genetics.107.085399.
33. Kafri R, Bar-Even A, Pilpel Y (2005) Transcription control reprogramming in genetic backup circuits. Nature genetics 37: 295–299. doi:10.1038/ng1523.
34. Kafri R, Levy M, Pilpel Y (2006) The regulatory utilization of genetic redundancy through responsive backup circuits. Proceedings of the National Academy of Sciences of the United States of America 103: 11653–11658. doi:10.1073/pnas.0604883103.
35. DeLuna A, Springer M, Kirschner MW, Kishony R (2010) Need-based up-regulation of protein levels in response to deletion of their duplicate genes. PLoS biology 8: e1000347. doi:10.1371/journal.pbio.1000347.
36. Agris PF (2004) Decoding the genome: a modified view. Nucleic acids research 32: 223–238. doi:10.1093/nar/gkh185.
37. Begley U, Dyavaiah M, Patil A, Rooney JP, DiRenzo D, et al. (2007) Trm9-catalyzed tRNA modifications link translation to the DNA damage response. Molecular cell 28: 860–870. doi:10.1016/j.molcel.2007.09.021.
38. Kalhor HR, Clarke S (2003) Novel methyltransferase for modified uridine residues at the wobble position of tRNA. Molecular and cellular biology 23: 9283–9292.
39. Braglia P, Percudani R, Dieci G (2005) Sequence context effects on oligo(dT) termination signal recognition by Saccharomyces cerevisiae RNA polymerase III. The Journal of biological chemistry 280: 19551–19562. doi:10.1074/jbc.M412238200.
40. Zhang G, Lukoszek R, Mueller-Roeber B, Ignatova Z (2011) Different sequence signatures in the upstream regions of plant and animal tRNA genes shape distinct modes of regulation. Nucleic Acids Research 39: 3331–3339.
41. Hernandez N (2001) Small nuclear RNA genes: a model system to study fundamental mechanisms of transcription. The Journal of biological chemistry 276: 26733–26736. doi:10.1074/jbc.R100032200.
42. Giuliodori S, Percudani R, Braglia P, Ferrari R, Guffanti E, et al. (2003) A composite upstream sequence motif potentiates tRNA gene transcription in yeast. Journal of molecular biology 333: 1–20.
43. Bailey TL, Elkan C (1994) Fitting a mixture model by expectation maximization to discover motifs in biopolymers. Proceedings / . International Conference on Intelligent Systems for Molecular Biology ;

ISMB International Conference on Intelligent Systems for Molecular Biology 2: 28–36.
44. Trotter EW, Kao CM-F, Berenfeld L, Botstein D, Petsko G a, et al. (2002) Misfolded proteins are competent to mediate a subset of the responses to heat shock in Saccharomyces cerevisiae. The Journal of biological chemistry 277: 44817–44825. doi:10.1074/jbc.M204686200.
45. Travers KJ, Patil CK, Wodicka L, Lockhart DJ, Weissman JS, et al. (2000) Functional and genomic analyses reveal an essential coordination between the unfolded protein response and ER-associated degradation. Cell 101: 249–258.
46. Mitchell A, Romano GH, Groisman B, Yona A, Dekel E, et al. (2009) Adaptive prediction of environmental changes by microorganisms. Nature 460: 220–224. doi:10.1038/nature08112.
47. Kaganovich D, Kopito R, Frydman J (2008) Misfolded proteins partition between two distinct quality control compartments. Nature 454: 1088–1095. doi:10.1038/nature07195.
48. Spokoini R, Moldavski O, Nahmias Y, England JL, Schuldiner M, et al. (2012) Confinement to organelle-associated inclusion structures mediates asymmetric inheritance of aggregated protein in budding yeast. Cell reports 2: 738–747. doi:10.1016/j.celrep.2012.08.024.
49. Kanehisa M, Goto S, Sato Y, Furumichi M, Tanabe M (2012) KEGG for integration and interpretation of large-scale molecular data sets. Nucleic acids research 40: D109–14. doi:10.1093/nar/gkr988.
50. Kanehisa M, Goto S (2000) KEGG: kyoto encyclopedia of genes and genomes. Nucleic acids research 28: 27–30.
51. Subramanian A, Tamayo P, Mootha VK, Mukherjee S, Ebert BL, et al. (2005) Gene set enrichment analysis: a knowledge-based approach for interpreting genome-wide expression profiles. Proceedings of the National Academy of Sciences of the United States of America 102: 15545–15550. doi:10.1073/pnas.0506580102.
52. Mootha VK, Lindgren CM, Eriksson K-F, Subramanian A, Sihag S, et al. (2003) PGC-1alpha-responsive genes involved in oxidative phosphorylation are coordinately downregulated in human diabetes. Nature genetics 34: 267–273. doi:10.1038/ng1180.
53. Bailly-Bechet M, Borgs C, Braunstein A, Chayes J, Dagkessamanskaia A, et al. (2011) Finding undetected protein associations in cell signaling by belief propagation. Proceedings of the National Academy of Sciences of the United States of America 108: 882–887. doi:10.1073/pnas.1004751108.
54. Ihmels J, Collins SR, Schuldiner M, Krogan NJ, Weissman JS (2007) Backup without redundancy: genetic interactions reveal the cost of duplicate gene loss. Molecular systems biology 3: 86. doi:10.1038/msb4100127.
55. Papp B, Pál C, Hurst LD (2004) Metabolic network analysis of the causes and evolution of enzyme dispensability in yeast. Nature 429: 661–664. doi:10.1038/nature02636.
56. Kafri R, Dahan O, Levy J, Pilpel Y (2008) Preferential protection of protein interaction network hubs in yeast: Evolved functionality of genetic redundancy. Proceedings of the National Academy of Sciences 105: 1243–1248. doi:10.1073/pnas.0711043105.

57. Hillenmeyer ME, Fung E, Wildenhain J, Pierce SE, Hoon S, et al. (2008) The chemical genomic portrait of yeast: uncovering a phenotype for all genes. Science (New York, NY) 320: 362–365. doi:10.1126/science.1150021.
58. Giaever G, Chu AM, Ni L, Connelly C, Riles L, et al. (2002) Functional profiling of the Saccharomyces cerevisiae genome. Nature 418: 387–391. doi:10.1038/nature00935.
59. Gingold H, Dahan O, Pilpel Y (2012) Dynamic changes in translational efficiency are deduced from codon usage of the transcriptome. Nucleic acids research 40: 10053–10063. doi:10.1093/nar/gks772.
60. Moqtaderi Z, Wang J, Raha D, White RJ, Snyder M, et al. (2010) Genomic binding profiles of functionally distinct RNA polymerase III transcription complexes in human cells. Nature structural & molecular biology 17: 635–640. doi:10.1038/nsmb.1794.
61. Patil A, Chan CTY, Dyavaiah M, Rooney JP, Dedon PC, et al. (2012) Translational infidelity-induced protein stress results from a deficiency in Trm9-catalyzed tRNA modifications. RNA biology 9: 990–1001. doi:10.4161/rna.20531.
62. Paredes J a, Carreto L, Simões J, Bezerra AR, Gomes AC, et al. (2012) Low level genome mistranslations deregulate the transcriptome and translatome and generate proteotoxic stress in yeast. BMC biology 10: 55. doi:10.1186/1741-7007-10-55.
63. Shalgi R, Hurt JA, Krykbaeva I, Taipale M, Lindquist S, et al. (2012) Widespread Regulation of Translation by Elongation Pausing in Heat Shock. Molecular cell 49: 439–452. doi:10.1016/j.molcel.2012.11.028.
64. Liu B, Han Y, Qian S-B (2013) Cotranslational Response to Proteotoxic Stress by Elongation Pausing of Ribosomes. Molecular cell 49: 453–463. doi:10.1016/j.molcel.2012.12.001.
65. Kafri R, Springer M, Pilpel Y (2009) Genetic redundancy: new tricks for old genes. Cell 136: 389–392. doi:10.1016/j.cell.2009.01.027.
66. Costanzo M, Baryshnikova A, Bellay J, Kim Y, Spear ED, et al. (2010) The genetic landscape of a cell. Science (New York, NY) 327: 425–431. doi:10.1126/science.1180823.
67. Schuldiner M, Collins SR, Thompson NJ, Denic V, Bhamidipati A, et al. (2005) Exploration of the function and organization of the yeast early secretory pathway through an epistatic miniarray profile. Cell 123: 507–519. doi:10.1016/j.cell.2005.08.031.
68. Zaborske J, Pan T (2010) Genome-wide analysis of aminoacylation (charging) levels of tRNA using microarrays. Journal of visualized experiments : JoVE. doi:10.3791/2007.
69. Girstmair H, Saffert P, Rode S, Czech A, Holland G, et al. (2013) Depletion of Cognate Charged Transfer RNA Causes Translational Frameshifting within the Expanded CAG Stretch in Huntingtin. Cell reports 3: 148–159. doi:10.1016/j.celrep.2012.12.019.
70. Chan PP, Lowe TM (2009) GtRNAdb: a database of transfer RNA genes detected in genomic sequence. Nucleic acids research 37: D93–7. doi:10.1093/nar/gkn787.
71. Baudin A, Ozier-Kalogeropoulos O, Denouel A, Lacroute F, Cullin C (1993) A simple and efficient method for direct gene deletion in Saccharomyces cerevisiae. Nucleic acids research 21: 3329–3330.

72. Wach A (1996) PCR-synthesis of marker cassettes with long flanking homology regions for gene disruptions in S. cerevisiae. Yeast (Chichester, England) 12: 259–265. doi:10.1002/(SICI)1097-0061(19960315)12:3<259::AID-YEA901>3.0.CO;2-C.
73. Goldstein AL, McCusker JH (1999) Three new dominant drug resistance cassettes for gene disruption in Saccharomyces cerevisiae. Yeast (Chichester, England) 15: 1541–1553. doi:10.1002/(SICI)1097-0061(199910)15:14<1541::AID-YEA476>3.0.CO;2-K.

Figure Legends

Figure 1. Creation and analysis of tRNA deletion library.

(A) Schematic representation of the deletion process. 204 different tRNA strains were created using homologous recombination. In each strain, a different tRNA gene was replaced by a hygromycin B resistance marker

(B) Schematic representation of growth measurements, analysis, and scoring. For each strain, relative-growth-rate and relative-growth-yield are calculated in relation to the wild-type strain. These parameters are then projected on a distribution of the wild-type growth parameters. Sigma (σ) is calculated according to the formula and denotes the number of standard deviations from the mean of the wild-type (see also Supplemental figure S1A). The color in the histogram are areas were: $\sigma<-3$ (blue), $-3<\sigma<-2$ (cyan), $2<\sigma<3$ (yellow) and $3<\sigma$ (red). The same color code is used to define phenotypes in the pie charts (C and D).

(C-D) Distribution of phenotypes for the tRNA deletion library in rich medium, according to two growth parameters: relative growth yield (C) relative growth rate (D). Deletion strains were assigned to categories according to their σ values. Any absolute σ value larger than 2 was considered as non-normal phenotype, where negative sigma denotes impairment (worse than the wild-type) and positive sigma denotes improvement (better than the wild-type). Any absolute σ value larger than 3 was considered as a strong phenotype. Thus, highly impaired for $\sigma<-3$, impaired for $-2>\sigma>-3$, improved for $2<\sigma<3$, and highly improved for $\sigma>3$, see also Supplemental figure S1B.

Figure 2. Screening the tRNA deletion library across various growth conditions.

(A) Percent of strains exhibiting a growth yield phenotype in various conditions. The color indicates the type of phenotype: impaired (blue) or improved (red). **(B)** Percent of strains exhibiting a growth rate phenotype in various conditions. **(C-D)** The σ values measured for both the growth yield (C) and the growth rate (D) for all deletion strains across six conditions.

The color bar indicates the σ values, red denoting improvement and blue impairment. Each row denotes a tRNA deletion strain and each column denotes different growth condition. Strains are ordered on the y-axis according to amino acids (denoted by letter) and further separated into families (denoted by lines within the amino-acid box). Black rows denote lethal strains. Gray rows indicate strains for which the respective value was not measured.

Figure 3. Extensive redundancy underlies robustness to tRNA gene deletion.

(A) Schematic representation of the genetic interactions within and between tRNA families. Families are denoted by dark grey circles and grouped (black dashed line) according to their tRNA copy number. Each family is denoted by its anti-codon and amino-acid. A protein-coding gene i.e. *TRM9* is denoted by a grey box. Each filled circle indicates a tRNA deletion strain. The lines connecting the deletion strains denote a co-deletion of these genes (a multi-tRNAs deletion strain). The color of the filled circles and lines denote the severity of the growth phenotype for the respective strain: blue for normal growth, purple for impaired growth (worse than wild-type) and red for lethality. **(B)** Epistasis values for multi-tRNAs deletion strains which contain the deletion of *tL(GAG)* and either:

one *tL(UAG)* gene, two *tL(UAG)* genes, *tL(CAA)* (which is a tRNA of different Leucine family), and *tW(CCA)* (which is a non-Leucine tRNA) as controls.

(C) Epistasis values for multi-tRNAs deletion strains which contain the deletion of *trm9* with: the singleton *tR(CCU)*, and *tR(ACG)* which is a tRNA of different Arginine family and *tW(CCA)* which is a non- Arginine tRNA as controls. In both (B) and (C) epistasis values of the relative growth yield and growth rate are indicated in grey and green respectively. Data is presented as mean of 3 biological repetitions +/- SEM.

Figure 4. Differential contribution of identical tRNA gene copies.

(A-B) Relative growth yield values of the tRNA deletion library strains in rich medium (A) and low glucose (B), sorted by anti-codon and amino-acid identity along the x-axis. Each dot along the vertical lines denotes the value (data are represented as mean of 3 biological repetitions +/- SEM) of a deletion strain of different tRNA gene of the respective family. The horizontal lines mark two standard deviations around the mean of the wild-type. Dots above or below these lines are considered non-normal phenotypes (see also Supplemental figure S7).

(C) Relative growth yield values (data are presented as mean of 3 biological repetitions +/- SEM) of various double deletion combinations consisting of: five *tR(UCU)* family members, *tR(CCU)* and *trm9* deletion strains as indicated on the x-axis, along with the five members of the *tR(UCU)* family each denoted by a different shape and color in the legend. **(D)** Relative growth yield of the five *tR(UCU)* members across different growth conditions, indicated on the x-axis.

(E) Enrichment of conserved elements in tRNA genes divided according to phenotype observed in rich media for each growth parameter. Each column in the matrix denotes a conserved element as defined by [42]. Color bar indicates the $-\log_{10}$ of the hypergeometric p-value. **(F)** log10 E-value found by the MEME software for the most significant motif in a 9bp window starting from the position indicated by the x-axis. The LOGOs of the two significant motifs are displayed below, next to a number indicating its position. Position 0 is the first position of the mature tRNA.

Figure 5. Changes in the tRNA pool affect protein folding

(A-C) Relative growth rate (compare to wild-type) of the following five deletion strain: *tL(GAG)G* (blue), *tR(CCU)J* (red), *tiM(CAU)C* (green), *tH(GUG)G1* (magenta) and *tR(UCU)M2* (cyan). Strains were grown in media supplemented with increasing concentrations of the following proteotoxic agent: AZC (A) Tunicamycin (B) DTT (C).

(D) Percentage of cells that contain puncta in the populations of the above strains.

(E) Percentage of cells that contain puncta in the populations of the above strains following treatment with 2.5mM AZC. Data are presented as mean of 3 biological repetitions +/- SEM, in each repetition 500 cells were counted. (*) $P< 0.001$ by Students *t*-test.

(F-G) Images of representative fields for the wild-type and *tR(CCU)J* deletion strain, without treatment (F) and following treatment with 2.5mM AZC (G).

Figure 6. Molecular response to changes in the tRNA pool.

(A) Dendrogram created by clustering changes in gene expression for five representative deletion strains, for more information see Materials and Methods. **(B)** Fold change of the *COS8* (*YHL048W*) mRNA levels in each of the five deletion strains as measured by microarrays. **(C)** The fold change distribution of mRNA levels as measured by microarrays, of genes composing the Proteasome pathway by the KEGG database [49], for each of the listed tRNA deletion strains.

(D) mRNA Fold change of 6 representative genes from the proteasome pathway measured by RT-qPCR. Presented values are the mean of 3 biological repetitions +/- SEM. The strain colors are as in (C). If the mRNA fold change in a specific strain is significantly different from 0 (*t*-test) it is marked with:* ($p<0.05$) or ** ($p<0.005$).

(E) The fold change distribution of mRNA levels as measured by microarrays, of genes composing the Pol III RNA Polymerase machinery module by the KEGG database, for each tRNA deletion strain. **(F)** mRNA Fold change of 6 representative genes from the Pol III KEGG module measured by RT-qPCR. Presented values are the mean of 3 biological repetitions +/- SEM. The strain colors are as in figure (C). If the mRNA fold change in a specific strain is significantly different from 0 (*t*-test) it is marked with:* ($p<0.05$) or ** ($p<0.005$).

In all the sub-figures (C,D,E,F) values are plotted for the same five deletion strains: *tL(GAG)G* (blue), *tR(CCU)J* (red), *tiM(CAU)C* (green), *tH(GUG)G1* (magenta) and *tR(UCU)M2* (cyan).

Tables

Table 1. KEGG pathways differentiating between tRNA deletion sets

Higher in SC than in MC	Higher in MC than in SC
Proteasome (<1E-5)	Ribosome biogenesis in eukaryotes (<1E-5)
Oxidative phosphorylation (<1E-5)	RNA polymerase (<1E-5)
Endocytosis(2E-3)	Phenylalanine, tyrosine and tryptophan biosynthesis (<1E-5)
SNARE interactions in vesicular transport (2E-3)	Pyrimidine metabolism (5E-5)
Protein processing in endoplasmic reticulum (2E-3)	Ribosome (1E-4)
Starch and sucrose metabolism (2E-3)	Lysine biosynthesis (1E-4)
Citrate cycle (TCA cycle) (0.01)	Histidine metabolism (4E-4)
Meiosis (0.01)	Cysteine and methionine metabolism (4E-4)
Homologous recombination (0.02)	Riboflavin metabolism (5E-3)
Mismatch Repair (0.02)	Arginine and proline metabolism (8E-3)
Cell cycle (0.02)	Valine, leucine and isoleucine biosynthesis (0.01)
MAPK signaling pathway - yeast (0.02)	Purine metabolism (0.03)
Fructose and mannose metabolism (0.02)	Sulfur metabolism (0.03)
Nitrogen Metabolism (0.02)	Tyrosine Metabolism (0.03)
Phagosome (0.03)	Folate biosynthesis (0.04)

KEGG pathways [49] for which changes in genes expression are significantly different between the two groups of tRNA deletion strains: MC (multi-copy) group (*ΔtH(GUG)G1* and *ΔtR(UCU)M2*) vs. SC (single-copy) group (*ΔtL(GAG)G*, *ΔtR(CCU)J*, *ΔtiM(CAU)C*) calculated with GSEA [51,52]. In the first column are pathways, which are higher in SC vs. MC and vice versa in the second column. The values are corrected for multiple hypothesis and the FDR q-values are indicated next to each pathway.

Supplemental Figures

Figure S1. Growth measurements parameters.

(A) Schematic growth curve of Optical Density (OD) vs. time. The red dots indicate the time points from which the growth rate (1) and growth yield (2) parameters are extracted. **(B)** Dot plot for all strains in the library grown in YPD. Each strain is represented by a blue dot, showing its sigma growth rate vs. its sigma growth yield values. The Pearson correlation coefficient is -0.019 indicating there is no correlation between the two parameters p-val 0.794.

Figure S2. Phenotypes cannot be explained by family size and amino-acid identity.

Sigma growth parameters for the tRNA library grown in rich medium are plotted in boxes sorted by either family size or amino-acid identity. For each box, the central mark is the median, the edges of the box are the 25th and 75th percentiles. Sigma growth yield by family size **(A)** sigma growth rate by family size **(B)** sigma growth yield by amino-acid **(C)** sigma growth rate by amino-acid **(D)**. Apart from the singletons whose deletion strains are often lethal or impaired, we could not explain the observed growth phenotypes, in either growth rate or yield, by either the size of the family, or the amino acid identity.

Figure S3. tRNA deletion phenotype are not correlated to the expression of nearby genes.

(A-B) the average expression level of the genes located upstream and downstream to the tRNA gene that was deleted in each strain vs. the sigma

growth yield (A) or the sigma growth rate (B). **(C)** Relative growth parameters of *tR(CCU)J* deletion (black), *tR(CCU)J* deletion containing a centromeric plasmid harboring the *tR(CCU)J* gene (gray) and a strain deleted for the *YJR055W* gene which is the protein-coding gene located downstream of *tR(CCU)J* (white). As can be seen only the *tR(CCU)J* deletion strain exhibits growth rate impairment while the two other strains do not.

Figure S4. Single tRNA genes can sustain wild-type growth upon deletion of multiple members in three gene families.

(A-B) Relative growth rate (red) and growth yield (blue) values of double deletion combinations containing members of the *tG(UCC)* family (A) and the *tS(UGA)* family (B). In each experiment the mean of 3 biological repetitions is presented +/- SEM. Two σ around the mean of the wild-type are indicated by red and blue lines around 1 (wild-type value).

Figure S5. Compensation within some tRNA families is due to plasticity of the pool and transcriptional changes of the remaining copies.

RT-qPCR measurement of the RNA levels of the *tS(UGA)* family**(A)** and *tL(UAG)* family **(B)** upon deletion of various members of the family. Results are reported in terms of log2 fold change of the expression level in each of the indicated deletion strain compared to the wild-type. In both (A) and(B) the * indicates cases in which the fold change was significantly different from zero (*t*-test, p-value <0.05).

Figure S6. Epistasis of trm9 deletion with Glutamic Acid tRNAs.

Examining a more general role for Trm9 in modulating the compensation between tRNA families we chose the second tRNA family that is modified by Trm9, *tE(UUC)*, and in addition we examined the *tE(UCU)* family. Together these two families decode in a split codon box, in a similar manner to the Arginine UCU and CCU families. We created 10 double deletions, each consisting of the enzyme along with one of the tRNA genes of the two glutamic acid families and analyzed their interactions by epistasis.

Epistasis values for co-deletion strains which contain the deletion of *trm9* with: the deletion of the two members of *tE(CUC)* family, and eight members of the *tE(UUC)* family. Epistasis values of the relative growth yield and growth rate are indicated in grey and green respectively. Data is presented as mean +/- SEM of 3 independent experiments.

Figure S7. Identical tRNA genes contribute differentially to the tRNA pool.

(A-B) Growth rate values of the tRNA deletion library in rich medium (A) and low glucose (B) sorted by families and amino-acid identity. The horizontal lines denote two standard deviations around the mean of the wild-type in that condition. Dots above or below these lines are considered phenotypes. **(C)** Relative growth yield values (data of 3 biological repetitions +/- SEM is presented) of five *tR(UCU)* deletion strains (Grey) and the corresponding complementation strains (White). Each complementation strain carries the deleted tRNA gene on a centromeric plasmid. The values are relative to the wild-type. In the complementation experiment, the wild-type harbors an empty plasmid. **(D)** Relative growth yield values of strain deleted for *tR(UCU)M2* gene

(a major copy of the *tR(UCU)* family- marked as *ΔM2*), and *ΔM2* strains containing different centromeric plasmids. Each centromeric plasmid carries the *tR(UCU)* tRNA flanked from each side by 200bp sequence identical to a the different members of the *tR(UCU)* family.

Figure S8. Expression changes of tRNA deletions.

Expression changes for the five deletion strains. Each row indicates a gene and each column is a tRNA deletion strain. The genes and strains are sorted according to the clustering results (see Materials and Methods). The Color bar indicates the log2 fold change. The groups of genes enriched for relative pathways are indicated on the right (locations were found by looking at the highest hypergeometric enrichments for varying window sizes).

Figure S9. Fold change of the Pol II pathway.

(A) The fold change distribution of mRNA levels as measured by microarrays, of genes composing the Pol II RNA Polymerase machinery by the KEGG database for each of the listed tRNA deletion strains. **(B)** mRNA Fold change of 3 representative genes from the Pol II pathway measured by RT-qPCR. Presented values are the mean of 3 biological repetitions +/- SEM. The strain colors are as in figure (A). If the mRNA fold change in a specific strain is significantly different from 0 (*t*-test) it is marked with:* ($p<0.05$) or ** ($p<0.005$).

In both sub-figures (A, B) values are plotted for the same five deletion strains: *tL(GAG)G* (blue), *tR(CCU)J* (red), *tiM(CAU)C* (green), *tH(GUG)G1* (magenta) and *tR(UCU)M2* (cyan).

Table S1.

Correlation between tRNA phenotype and expression of nearby genes.

Table S2.

List of all tRNA deletion strains in the library and their respective phenotypes across conditions.

Table S3.

List of double deletion strains and their phenotypes.

Table S4.

Microarray Fold change measurements for selected tRNA deletion strains

Table S5.

List of primers used to create the tRNA deletion strains.

Table S6.

List of primers used for RT-qPCR experiments.

Text S1.

Supplementary methods and note.

Figure 1
Click here to download Figure: F1.eps

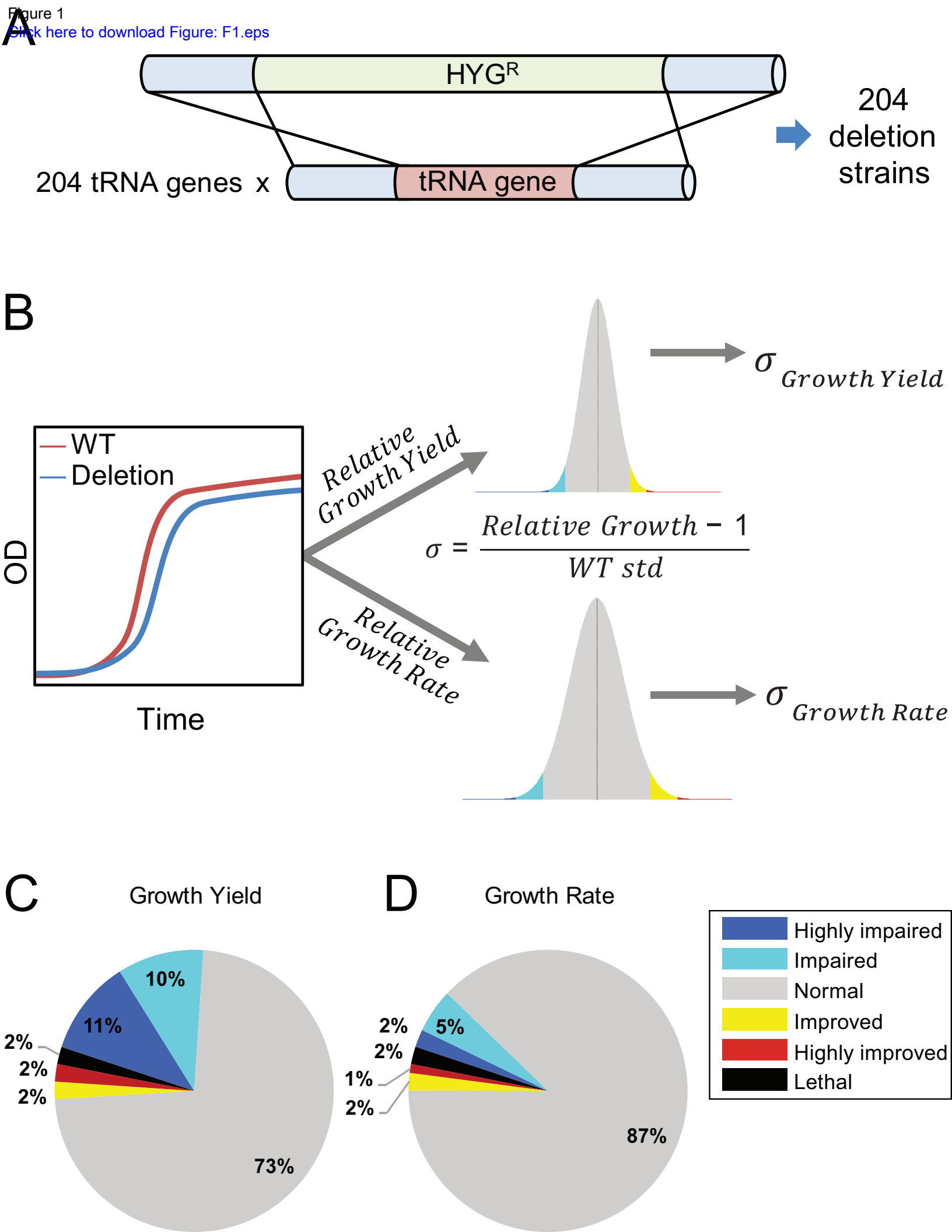

Figure 2

Click here to download Figure: F2.eps

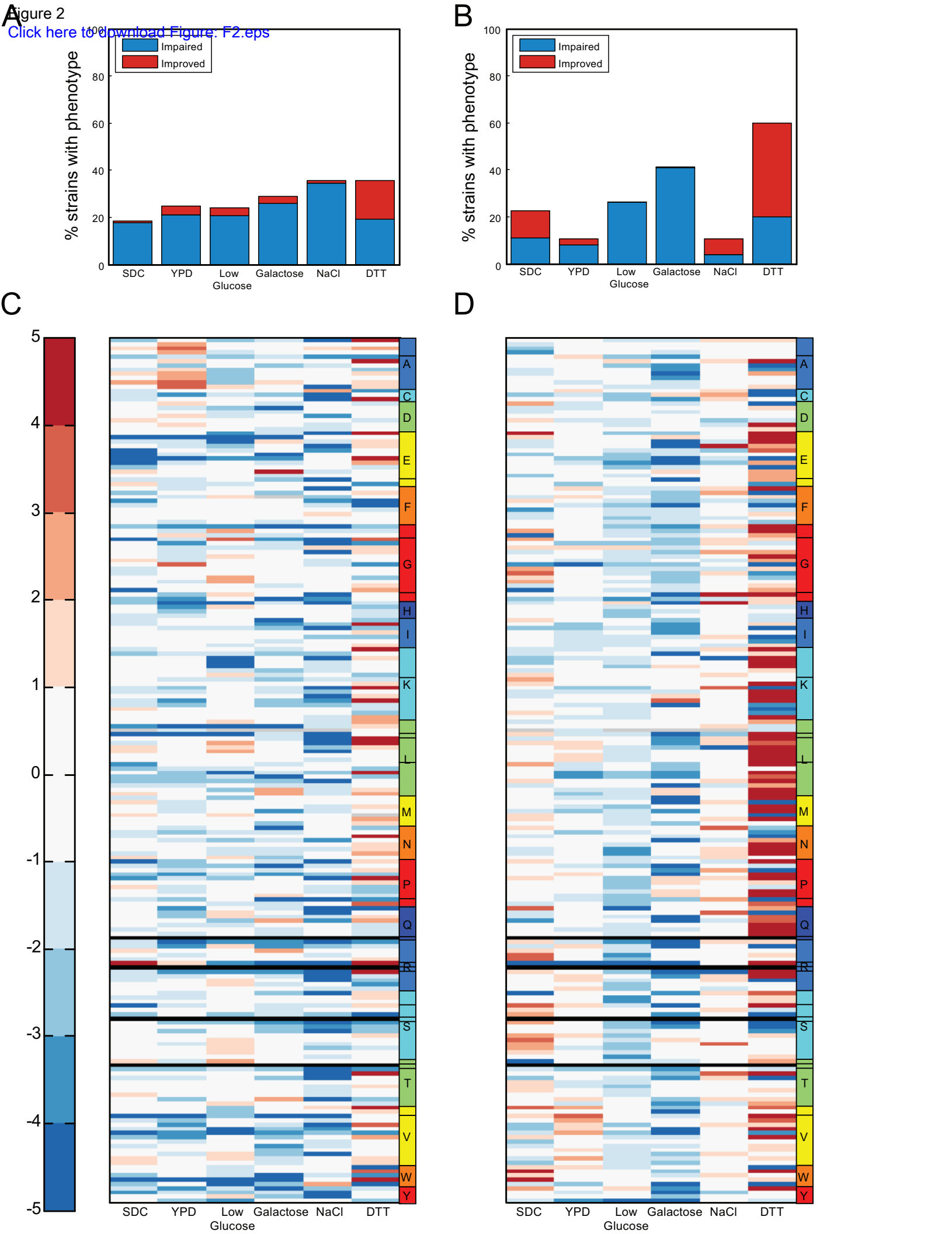

Figure 3

Click here to download Figure: F3.eps

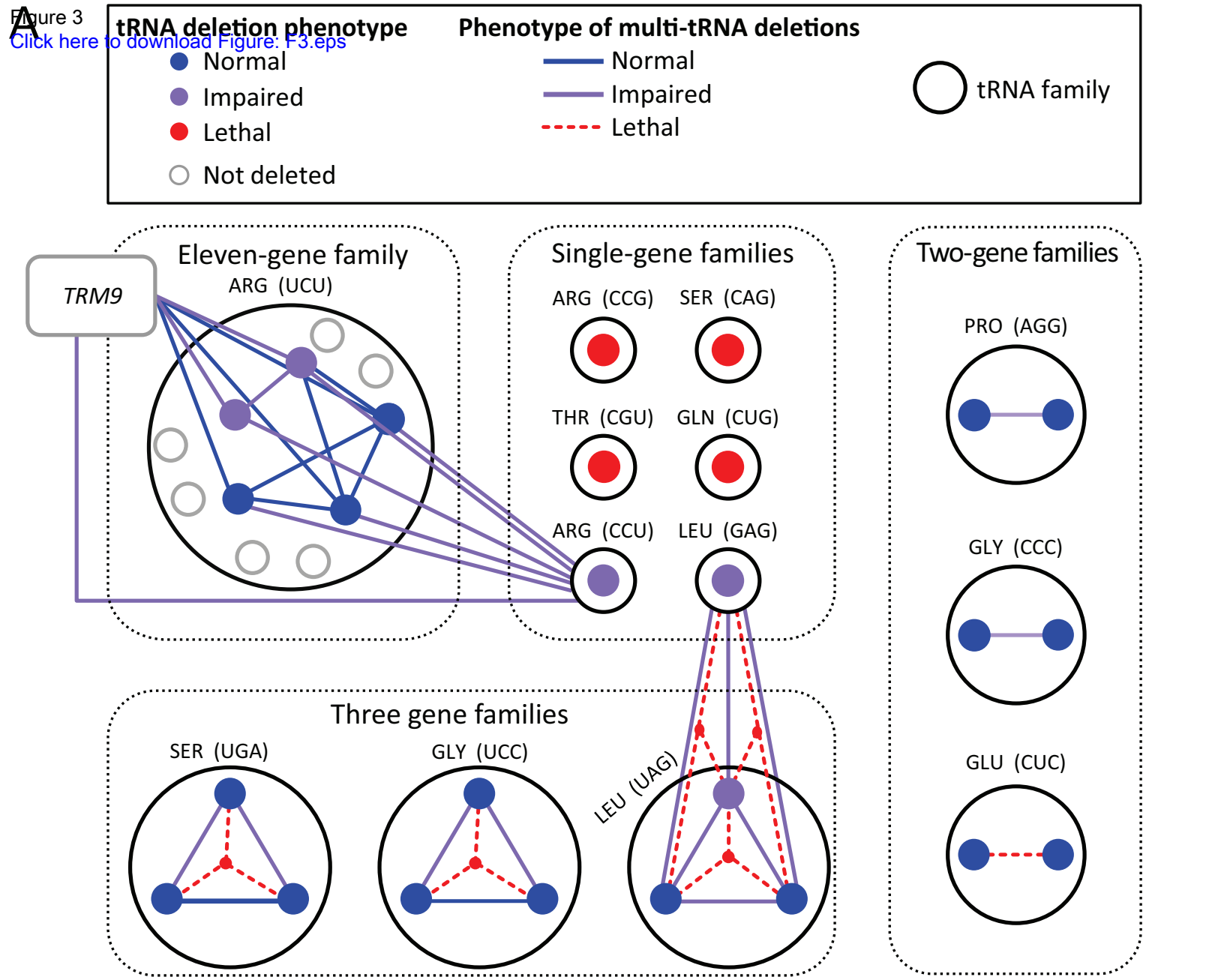

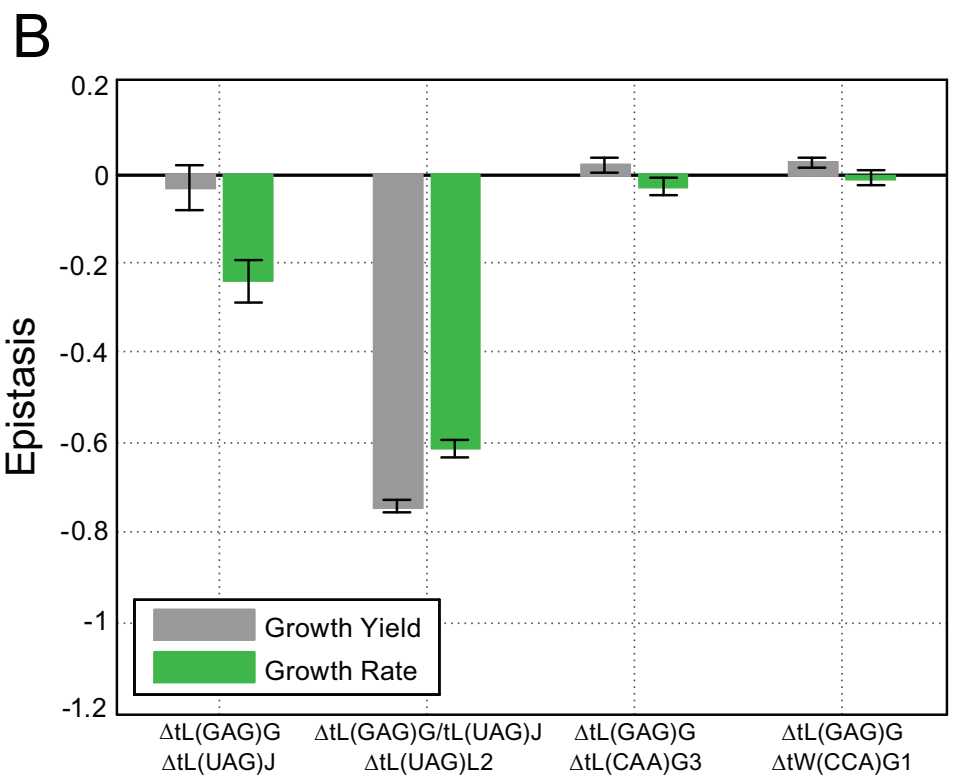

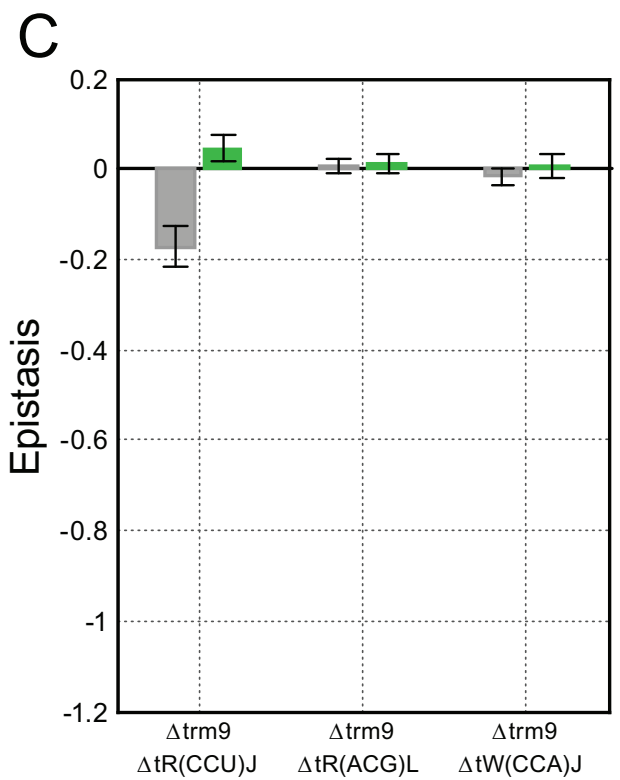

Figure 4

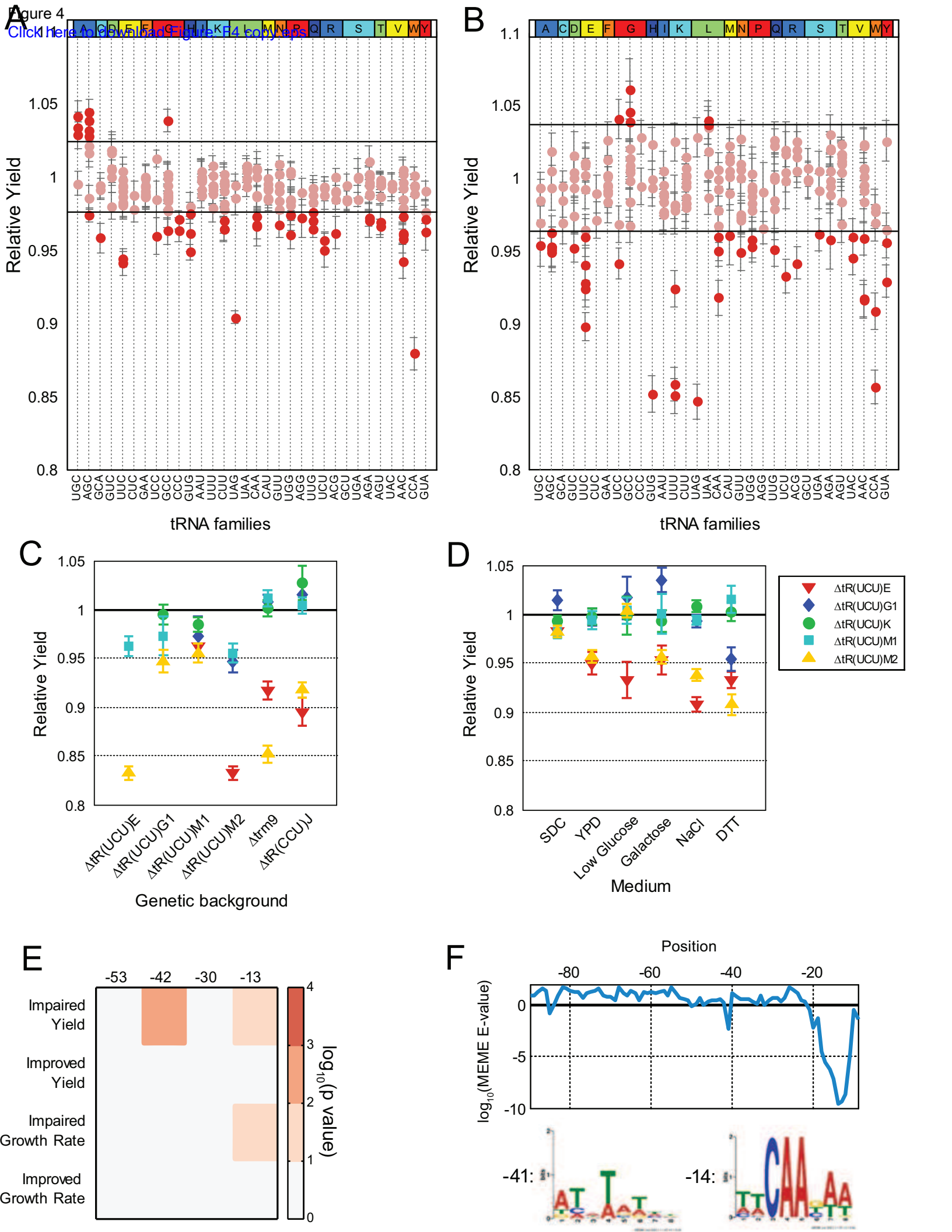

Figure 5
Click here to download Figure: F5.eps

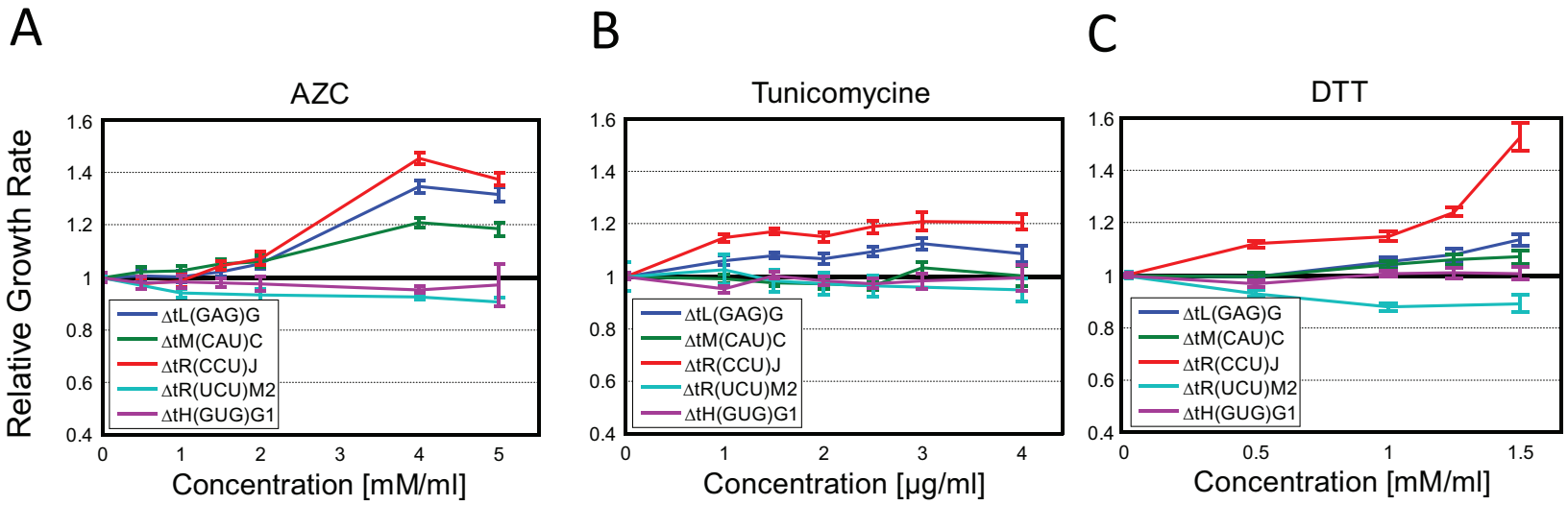

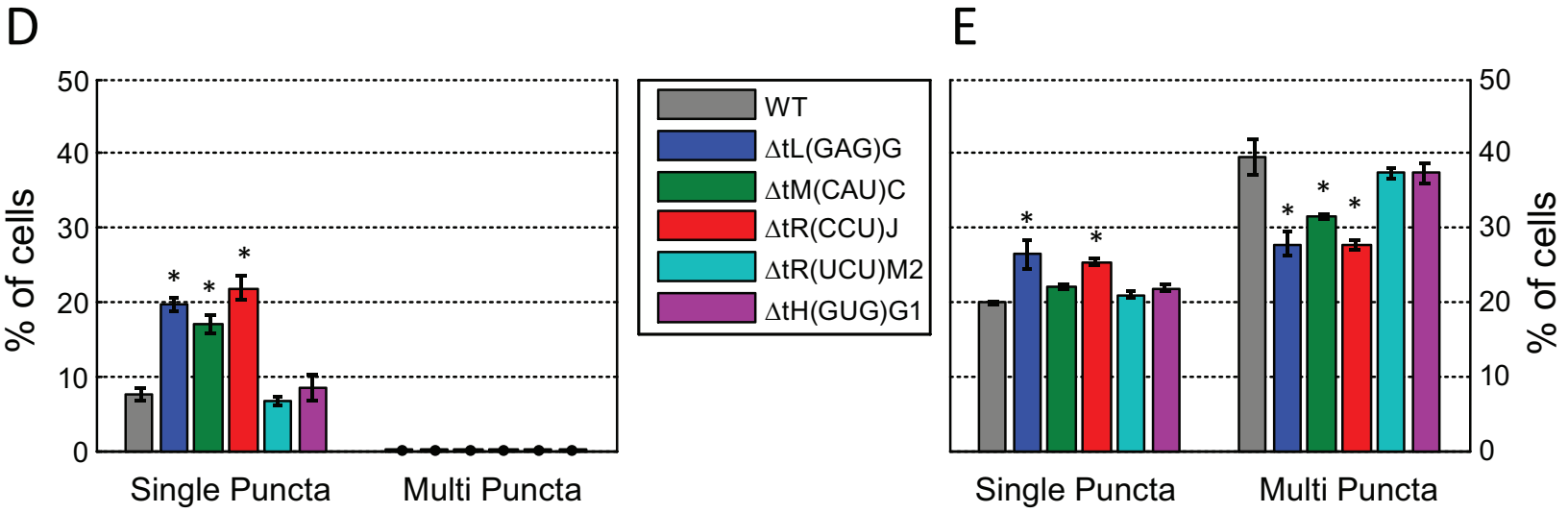

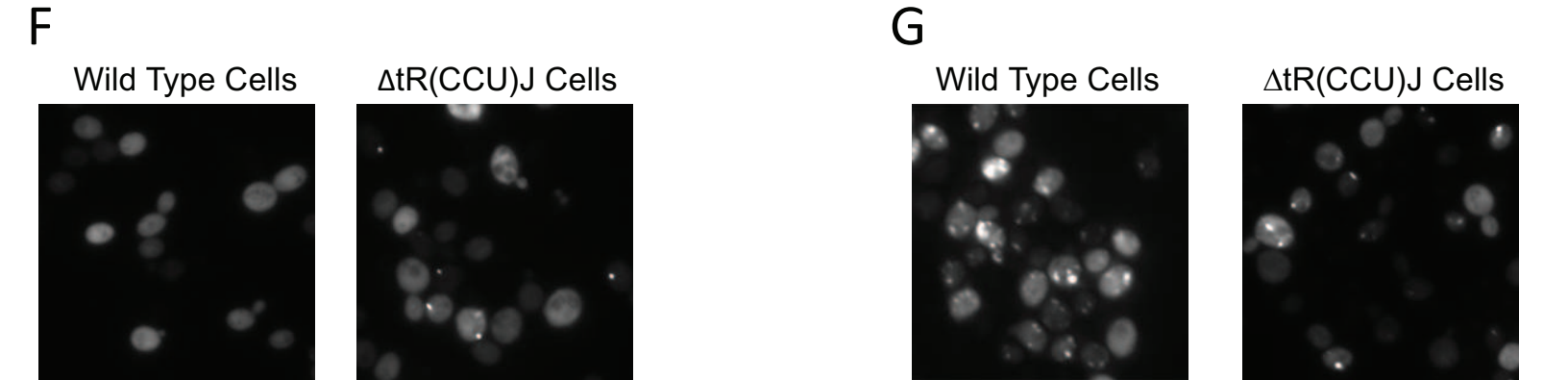

Figure 6
Click here to download Figure: F6.eps

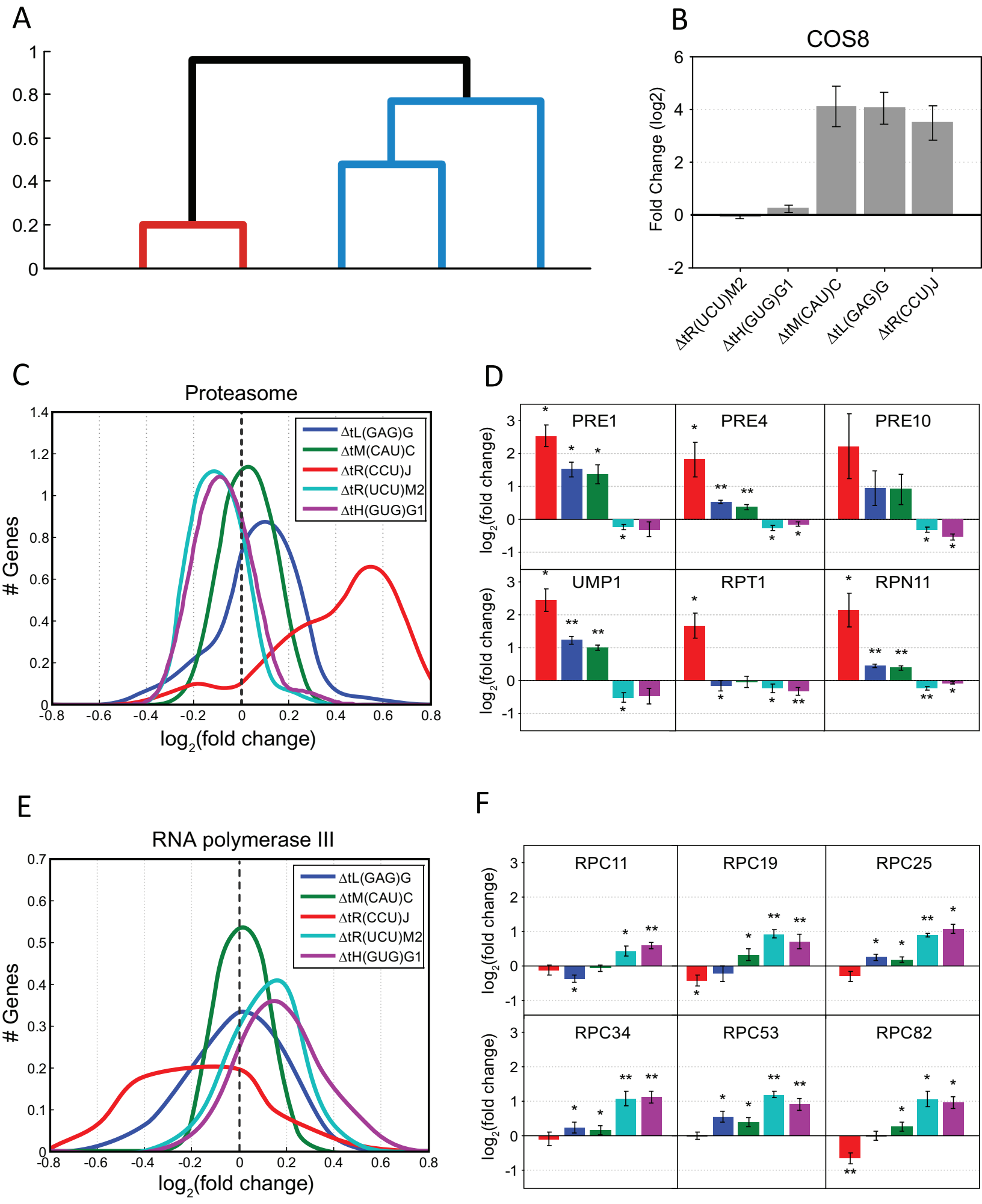

Supplemental Text

Materials and Methods

Yeast strains and plasmids

- *S. cerevisiae* strain Y5565 *(MATα can1Δ::MFA1pr-HIS3 mfα1Δ::MFα1pr-LEU2 lyp1Δ ura3Δ0 leu2Δ0)* was used as the genetic background for the tRNA deletion library strains and the double deletion strains.
- *S. cerevisiae* strain BY4743 *(MATa/α his3Δ1/his3Δ1 leu2Δ0/leu2Δ0 LYS2/lys2Δ0 met15Δ0/MET15 ura3Δ0/ura3Δ0)* was used for analysis of tRNA essentiality in tetrad analysis.
- pAG32 DEL-MARKER-SET (EOUROSCARF) [1] was used to amplify the Hygromycin B resistance marker.
- pAG25 DEL-MARKER-SET (EOUROSCARF) [1] was used to amplify the Nourseothricin resistance marker.
- pFA6a-kanMX6 [2] was used to amplify the Kanamycin resistance marker.
- pRS316- Centromeric plasmid [3] was used for tRNA complementation assays.

Creation of a tRNA deletion library

In similarity to the yeast gene deletion library [8], the tRNA deletion library was constructed using homologous recombination, replacing each tRNA gene with the HPH antibiotics cassette. The DNA template for the recombination event was created using two sequential PCR reactions. The first PCR reaction created the basic template for the recombination containing the antibiotic marker and a 23bp sequence homologous to the desired tRNA. The second PCR reaction served to lengthen this template so it contains 45bp homologues to the desired tRNA deletion. The first PCR reaction used primers containing a genomic sequence that flanks either the 5' or 3' end of the tRNA (directly proximal and distal to the start and end of the gene respectively), 18 and 17bp of sequence common to all gene disruptions as was used in the yeast deletion collection, a 20 base pairs unique sequence (the 'molecular bar-code' TAG) and 22 base pairs of sequence, homologous to the HPH gene. The template for this PCR reaction was the pAG32 plasmid, encoding the hygromycin B phosphotransferase conferring resistance to the antibiotic hygromycin B. The second PCR

reaction used two tRNA gene-specific 45 bp primers, to extend the tRNA specific homology of the first PCR product to a total of 45 bp. The product of the second PCR served for yeast transformation. For a full list of primers see Supplemental table S5.

Verification of tRNA deletion strains

For each tRNA deletion strain, five different colonies were selected, and verified by two PCR reactions. The junctions of the antibiotics cassette were amplified using two primer combinations. Each primer combination contained a primer homologous to sequence within antibiotics cassette of either the promoter or terminator of the marker gene, and a tRNA specific primer, homologous to sequence upstream or downstream of the tRNA deletion. Only colonies from which the correct products were amplified served for further analysis.

Verification of lethality of tRNA deletions by tetrad analysis

To confirm the essentiality of double and triple tRNA deletions, diploid strains were created by mating two deletion strains, either single or double deletions. These heterozygous diploids were sporulated in SC medium (1% potassium acetate) for three days at 25°C. The resulting tetrads were then dissected using a Micromanipulator (Singer). Spores were then allowed to germinate at 30°C on YPD plates and scored on plates containing the appropriate antibiotics. The essentiality of single tRNA genes was confirmed by deletion of the gene from a diploid strain, BY4347, in a similar manner to the construction of the tRNA deletion library. The resulting colonies were verified, grown on rich medium, sporulated and scored. At least 100 tetrads were scored for each such deletion.

Construction of complementation plasmids

In order to reintroduce into the cell a tRNA deleted gene we created a set of "complementation plasmids". Complementation plasmids were constructed for multiple tRNA genes using gene specific primers homologous to 200 bp up and down stream of the tRNA gene which was deleted in the library. Genomic DNA of Y5565 was used to amplify the desired tRNA gene, followed by cloning into the pRS316 centromeric plasmid.

Creation of multi-deletion tRNA strains

Double deletion of tRNA genes was constructed in a similar way to the creation of the tRNA deletion library strains. A strain from the tRNA deletion library served as the genetic

background for the deletion of an additional gene by means of homologues recombination. The sequential PCR was repeated for the second tRNA gene deletion using the same primers used for the creation of the tRNA deletion library. The templates for the first PCR round were either the pAG25 plasmid containing the nourseothricin N-acetyl-transferase that confers resistance to the antibiotics nourseothricin, or the pFA6a-kanMX6, encoding the kanamycin gene that confers resistance to the antibiotics G418. Triple deletions were created by mating double deletions with a single deletion.

Growth measurements and normalization

The measures obtained for each strain in the library were compared to wild-type values that were retrieved separately for each condition. The wild-type measures were done in three repeats and were then summarized by the mean and standard deviation values to generate normalized growth rate and normalized growth yield for each condition. This procedure allowed normalizing for potential variation between days, incubator slots, and locations of wells within the 96-well plate. These measures were obtained from three biological repeats containing wild-type cells in all plate positions, for all slots in the incubator. Each mutant was characterized by growth rate and growth yield. We consider a mutant as showing a phenotype if it deviated by more than two standard deviations from the wild-type mean in that condition in either growth rate or growth yield.

Double deletion epistasis calculations

The epistasis between any two deletion strains was calculated according to the non-scaled measure of epistatic interactions [9] using the following equation: $\varepsilon = W_{XY} - W_X W_y$ In which W_X and W_Y represent the growth values (separating growth rate and growth yield) of the single deletions and W_{XY} represents the growth values of the corresponding double deletion. The results of the calculation indicate the nature of the epistasis, $\varepsilon = 0$ indicates no epistasis, $\varepsilon < 0$ aggravation and $\varepsilon > 0$ buffering.

Note

No appreciable correlation between tRNA expression and the expression levels of nearby protein-coding genes

It has been demonstrated in the past (mainly for specific cases) that the expression of tRNA genes may affect the expression levels of nearby coding genes [6–8]. In order to explore a possible relation between the essentially of tRNA genes, as revealed here upon their deletion, and the expression of nearby genes we measured the correlation between the tRNA deletion phenotype and the expression level (as measured for the wild-type strain in our microarray data) of their upstream and downstream nearby genes. We found no correlation between the severity of growth yield or growth rate phenotypes and nearby gene expression level, indicating that high (or low) expression of a nearby gene is not a predictor of fitness change upon tRNA deletion (see Supplemental figure S3A,B and Supplemental table S1). In addition, we did not find any correlation between the distance to the closest genomic feature and the phenotype of the deletion strain.

Furthermore focusing on five tRNA deletions for which we measured genome wide expression changes, we examined the effect of the deletion on the expression levels of the adjacent genes. As can be seen in the following table:

Deletion Strain	Upstream			Downstream		
	Gene Name	Distance bp	$\log_2$ (Fold Change)	Gene Name	Distance bp	$\log_2$ (Fold Change)
ΔiM(CAU)C	YCR018C	-1017	0.21	YCR019W	2846	0.05
ΔR(CCU)J	YJR054W	-1006	0.27	YJR055W	146	-0.97
ΔtR(UCU)M2	YML071C	-253	-0.37	YML070W	1579	-0.38
ΔtH(GUG)G1	YGL205W	-221	0.79	YGL203C	1779	0.07
ΔL(GAG)G	YGR106C	-889	-0.12	YGR108W	2880	-0.37

Out of 10 protein-coding genes examined, only in two cases (*YJR055W* and *YGL205W*) we detect an appreciable change in the expression level (although in both cases it was less than two fold). This indicates that in most cases tRNAs deletion do not affect their surroundings.

The general lack of coordination between tRNA genes and nearby protein-coding genes is in agreement with the work of Conesa *et al*., [9], that have measured the expression level of all protein-coding genes in several Pol III mutants as well as few tRNA deletion strains. This analysis detected only a modest correlation between altered expression of Pol II-transcribed

genes and their proximity to class III genes.

For the deletion that demonstrated the highest fold change in the expression of a nearby gene (*tR(CCU)J)* and a severe phenotype, we verified that the fitness reduction observed in this strain is indeed due to the deletion of the tRNA gene using several different methods. First, using complementation assay we re-introduced the *tR(CCU)J* gene on a centromeric plasmid into the background of the deleted strain. This resulted in a complete abolishment of the fitness defect (Supplemental figure S3C). In addition, we measured the growth of a strain deleted for the *YJR055W* gene (the protein-coding gene located downstream *tR(CCU)J)* and found that unlike *tR(CCU)J* this strain does not exhibit a growth rate phenotype (Supplemental figure S3C). Taken together these two analysis demonstrate that the growth defect observed in cells deleted for *tR(CCU)J* is due to the lack of function of the CCU tRNA.

Supplemental references

1. Goldstein AL, McCusker JH (1999) Three new dominant drug resistance cassettes for gene disruption in Saccharomyces cerevisiae. Yeast (Chichester, England) 15: 1541–1553. doi:10.1002/(SICI)1097-0061(199910)15:14<1541::AID-YEA476>3.0.CO;2-K.

2. Wach A, Brachat A, Alberti-Segui C, Rebischung C, Philippsen P (1997) Heterologous HIS3 marker and GFP reporter modules for PCR-targeting in Saccharomyces cerevisiae. Yeast (Chichester, England) 13: 1065–1075. doi:10.1002/(SICI)1097-0061(19970915)13:11<1065::AID-YEA159>3.0.CO;2-K.

3. Sikorski RS, Hieter P (1989) A system of shuttle vectors and yeast host strains designed for efficient manipulation of DNA in Saccharomyces cerevisiae. Genetics 122: 19–27.

4. Brachmann CB, Davies A, Cost GJ, Caputo E, Li J, et al. (1998) Designer deletion strains derived from Saccharomyces cerevisiae S288C: a useful set of strains and plasmids for PCR-mediated gene disruption and other applications. Yeast (Chichester, England) 14: 115–132. doi:10.1002/(SICI)1097-0061(19980130)14:2<115::AID-YEA204>3.0.CO;2-2.

5. Elena SF, Lenski RE (1997) Test of synergistic interactions among deleterious mutations in bacteria. Nature 390: 395–398. doi:10.1038/37108.

6. Hull MW, Erickson J, Johnston M, Engelke DR (1994) tRNA genes as transcriptional repressor elements. Molecular and cellular biology 14: 1266–1277.

7. Kendall A, Hull MW, Bertrand E, Good PD, Singer RH, et al. (2000) A CBF5 mutation that disrupts nucleolar localization of early tRNA biosynthesis in yeast also suppresses tRNA gene-mediated transcriptional silencing. Proceedings of the National Academy of Sciences of the United States of America 97: 13108–13113. doi:10.1073/pnas.240454997.

8. Bolton EC, Boeke JD (2003) Transcriptional interactions between yeast tRNA genes, flanking genes and Ty elements: a genomic point of view. Genome research 13: 254–263. doi:10.1101/gr.612203.

9. Conesa C, Ruotolo R, Soularue P, Simms TA, Donze D, et al. (2005) Modulation of yeast genome expression in response to defective RNA polymerase III-dependent transcription. Molecular and cellular biology 25: 8631–8642. doi:10.1128/MCB.25.19.8631-8642.2005.

Figure S1

A

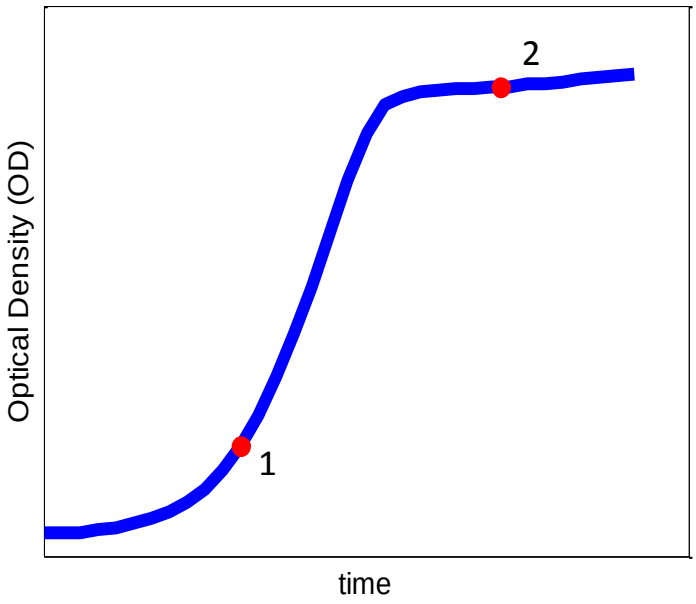
2
1
Optical Density (OD)
time

B

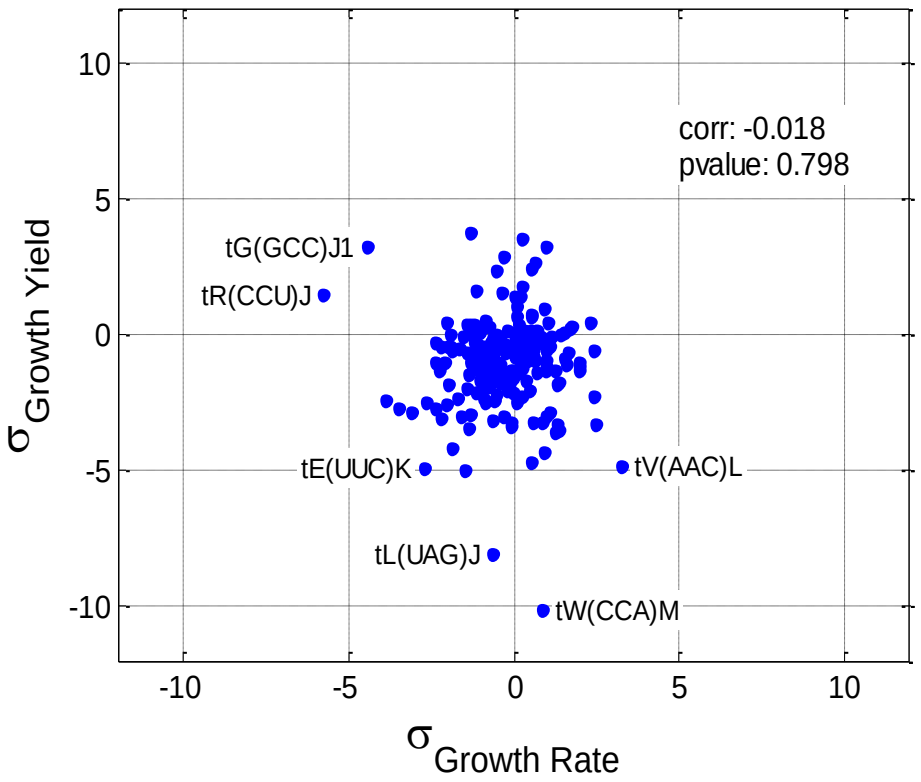
corr: -0.018
pvalue: 0.798
tG(GCC)J1
tR(CCU)J
tE(UUC)K
tV(AAC)L
tL(UAG)J
tW(CCA)M
10
5
0
-5
-10
-10
-5
0
5
10
σGrowth Yield
σGrowth Rate

Figure S2

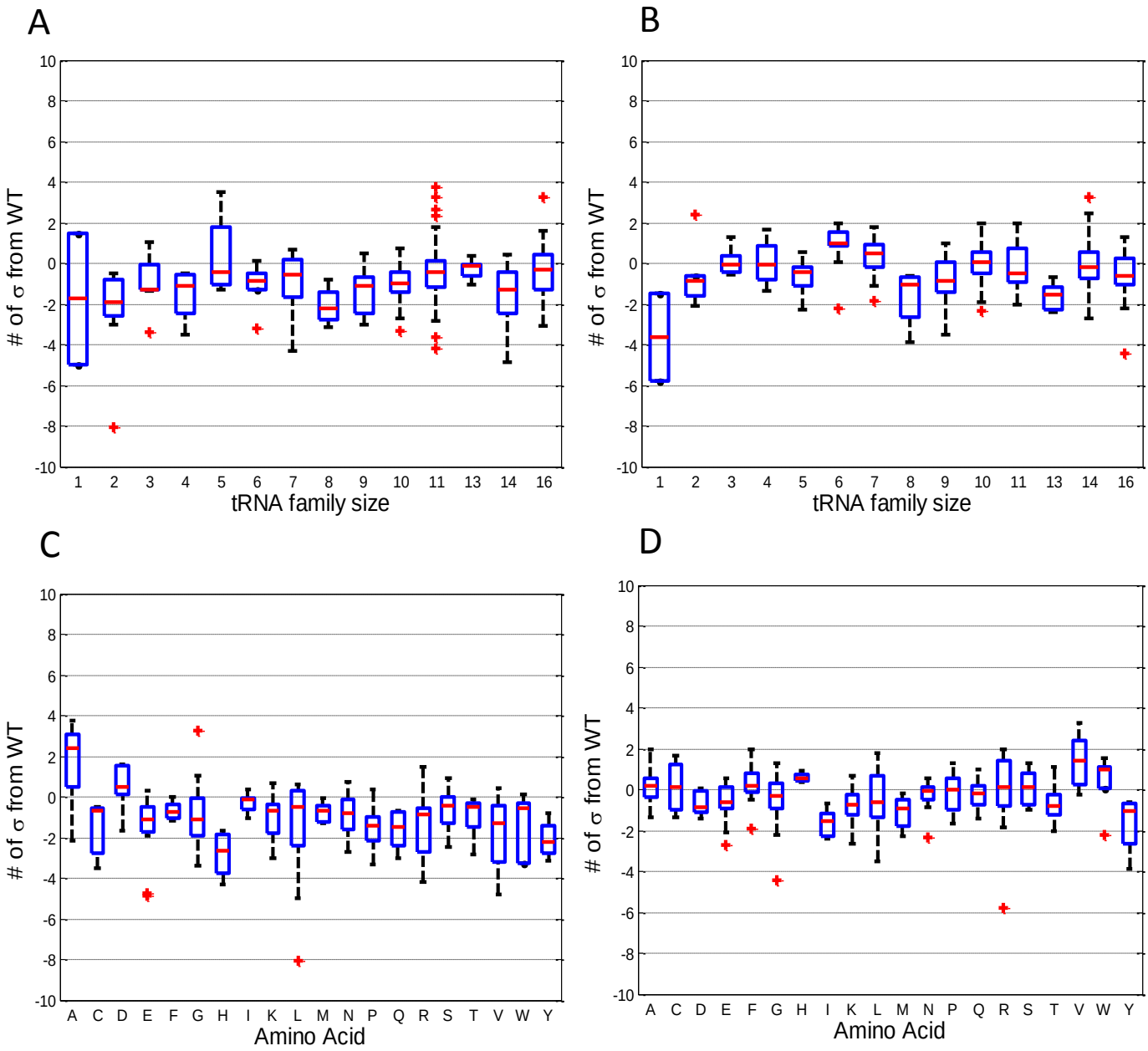
A
B
C
D
# of σ from WT
tRNA family size
Amino Acid
1 2 3 4 5 6 7 8 9 10 11 13 14 16
A C D E F G H I K L M N P Q R S T V W Y
10 8 6 4 2 0 -2 -4 -6 -8 -10

Figure S3

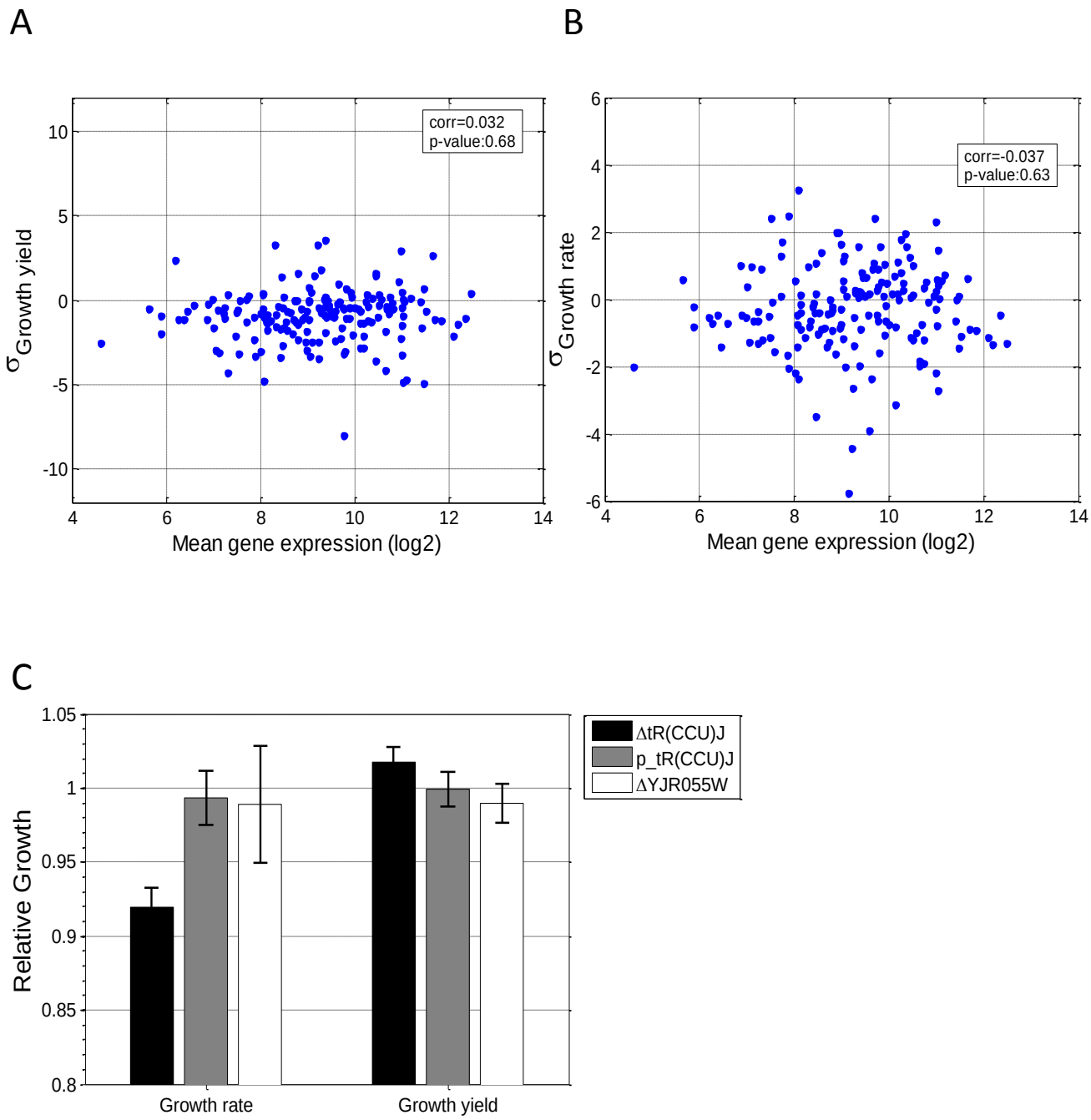
A
B
C
corr=0.032
p-value:0.68
σGrowth yield
Mean gene expression (log2)
corr=-0.037
p-value:0.63
σGrowth rate
Mean gene expression (log2)
Relative Growth
Growth rate
Growth yield
ΔtR(CCU)J
p_tR(CCU)J
ΔYJR055W

Figure S4

A

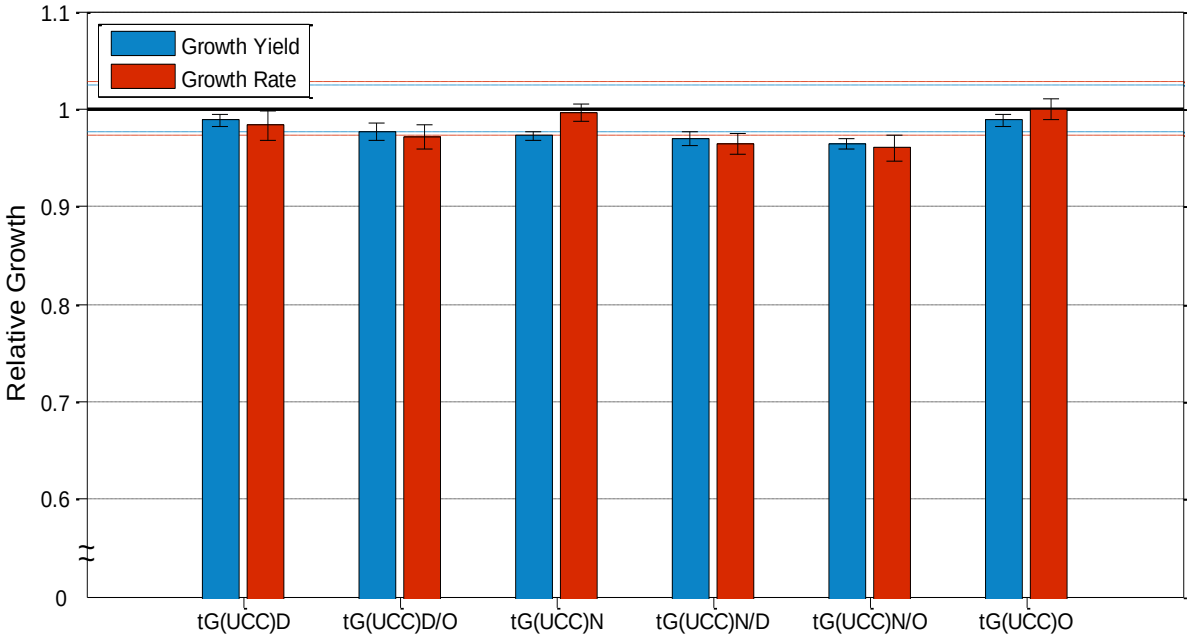
Growth Yield
Growth Rate
Relative Growth
1.1
1
0.9
0.8
0.7
0.6
0
tG(UCC)D
tG(UCC)D/O
tG(UCC)N
tG(UCC)N/D
tG(UCC)N/O
tG(UCC)O

B

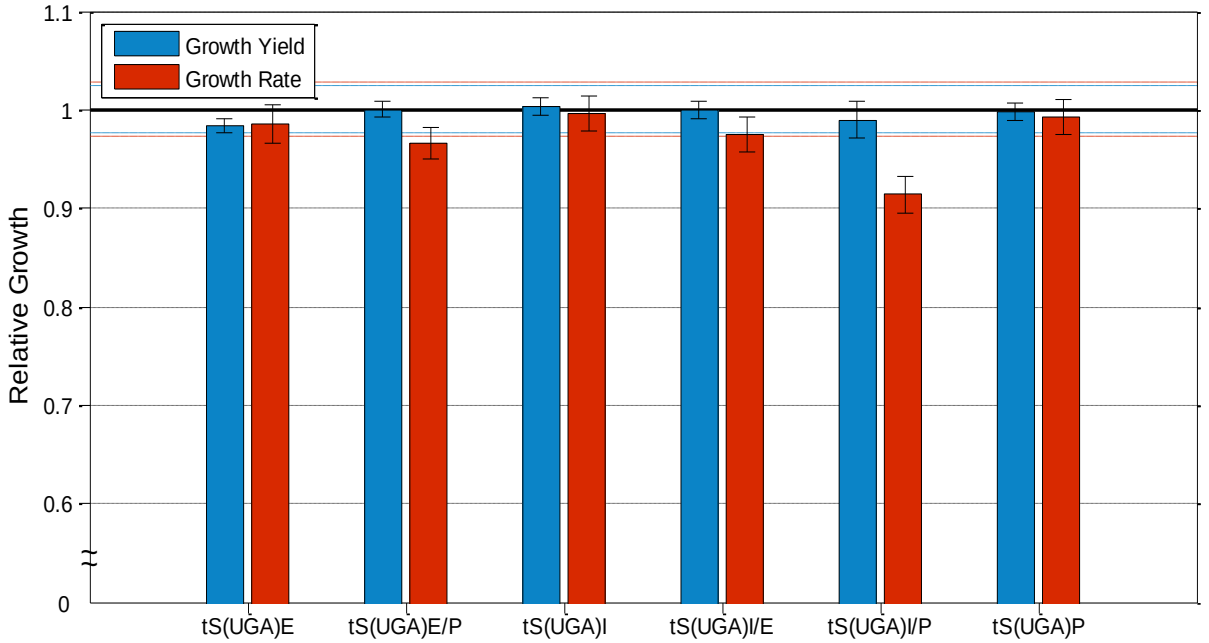
Growth Yield
Growth Rate
Relative Growth
1.1
1
0.9
0.8
0.7
0.6
0
tS(UGA)E
tS(UGA)E/P
tS(UGA)I
tS(UGA)I/E
tS(UGA)I/P
tS(UGA)P

Figure S5

A

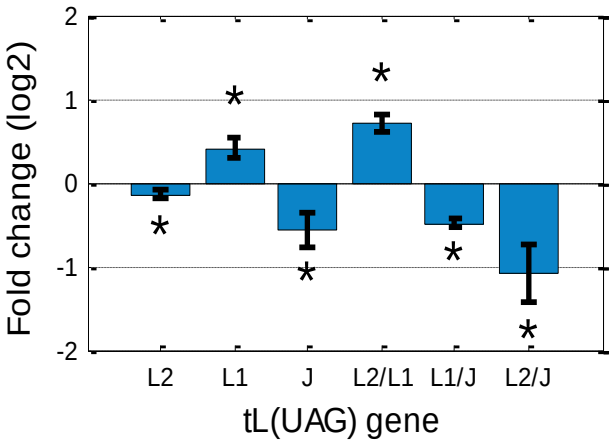
Fold change (log2)
2
1
0
-1
-2
L2
L1
J
L2/L1
L1/J
L2/J
tL(UAG) gene

B

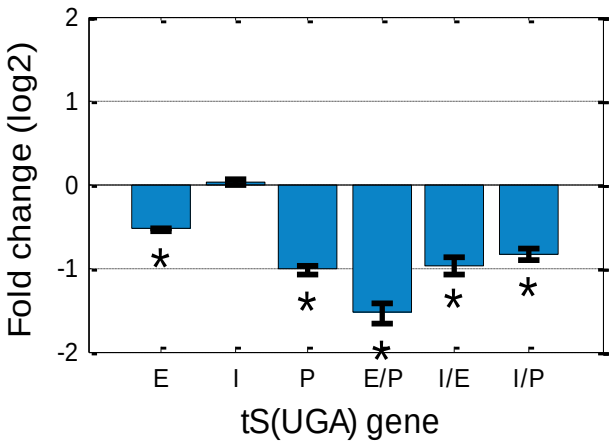
Fold change (log2)
2
1
0
-1
-2
E
I
P
E/P
I/E
I/P
tS(UGA) gene

Figure S6

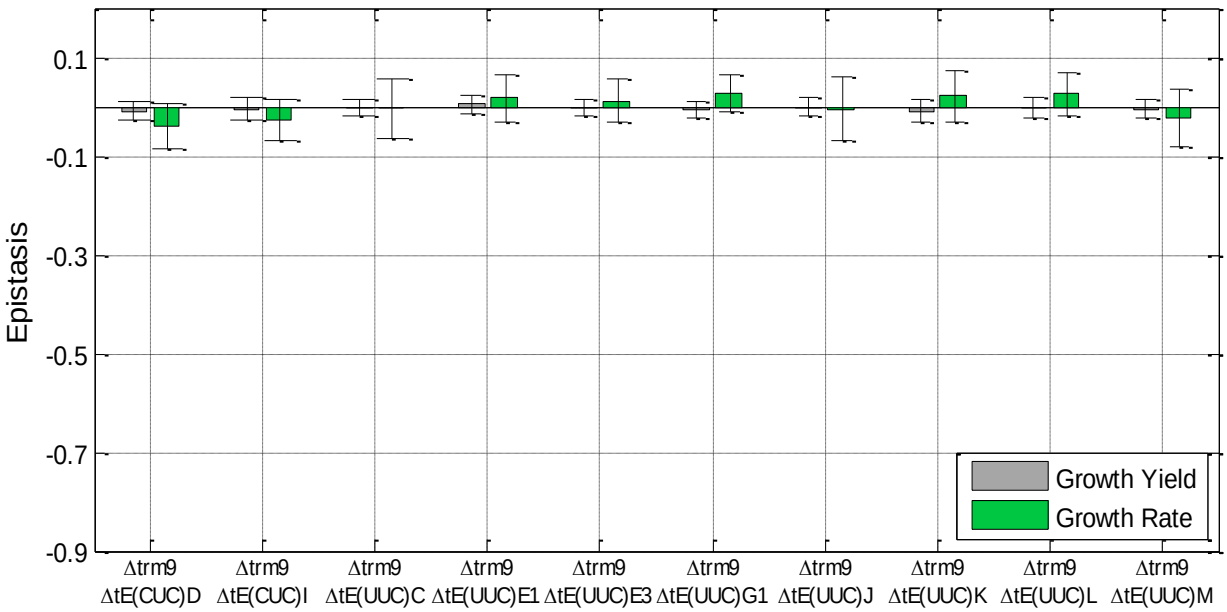
Epistasis
0.1
-0.1
-0.3
-0.5
-0.7
-0.9
Growth Yield
Growth Rate
Δtrm9 ΔtE(CUC)D
Δtrm9 ΔtE(CUC)I
Δtrm9 ΔtE(UUC)C
Δtrm9 ΔtE(UUC)E1
Δtrm9 ΔtE(UUC)E3
Δtrm9 ΔtE(UUC)G1
Δtrm9 ΔtE(UUC)J
Δtrm9 ΔtE(UUC)K
Δtrm9 ΔtE(UUC)L
Δtrm9 ΔtE(UUC)M

Figure S7

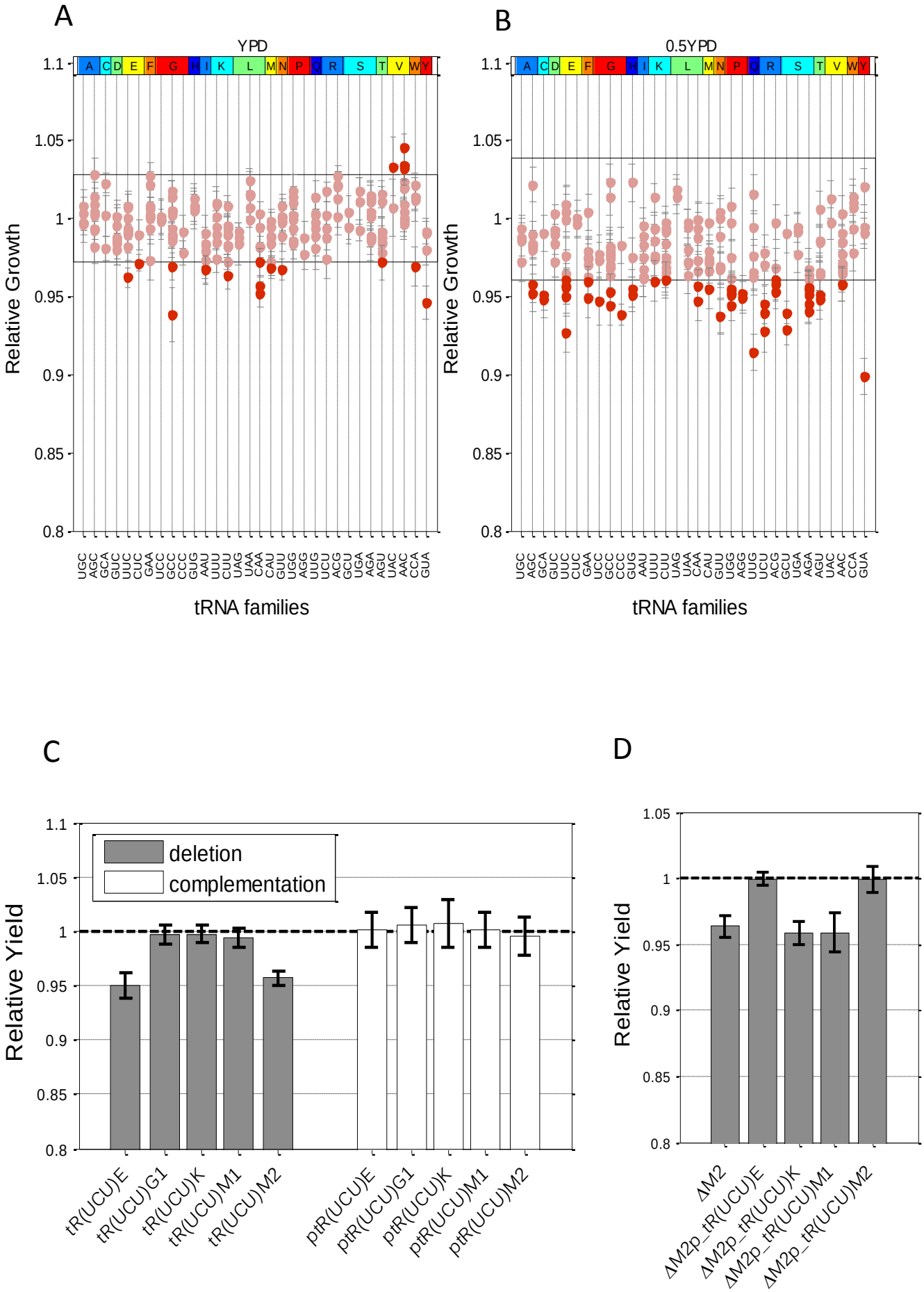
A
YPD
Relative Growth
tRNA families
B
0.5YPD
Relative Growth
tRNA families
C
deletion
complementation
Relative Yield
tR(UCU)E
tR(UCU)G1
tR(UCU)K
tR(UCU)M1
tR(UCU)M2
ptR(UCU)E
ptR(UCU)G1
ptR(UCU)K
ptR(UCU)M1
ptR(UCU)M2
D
Relative Yield
ΔM2
ΔM2p_tR(UCU)E
ΔM2p_tR(UCU)K
ΔM2p_tR(UCU)M1
ΔM2p_tR(UCU)M2

Figure S8

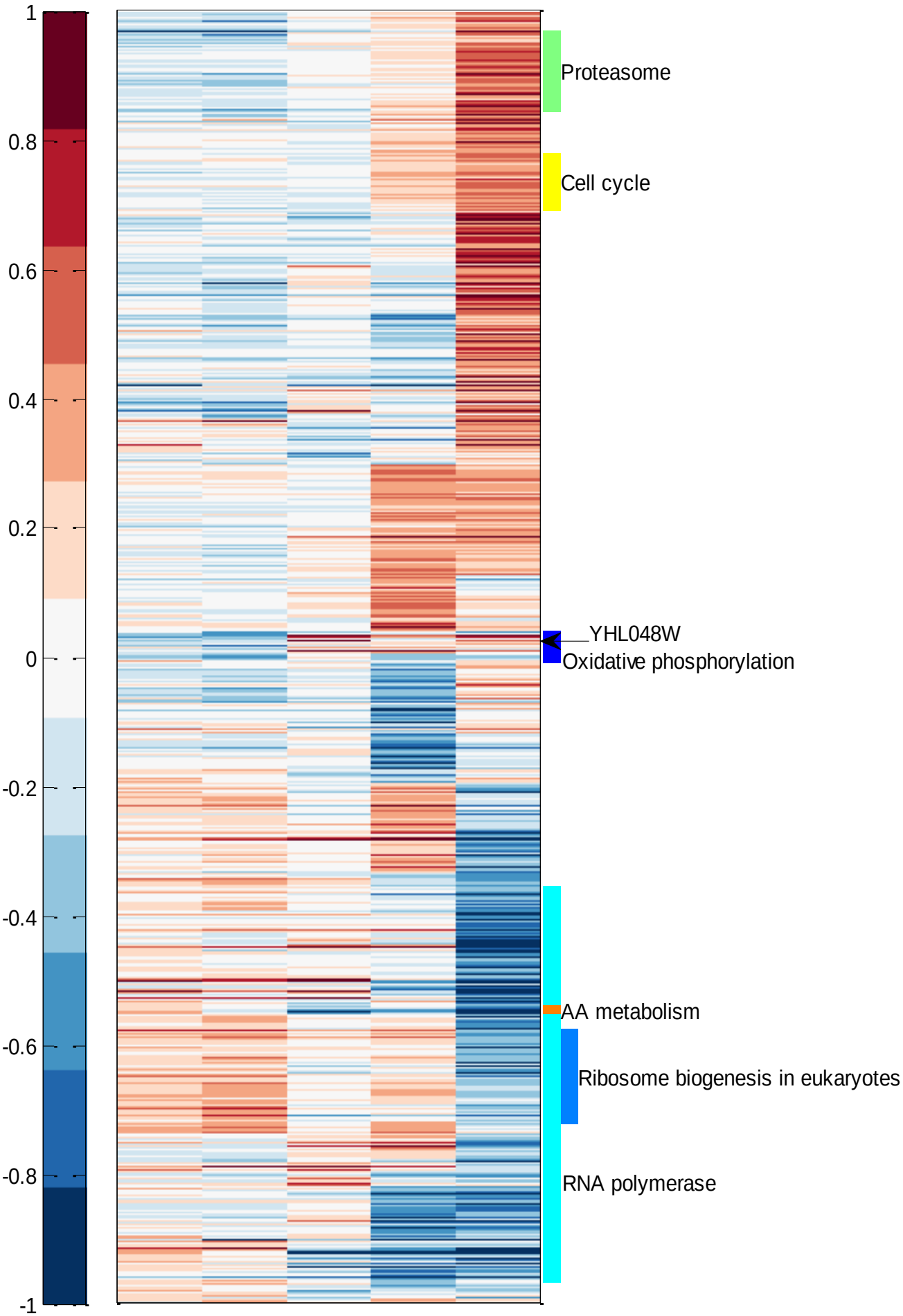
1
0.8
0.6
0.4
0.2
0
-0.2
-0.4
-0.6
-0.8
-1
Proteasome
Cell cycle
YHL048W
Oxidative phosphorylation
AA metabolism
Ribosome biogenesis in eukaryotes
RNA polymerase

Figure S9

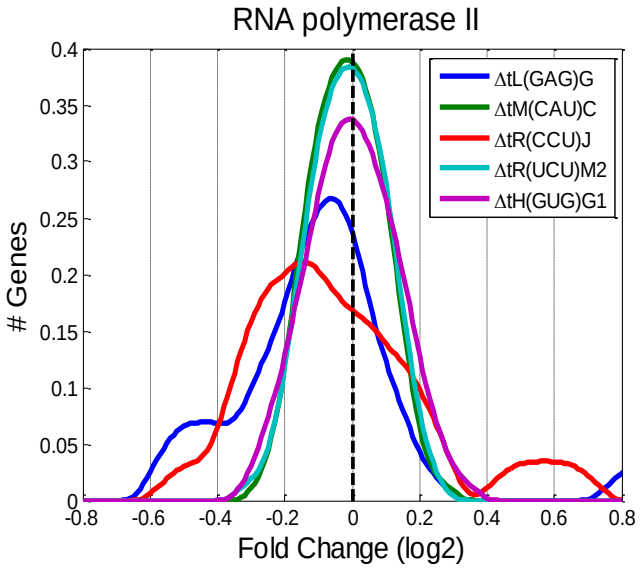
RNA polymerase II
Genes
Fold Change (log2)
ΔtL(GAG)G
ΔtM(CAU)C
ΔtR(CCU)J
ΔtR(UCU)M2
ΔtH(GUG)G1

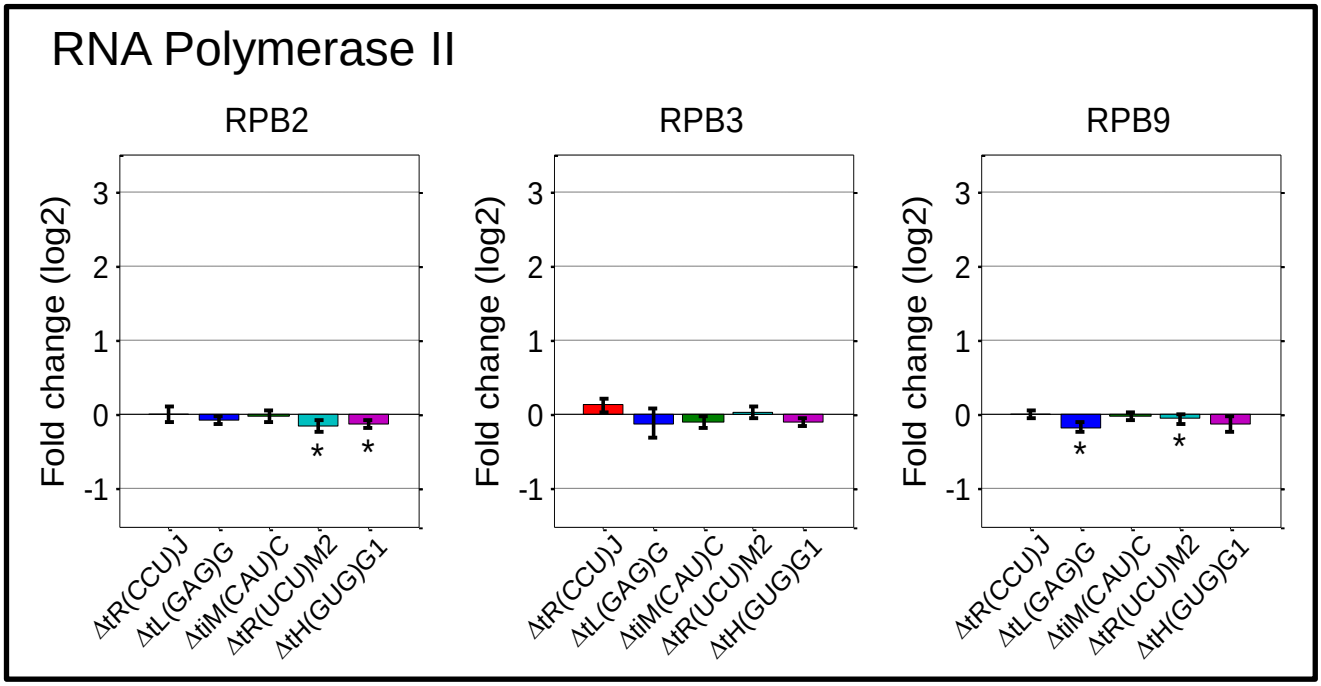
RNA Polymerase II
RPB2
RPB3
RPB9
Fold change (log2)
ΔtR(CCU)J
ΔtL(GAG)G
ΔtiM(CAU)C
ΔtR(UCU)M2
ΔtH(GUG)G1

Table S1. Correlation between tRNA phenotype and expression of nearby genes.

	Upstream Gene	**Downstream Gene**	**Average (up & down genes)**	**Minimal distance**
yield phenotype	r=0.06 p-value:0.41	r=-0.02 p-value:0.78	r=0.03 p-value:0.68	r=0.06 p-value:0.36
absolute yield phenotype (no matter whether it is impairment or improvement)	r=-0.03 p-value:0.71	r=0.02 p-value:0.80	r=0.01 p-value:0.95	r=0.07 p-value:0.37
growth phenotype	r=-0.01 p-value:0.92	r=-0.05 p-value:0.50	r=-0.04 p-value:0.63	r=0.04 p-value:0.61
absolute growth phenotype (no matter whether it is impairment or improvement)	r=-0.02 p-value:0.78	r=-0.04 p-value:0.60	r=-0.04 p-value:0.61	r=0.12 p-value:0.08
any absolute phenotype (growth rate/growth yield impairment/ improvement)	r=-0.02 p-value:0.77	r=-0.01 p-value:0.86	r=0.00 p-value:0.99	r=0.08 p-value:0.24

The table shows the correlation (r) and the p-value between the deletion strain phenotypes and the expression of nearby genes. Each row shows the correlation between the sigma value of the growth yield/growth rate in rich medium (YPD) and the expression of the nearby gene/s taken from the microarray wild-type measurements (columns 1-3) and the distance to the closest genomic feature (column 4).